

A CORRELATIVE STUDY OF THE UV SPECTRA OF INDOLE  
AND THE AZAINDOLES INCLUDING PURINE:  
A SYMBIOTIC COMPUTATIONAL AND  
EXPERIMENTAL APPROACH

Thesis for the Degree of Ph. D.  
MICHIGAN STATE UNIVERSITY  
RICHARD WAYLAND WAGNER  
1971



This is to certify that the

thesis entitled

A CORRELATIVE STUDY OF THE UV SPECTRA OF INDOLE  
AND THE AZAINDOLES INCLUDING PURINE:  
A SYMBIOTIC COMPUTATIONAL AND EXPERIMENTAL APPROACH

presented by

Richard W. Wagner

has been accepted towards fulfillment  
of the requirements for

Ph. D. degree in Biophysics

W. G. St. Seymour  
Major professor

Date Aug. 9<sup>th</sup> 1971

## ABSTRACT

A CORRELATIVE STUDY OF THE UV SPECTRA OF INDOLE  
AND THE AZAINDOLES INCLUDING PURINE:  
A SYMBIOTIC COMPUTATIONAL AND EXPERIMENTAL APPROACH

By

Richard Wayland Wagner

The ultraviolet spectral characteristics of indole, the mono and some diazaindoles and purine were compared and correlated. The characteristics included vapor and solution absorption measurements, polarization measurements, fluorescence and phosphorescence. To further aid these correlations Pariser-Parr-Pople calculations were carried out. Agreement between the calculated observables and the experimental values was quite good. In addition the calculated  $\pi$ -electron charge densities and permanent dipole moments for the ground and two lowest excited singlet states were correlated with the absorption and fluorescence shifts in various solvents.

The  ${}^1L_a \leftarrow {}^1A$  transition was energetically lower than the other singlet transitions for all molecules except those with an aza nitrogen substitution in the pyrrolic ring. For these molecules the  ${}^1L_b \leftarrow {}^1A$  transition was lowest. The vapor absorption spectra of indole, indazole, benzimidazole and 7-azaindole exhibited an anomalous temperature dependent effect. As the temperature was increased the  ${}^1L_a/{}^1L_b$  transition ratio increased. This was attributed to a vibronic coupling scheme.

Richard Wayland Wagner

The vapor phase  ${}^1L_b \leftarrow {}^1A$  transition displayed less vibrational structure as more aza nitrogens were introduced into the indole ring. With three aza nitrogens (purine) no vibrational structure was evident.

The biological significance of these results remains obscure. The spectral phenomena probably reflect the subtle differences in the electronic structure these molecules possess. This structure is biologically manifested in the chemical reactions in which these molecules participate. Thus these results indicate that slight differences in molecular architecture lead to quite varied biological functions.



A CORRELATIVE STUDY OF THE UV SPECTRA OF INDOLE  
AND THE AZAINDOLES INCLUDING PURINE:  
A SYMBIOTIC COMPUTATIONAL AND EXPERIMENTAL APPROACH

By

Richard Wayland Wagner

A THESIS

Submitted to

Michigan State University

in partial fulfillment of the requirements

for the degree of

DOCTOR OF PHILOSOPHY

Department of Biophysics

1971

## DEDICATION

To Ann, Terri, Deborah and especially Marlene  
for the patience afforded the only male member of the household  
during his studies for this degree

## ACKNOWLEDGMENTS

I wish to thank my thesis advisor, Dr. M. Ashraf El-Bayoumi, for his guidance and encouragement throughout the performance of the various phases leading to this dissertation. His friendship is appreciated and his vitality and flexibility is admired.

I am also indebted to Dr. Petr Hochmann for his willingness to lead me into the quantum chemical jungle. His computer program was used in performing the calculations whose results are presented here. In addition he spent many (pleasant for me!) hours discussing quantum mechanical features underlying this program.

Other members of the department and research group must also be recognized. Many fruitful discussions were held with Dr. Kenneth C. Ingham and Dr. Fred Watson which cemented many spectroscopic ideas. The banter we exchanged also helped make the frustrations of this work more bearable. The photographic facilities and aid provided by Prof. J. I. Johnson and by John Haight are also greatly appreciated.

Finally I wish to acknowledge my gratitude to my initial major professor, Dr. Leroy G. Augenstein, whose untimely death severed a relationship which was particularly influential.

## TABLE OF CONTENTS

LIST OF TABLES	vi
LIST OF FIGURES	vii
CHAPTER I INTRODUCTION	1
CHAPTER II THEORETICAL CALCULATIONS	8
I. Introduction	8
II. Background for Theoretical Calculations	8
III. Format for the Calculations	27
CHAPTER III EXPERIMENTAL PROCEDURES	40
I. Vapor Absorption Spectra	40
II. Solution Absorption Spectra	42
III. Emission Spectra	42
IV. Solvents	45
V. Experimentally Studied Molecules	46
CHAPTER IV ANALYSIS OF SPECTRAL DATA FOR EACH MOLECULE	48
INDOLE	48
I. Vapor Absorption Spectra	48
II. Polarization Measurements of Fluorescence Excitation	55
III. Solution Absorption Spectra	57
IV. Fluorescence Spectra	61
V. Phosphorescence Spectra	72
VI. Theoretical Calculations	74
VII. Correlations and Summary	78
INDAZOLE	81
I. Vapor Absorption Spectra	81
II. Polarization Measurements of Fluorescence Excitation	84
III. Solution Absorption Spectra	84
IV. Fluorescence Spectra	87
V. Phosphorescence Spectra	88
VI. Correlations and Summary	89
BENZIMIDAZOLE	90
I. Vapor Absorption Spectra	90
II. Polarization Measurements of Fluorescence Excitation	93
III. Solution Absorption Spectra	94
IV. Fluorescence Spectra	98
V. Phosphorescence Spectra	100
VI. Theoretical Calculations	102
VII. Correlations and Summary	102

4-AZAINDOLE	109
I. Absorption and Fluorescence Spectra	109
II. Theoretical Calculations	110
III. Correlations and Summary	110
5-AZAINDOLE	110
I. Absorption and Fluorescence Spectra	110
II. Theoretical Calculations	110
III. Correlations and Summary	111
6-AZAINDOLE	111
I. Absorption and Fluorescence Spectra	111
II. Theoretical Calculations	111
III. Correlations and Summary	112
7-AZAINDOLE	112
I. Vapor Absorption Spectra	112
II. Solution Absorption Spectra	115
III. Fluorescence Spectra	118
IV. Theoretical Calculations	120
V. Correlations and Summary	120
BENZOTRIAZOLE	125
I. Vapor Absorption Spectra	125
II. Polarization Measurements of Fluorescence Excitation	129
III. Solution Absorption Spectra	130
IV. Fluorescence Spectra	131
V. Phosphorescence Spectra	132
VI. Correlations and Summary	132
4-AZABENZIMIDAZOLE	134
I. Vapor Absorption Spectra	134
II. Absorption and Fluorescence Spectra	137
III. Theoretical Calculations	139
IV. Correlations and Summary	139
5-AZABENZIMIDAZOLE	141
I. Absorption and Fluorescence Spectra	141
II. Theoretical Calculations	142
III. Correlations and Summary	143
PURINE	143
I. Vapor Absorption Spectra	143
II. Transition Assignments	145
III. Absorption and Fluorescence Spectra	146
IV. Phosphorescence Spectra	151
V. Theoretical Calculations	152
VI. Correlations and Summary	155
CHAPTER V INTERMOLECULAR CORRELATION OF THE SPECTRAL DATA	159
BIBLIOGRAPHY	178

## LIST OF TABLES

Table 1.	Semiempirical Parameters.	35
Table 2.	Comparison of Experimental and Calculated Values for Test Molecules.	37
Table 3a.	Solvent Effects on Indole Absorption.	59
Table 3b.	Indole: Comparable Maxima in 2 Solvents.	59
Table 4.	Indole Emission in Various Solvents.	65
Table 5.	Effect of pH on Fluorescence in Indoles (Reference 40).	71
Table 6.	Calculation Results for Indole.	75
Table 7.	Solvent Effects on Azaindole Spectra.	85
Table 8.	Calculation Results for the Azaindoles.	103
Table 9.	Purine Absorption and Luminescence.	147
Table 10.	Effects of pH on Purine Absorption or Fluorescence.	149
Table 11.	Calculation Results for Purine.	149

## LIST OF FIGURES

Figure 1.	Molecules of Biological Interest Containing an Indole or Purine Chromophore.	2
Figure 2.	Molecules Investigated in this Study.	6
Figure 3.	Luminescence Apparatus.	43
Figure 4.	Indole Vapor Absorption Spectrum.	50
Figure 5.	Indole Vapor Absorption Spectra as a Function of Temperature.	53
Figure 6.	Solvent Effects on the Absorption Spectrum of Indole (after Chignell and Gratzer <sup>20</sup> ).	58
Figure 7.	Calculated Charge Densities and Bond Lengths for Indole.	77
Figure 8.	Indazole Vapor Absorption Spectrum.	82
Figure 9.	Indazole Vapor Absorption Spectra as a Function of Temperature.	83
Figure 10.	Benzimidazole Vapor Absorption Spectrum.	91
Figure 11.	Benzimidazole Vapor Absorption Spectra as a Function of Temperature.	92
Figure 12.	Benzimidazole Absorption Spectra in Basic, Neutral and Acidic Solution.	97
Figure 13.	Benzimidazole Fluorescence Spectra in Basic, Neutral and Acidic Solution.	99
Figure 14.	Benzimidazole Phosphorescence in Ethanol at 77° K.	101
Figure 15.	Calculated Charge Densities and Bond Lengths for Benzimidazole.	107
Figure 16.	7-Azaindole Vapor Absorption Spectrum.	113
Figure 17.	7-Azaindole Vapor Absorption Spectra as a Function of Temperature.	114

Figure 18.	Calculated Charge Densities and Bond Lengths for 7-Azaindole.	122
Figure 19.	Benzotriazole Vapor Absorption Spectrum.	126
Figure 20.	Benzotriazole Vapor Absorption Spectra as a Function of Temperature.	127
Figure 21.	4-Azabenzimidazole Vapor Absorption Spectrum.	135
Figure 22.	4-Azabenzimidazole Vapor Absorption Spectra as a Function of Temperature.	136
Figure 23.	Purine Vapor Absorption Spectrum.	144
Figure 24.	Calculated Charge Densities and Bond Lengths for Purine.	154



## CHAPTER I

### INTRODUCTION

Indole is a unique and interesting molecule to spectroscopists, biochemists and biophysicists. It is the chromophore of tryptophan, an amino acid found in most proteins. Tryptophan's maximum extinction coefficient (at 280 nm) is five times that of tyrosine (at 278 nm) and fifteen times that of phenylalanine (at 260 nm) which are the other amino acids absorbing light in the UV region of the electromagnetic spectrum. Thus tryptophan accounts for most of the energy deposition from UV irradiation in proteins (this statement obviously isn't true for certain proteins which don't contain tryptophan, e.g. ribonuclease).

The indole chromophore is also contained in several other molecules of biological significance. A representative group of these molecules is depicted in Figure 1. As can be seen from the figure these molecules may be considered as an indole molecule with attached substituent groups. Serotonin is a transmitter substance found at chemical synapses between neurons. It has also been found to block the action of adrenaline at chemical synapses which utilize adrenaline as a chemical transmitter substance. Indole acetic acid (IAA) is an auxin or plant growth hormone. Lysergic acid is an alkaloid which has achieved recent prominence as the basis of the hallucinogen LSD.

If one takes indole and judiciously replaces three carbons with three aza nitrogens purine could be produced. The nitrogen - carbon replacement would have to occur at the 3, 5, and 7 positions to form this base. Purine is the chromophoric basis of another group of biologically important molecules. Adenine and guanine are two of the

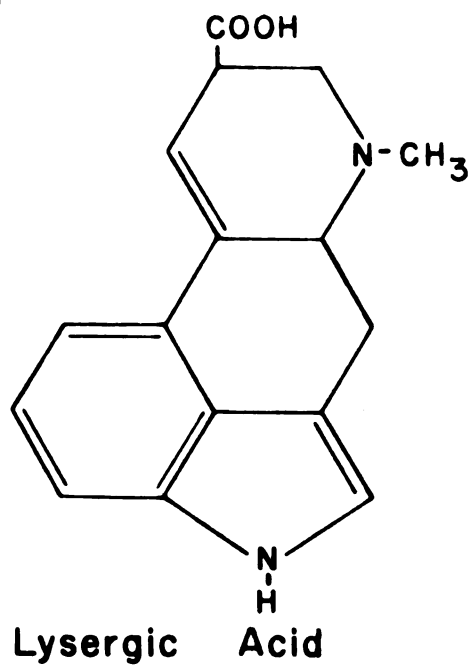
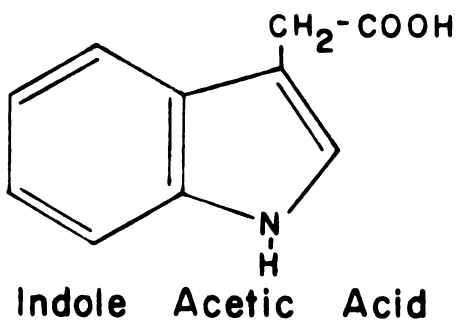
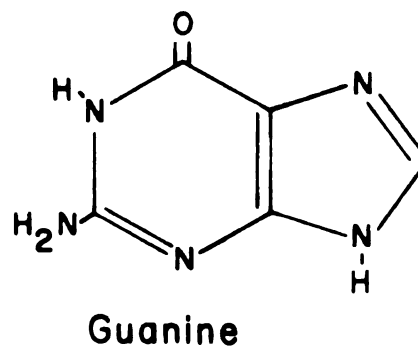
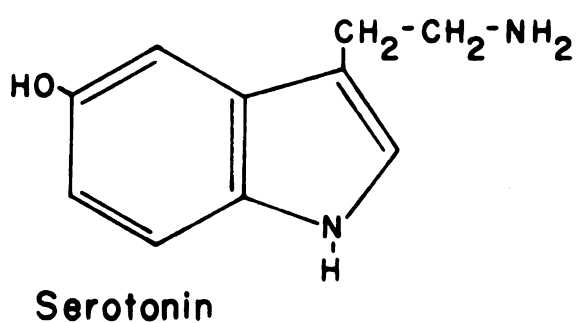
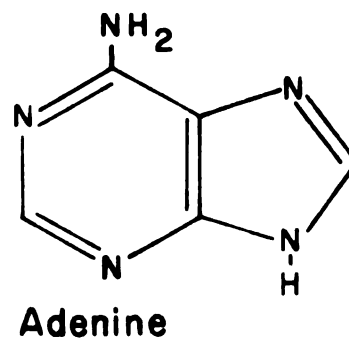
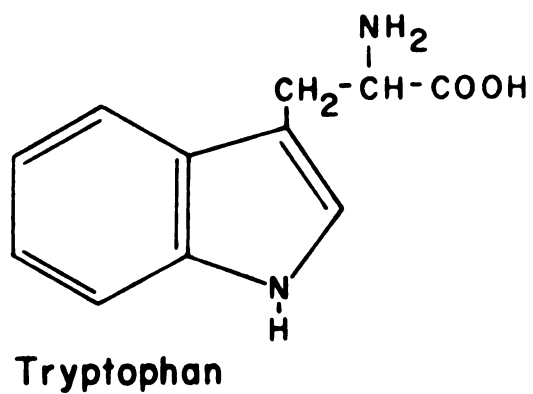


**Figure 1. Molecules of Biological Interest Containing an Indole or Purine Chromophore.**

bases found in the DNA and RNA genetic molecules. These base structures are also shown in Figure 1. Purine is the chromophoric basis of ATP which is a very important intermediary in metabolism. The purine structure is also found in the NAD coenzyme molecule. Although an extensive number of spectroscopic investigations have been made of the purines, relatively few of these have been concentrated on purine itself. Most of the effort has been directed toward the purines found in biological systems such as adenine, guanine and hypoxanthine. However to interpret the spectroscopic data amassed for these molecules, one could begin with purine as the basis molecule and consider the other purines as purine with various substituents. This would assume the spectroscopic nature of purine was known. Obviously this approach hasn't been taken since there is paltry data available for purine.

Spectroscopic investigations of these biologically significant molecules can yield information which is useful in at least two respects. First there has been much attention devoted to the effects of radiation on biological systems. Radiation Biophysics has historically been an important investigative avenue. The spectroscopically investigated properties of biological molecules have been found to shed light on the effects of radiation. Knowledge about the interactions of UV electromagnetic radiation with these molecules fosters an understanding of the available pathways for irradiation deposited energy. A second use for the spectroscopic information pertains to the structure of these molecules. They are not static models composed of units of mass or electrical charge. Their biological relevance recalls the concept that they are dynamic systems. One should probe various physical aspects of these molecules to learn about their structure and its relationship to

their function. UV spectroscopic investigations are probes which can yield information about the electronic portion of the molecular structure. Since the electronic portion participates in chemical reactions it is particularly important to obtain knowledge of this molecular component. In addition these spectroscopic studies give some insight into the dynamic qualities of the electronic component.

Obviously there are several possible spectroscopic studies which could be done. The approach used in this study is somewhat different than in most previously attempted investigations. It seemed strange that the closely related chromophores, indole and purine, are found in such a wide variety of biological molecules. The biological function of these molecules is also widely variant even though the chromophoric difference consists of only an interchange of three carbons and three nitrogens. It is possible that the differences in ecological usage of these chromophores is related to the presence or absence of the aza nitrogens. There is a chromophoric family of molecules which consists of indole, monoaza, diaza and triaza indoles. This family is formed by successive aza nitrogen substitutions at different positions in the indole molecule. There are a large but finite number of such substitutions which can be made. If three substitutions are made at specific positions the triaza-indole called purine is formed. Thus it was decided to undertake a systematic study of this aza-indole molecule family in an attempt to characterize the spectroscopic effects of aza nitrogen substitution on indole. In this manner it was hoped that information would be revealed about the inherent electronic differences between indole and purine. With so many possible aza-indoles to study, time dictated that only a fraction of them be investigated. The choice was further

simplified by the commercial availability of azaindoles as well as the accessibility of previously published data for molecules in this family. After this paring the molecules which were investigated in this study are shown in Figure 2.

In order to reach the objectives of this study it was decided that a correlative investigation of the UV spectroscopic data for these molecules should be done. All available published experimental data would be used. This would be augmented by experimental work performed in this laboratory. In addition it was decided that theoretical calculations should be undertaken to add another dimension to our concept of the electronic structure and spectroscopic properties of these molecules. It was hoped that a unified picture of the electronic structure would be developed which could explain the spectroscopic data. In addition it was hoped that this spectral data unification would incorporate the effects of the molecular environment on the spectroscopic properties of these molecules.

One of the obvious spectroscopic features not present for indole but which azaindoles might possess is the  $n \rightarrow \pi^*$  transition. This transition consists of the promotion of an electron from the electron lone pair or nonbonding orbital on an aza nitrogen to an antibonding  $\pi^*$  orbital. It is characterized by its weak intensity resulting from the negligible overlap of the nonbonding and antibonding orbitals. The other transition which should occur for both indole and the azaindoles is the  $\pi \rightarrow \pi^*$  transition. It consists of an electron promotion from a bonding  $\pi$  orbital to an antibonding  $\pi^*$  orbital and is usually intense due to the overlap of these two orbitals. It will become apparent in this study that both transitions are important spectral properties of

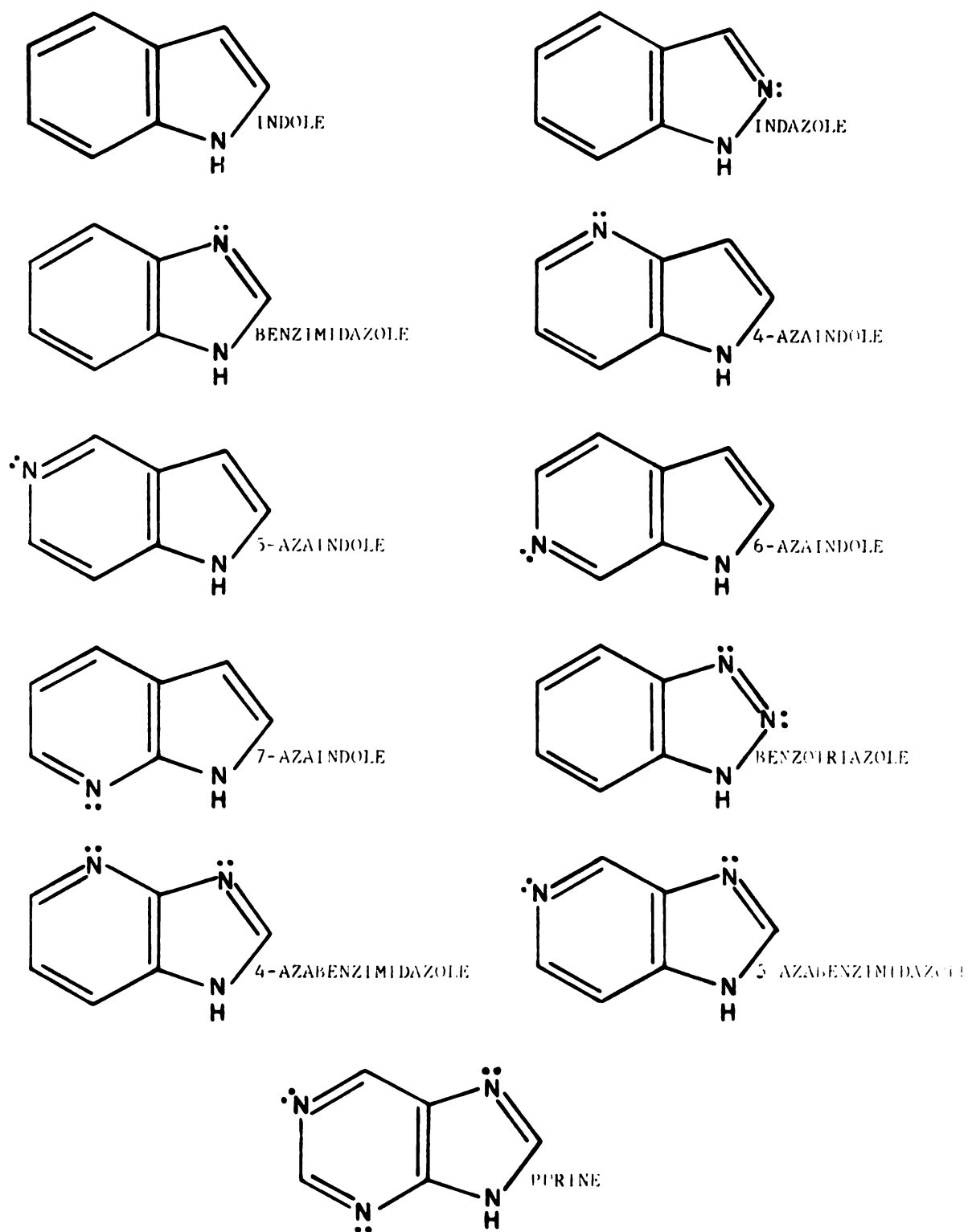


Figure 2. Molecules Investigated in this Study.

these molecules.

With this brief background we are ready to proceed to the rest of this dissertation. The next chapter will outline the method for performing the theoretical calculations. Chapter 3 will be a discussion of the experimental techniques and apparatus employed in this study. Chapter 4 will be compilation and discussion of all the available data for the investigated molecules. The data for each molecule will be discussed separately and will include results personally obtained during the course of this study. The final chapter will be devoted to a discussion of the trends and correlations which occur in this family of molecules. It will be concluded with a few statements concerning the accomplishments of this correlative undertaking.

## CHAPTER II

### THEORETICAL CALCULATIONS

#### I. Introduction

One of the powerful tools for studying the electronic structure of molecules is the performance of correlative theoretical calculations of certain molecular observables for a given class of molecules. An examination of trends in properties such as ionization potentials, electron affinities, transition energies and intensities often yields valuable information. It is also possible to then compare the calculated observables with corresponding experimental results. This gives one a feeling for how reliable the calculated observables are, allows further correlations between theoretical and experimental quantities and gives the freedom of predicting values for which no experimental results are available. Of course this is all predicated on the validity of the theoretical calculations.

The following sections will be devoted to this question of validity. Pariser-Parr-Pople type calculations were made of the molecules under study. The general theoretical background for these calculations will be described, followed by the rationale used here in specifically performing them. The form, parametrization, and type of input and output used here will also be presented.

1,2,3

#### II. Background for Theoretical Calculations

To date the most powerful and fruitful approach for the analytical calculation of physically interpretable quantities pertaining to molecules is that of Quantum Mechanics. By solving the Time Independent



## Schrodinger Equation

$$\hat{H} \Psi = W \Psi \quad (1)$$

many molecular properties may be examined. For any molecule the

Hamilton operator  $\hat{H}$  may be represented by

$$\begin{aligned} \hat{H} = & -\sum_{\alpha=1}^K \frac{\hbar^2}{2M_{\alpha}} \nabla_{\alpha}^2 - \sum_{i=1}^N \frac{\hbar^2}{2m_i} \nabla_i^2 + \frac{1}{2} \sum_{i \neq j}^{N,N} \frac{e^2}{|r_i - r_j|} + \frac{1}{2} \sum_{\alpha \neq \beta}^{K,K} \frac{Z_{\alpha} Z_{\beta} e^2}{|R_{\alpha} - R_{\beta}|} \\ & - \frac{1}{2} \sum_{i,\alpha}^{N,K} \frac{Z_{\alpha} e^2}{|R_{\alpha} - r_i|} \end{aligned} \quad (2)$$

where the K nuclei of the molecule are indexed by the values of  $\alpha$ , with charge  $Z_{\alpha}e$  and mass  $M_{\alpha}$ , and the N electrons are indexed by the values of  $i$ . However this representation has been formulated with the following assumptions.

**Assumption 1:** A non-relativistic representation is adequate for reproducing the observables under study. That is, relativistic corrections are of such a magnitude as to be negligible. Thus non-electrostatic interactions are ignored.

**Assumption 2:** All molecular electrons and nuclei are regarded as point charges. Terms which are neglected by this assumption (such as that due to nuclear quadrupole) are of the order of relativistic corrections.

**Assumption 3:** The molecule under investigation is isolated and not subject to any external fields. Stationary state values of  $\Psi$  adequately provide the observables of interest. Thus  $\Psi$  is a function of spatial and spin variables only.

Unfortunately even with these assumptions it is impossible to exactly solve Equation 1 except in the most elementary cases. Further assumptions must be made to simplify the analysis. These assumptions, as well as the preceding ones, are primarily based on our physical intuition regarding the system being studied.

For the molecules studied here, only those properties primarily due to the electrons are of interest. Since  $\frac{m_e}{M_\alpha} \ll 1$

Assumption 4: The separability of the electron and nuclear motions in the sense of the Born - Oppenheimer (Adiabatic) Approximation is assumed. The electronic part of the wave function is then an eigenfunction of the Hamiltonian:

$$\hat{H} = - \sum_{i=1}^N \frac{\hbar^2}{2m_i} \nabla_i^2 + \frac{1}{2} \sum_{i \neq j}^{N,N} \frac{e^2}{|r_i - r_j|} - \frac{1}{2} \sum_{\alpha,i}^{K,N} \frac{Z_\alpha e^2}{|R_\alpha - r_i|} \quad (3)$$

This eigenfunction is determined only for the nuclear configuration which corresponds to the equilibrium geometry of the molecule in the ground state. Therefore all properties of molecular excited states evaluated within this approximation are those of vertical states (see Franck - Condon Principle). The wave function now only depends explicitly on the electronic spatial and spin coordinates. This wave function may be represented as a linear combination of Slater determinants. Let  $\Delta_K$  denote the following Slater determinant:

$$\Delta_K = \frac{1}{\sqrt{N!}} \sum_P (-1)^P \hat{P} [X_{K_1}(1), X_{K_2}(2), \dots, X_{K_N}(N)] \quad (4)$$

where  $\chi_{K_1}$  is the  $K_1$ -th spin orbital. By using this representation the requirement of an antisymmetric wave function with respect to electron coordinate transpositions (Pauli Exclusion Principle) will be satisfied.

It is apparent from the normalization factor in Equation 4 that

**Assumption 5:** The spin orbitals comprise an orthonormalized set.

They can be written as a simple product of MO and spin

functions  $\eta(s)$ :  $\phi(r)\eta(s)$ . (The  $\eta(s)$  are either  $\alpha$  or  $\beta$ )

The molecular orbitals are the eigenfunctions of an effective one-electron Hamiltonian which will be specified later. Since the wave function is represented as a linear combination of Slater determinants:

$$\psi = \sum_K C_K \Delta_K \quad (5)$$

Since  $\hat{H}$  does not contain any spin dependent operator,  $\hat{S}_z$  and  $\hat{S}^2$  commute with  $\hat{H}$ . Therefore the eigenfunction of  $\hat{H}$  can be simultaneously made the eigenfunction of  $\hat{S}_z$  and  $\hat{S}^2$ . This condition restricts the class of wave functions which are eigenfunctions of  $\hat{H}$ . However the same function may be used to calculate both energy and spin related observables. This is important when molecular states of a particular multiplicity are under scrutiny.

Although molecular calculations could be made in principle with these assumptions they would rapidly become intractable without some further restrictions. These restrictions are made to simplify the computations which must be performed.

**Assumption 6:** A one - electron effective Hamiltonian will be used. Its form will be specified later.

This operator will serve as a generator of electronic molecular orbitals which form the eigenfunctions. The molecular orbitals (MO)

are a property of the molecule and are of the form illustrated in Assumption 5. Each electron is assigned to an MO. When the MO are written in the product form of Assumption 5 it is possible to place two electrons in each spatial function  $\phi(r)$ . This does not violate the Pauli Exclusion Principle since the accompanying spin coordinates may have either of the two allowed values,  $\alpha$  or  $\beta$ .

Certain requirements of the  $\Delta_K$  in Equation 5 must be met before the  $\psi$  defined by Equation 5 is an eigenfunction of the Hamiltonian of Equation 3. The  $\Delta_K$  must be functions which comprise a complete orthonormalized set with respect to quadratically integrable antisymmetric  $N$  - electron functions. The  $C_K$  in Equation 5 are determined by the infinite order eigenvector equation. However the  $N$  - order Slater determinants, constructed from the complete set of orthonormalized spin orbitals  $X$ , make such a complete orthonormalized set of  $N$  - electron wave functions. Equation 5 is thus an eigenfunction of the stated Hamiltonian. This equation is the basis of Configuration Interaction which is an expansion over a complete set of  $N$  - particle functions. In the calculations performed here

**Assumption 7:** A Limited Configuration Interaction (LCI) involving a truncated set of ground and monoexcited states is used. This assumption is made for two reasons. First experience has shown that the ground state and monoexcited states make the largest contribution to calculated properties of the ground and lowest excited states. Second the computers used in performing these calculations have only a finite capacity so truncation must be performed.

Obviously the function  $\psi$  is not analytically correct and is completely undetermined as it has been written. It only approximates

the "correct" solution to the Schrodinger Equation. However to obtain the best eigenvalue which may be compared to the experimentally determined energy, some mechanistic procedure must be found to improve successive "guesses" of the true wavefunction. Such a procedure is found in the Variational Theorem where for

$$W = \min_{\psi} \frac{\int \psi^* \hat{H} \psi d\tau}{\int \psi^* \psi d\tau} \quad \text{Variational Theorem} \quad (6)$$

values of  $\psi$  are guessed over and over

$$E = \frac{\int \psi^* \hat{H} \psi d\tau}{\int \psi^* \psi d\tau} \quad (7)$$

and

$$E \geq W \quad (8)$$

In this case  $W$  corresponds to the molecular ground state energy. The value of  $\psi$  which minimizes this energy will not in principle be a good function for calculating any other energy state or any other observable. However these functions together with Configuration Interaction will be used here. The parametrization which is outlined later partially overcomes this obstacle. For the molecules studied here the Variational Theorem is modified to the Linear Variational Principle. This principle is used to determine the expansion coefficients  $C_K$  in Equation 5. Using the form of Equation 5

$$\sum_{J=1}^L C_J (H_{IJ} - S_{IJ} E) = 0 \quad (9)$$

where

$$H_{IJ} = H_{JI}^* = \int \Delta_I^* \hat{H} \Delta_J d\tau(1, 2, \dots, N) \quad \text{and} \quad (10)$$

$$S_{IJ} = S_{JI}^* = \int \Delta_I^* \Delta_J d\tau(1, 2, \dots, N)$$

There are L such linear equations and the nontrivial solution for the coefficients requires the Secular Equation

$$|(H_{IJ} - S_{IJ}E)| = 0 \quad (11)$$

This yields L roots for  $E_I$  which converge to  $W_I$  from above as more independent  $\Delta_I$  are added, increasing the value of L.

At this point a closer examination of the Secular Equation is warranted. Without loss of generality the  $X_i$  and  $\phi_i$  functions composing  $\Delta_I$  may be assumed to be orthonormal as intimated in Assumption 5 so

$$S_{IJ} = \delta_{IJ} \quad (12)$$

The Hamiltonian is now broken up

$$\hat{H}_2(1,2,\dots,N) = \sum_i^N \hat{H}_K(i) + \frac{1}{2} \sum_{i,j}^{N,N} \frac{e^2}{|r_i - r_j|} \quad (13)$$

where obviously

$$\hat{H}_K(i) = -\frac{\hbar^2}{2m_i} \nabla_i^2 - \sum_{\alpha}^K \frac{Z_{\alpha} e^2}{|R_{\alpha} - r_i|} \quad (14)$$

It is judicious to delineate four possible cases:

Case 1:  $\Delta_I$  and  $\Delta_J$  are identical.

Case 2:  $\Delta_I$  and  $\Delta_J$  differ by only one spin orbital with  $X_m$  entering  $\Delta_I$  where  $X_p$  enters  $\Delta_J$ .

Case 3:  $\Delta_I$  and  $\Delta_J$  differ by two spin orbitals with  $X_m$  and  $X_n$  entering  $\Delta_I$  where  $X_p$  and  $X_q$  enters  $\Delta_J$ .

Case 4:  $\Delta_I$  and  $\Delta_J$  differ by three or more spin orbitals.

Each term in the Secular Equation can be evaluated for these cases by using the Slater Rules. In light of Equation 12

$$S_{IJ} = \begin{cases} 1 & \text{for Case 1} \\ 0 & \text{otherwise} \end{cases} \quad (15)$$

$$H_{IJ} = \begin{cases} \sum_i^N (I_i' + \frac{1}{2} \sum_j^N (J_{ij}' - K_{ij}')) & \text{for Case 1} \\ I_{mp}' + \sum_{i \neq m, p}^N [(im|ip)' - (im|pi)'] & \text{for Case 2} \\ 0 + (mn|pq)' - (mn|qp)' & \text{for Case 3} \\ 0 & \text{for Case 4} \end{cases} \quad (16)$$

where the primes denote spin orbitals and

$$\begin{aligned} I_{ii}' &= I_i' = \int \chi_i^*(a) \hat{H}_K(a) \chi_i(a) d\tau(a) \\ I_{ij}' &= \int \chi_i^*(a) \hat{H}_K(a) \chi_j(a) d\tau(a) \\ (ik|jl)' &= \int \chi_i^*(a) \chi_k^*(b) \frac{e^2}{|r_a - r_b|} \chi_j(a) \chi_l(b) d\tau(a) d\tau(b) \\ J_{ij}' &= (ij|ij)' \quad \text{is the Coulomb Integral} \\ K_{ij}' &= (ij|ji)' \quad \text{is the Exchange Integral} \end{aligned} \quad (17)$$

It is possible to switch from spin orbitals to space orbitals easily.

$$I_{ij}' = \begin{cases} I_{ij} & \text{if } \chi_i \text{ and } \chi_j \text{ have the same spin.} \\ 0 & \text{otherwise.} \end{cases} \quad (18)$$

$$I_{ii}' = I_{ii} = I_i \quad (19)$$

$$(ik|jl)' = \begin{cases} (ik|jl) & \text{if } \chi_i \text{ and } \chi_j \text{ have the same spin and} \\ & \chi_k \text{ and } \chi_l \text{ have the same spin.} \\ 0 & \text{otherwise.} \end{cases} \quad (20)$$

$$\begin{aligned}
 J'_{ij} &= J_{ij} \\
 K'_{ij} &= \begin{cases} K_{ij} & \text{if } X_i \text{ and } X_j \text{ have the same spin.} \\ 0 & \text{otherwise} \end{cases}
 \end{aligned}
 \quad (21)$$

It is now possible to calculate (at least symbolically) the expectation value for the ground state energy of a given molecule. Each spatial MO used has two electrons in it with opposing spins forming a Closed Shell Configuration. For this case

$$E_N = \sum_{i=1}^N (2I_i + \sum_{j \neq i}^N (2J_{ij} - K_{ij})) \quad (22)$$

where  $N = N/2$ .

So far it has not been apparent how to use the Variational Theorem to best advantage in calculating the minimum  $E$ . This is accomplished by carrying out a variational calculation using the method of Lagrangian Undetermined Multipliers.

It is asked that

$$\mathcal{E} = E_N - 2 \sum_{i,j}^N \epsilon_{ij} S_{ij} \quad (23)$$

be a minimum or  $\delta \mathcal{E} = 0$ . This gives

$$0 = \sum_{i=1}^N \int \delta \phi_i \left[ 4 \hat{H}_K \phi_i + \sum_{j=1}^N (8 J_{ij} \phi_i - 4 K_{ij} \phi_i - 4 \epsilon_{ij} \phi_j) \right] \quad (24)$$

$$\begin{aligned}
 \text{where } J_{ij} &= \iint \phi_i^2(a) \frac{e^2}{|r_a - r_b|} \phi_j^2(b) d\tau(a) d\tau(b) = \int \phi_i^*(a) J_{ij}(a) \phi_i(a) d\tau(a) \\
 &= \int \phi_j^*(b) J_{ij}(b) \phi_j(b) d\tau(b)
 \end{aligned}
 \quad (25)$$

or  $\hat{J}_{ij}(a) \phi_i(a) = \left[ \int \phi_j^*(b) \frac{e^2}{|r_a - r_b|} \phi_j(b) d\tau(b) \right] \phi_i(a)$



$$\begin{aligned}
\text{and } K_{ij} &= \iint \phi_i^*(a) \phi_j(a) \frac{e^2}{|r_a - r_b|} \phi_i(b) \phi_j^*(b) d\tau(a) d\tau(b) \\
&= \int \phi_i^*(a) K_j(a) \phi_i(a) d\tau(a) = \int \phi_j^*(b) K_i(b) \phi_j(b) d\tau(b) \\
\text{or } \hat{K}_j(a) \phi_i(a) &= \left[ \int \phi_j^*(b) \frac{e^2}{|r_a - r_b|} \phi_i(b) d\tau(b) \right] \phi_j(a)
\end{aligned} \quad (26)$$

Since equation 24 is nontrivially satisfied when the term in the bracket is zero

$$[\hat{H}_K(a) + \sum_{j=1}^N (2J_j(a) - K_j(a))] \phi_i(a) = \sum_{j=1}^N \epsilon_{ij} \phi_j(a) \quad (27)$$

$$\text{without loss of generality } \epsilon_{ij} = \epsilon_i \delta_{ij} \quad (28)$$

which finally yields

$$\hat{F}(a) \phi_i(a) = \epsilon_i \phi_i(a) \quad (29)$$

These are the Hartree-Fock integro-differential equations. Since the  $\hat{F}$  depends explicitly on the functions  $\phi_i$  the tact is to guess a starting set  $\phi_i$ , evaluate  $\hat{F}$ , solve Equation 29 and iterate until self-consistency is attained. This is known as the Self-Consistent Field (SCF) method.

The transformation of Equation 28 is not difficult to perform and may be done in general. However for most molecules it is difficult to solve the Hartree-Fock formulation (Equation 29). A judicious choice of MO would alleviate this problem. The MO may be of any form. However one form has gained popularity because it is based on a subset of orbitals whose properties are known.

**Assumption 8:** The Molecular Orbitals are constructed of a Linear Combination of Atomic Orbitals (LCAO).

$$\phi_i = \sum_p^m C_{ip} \chi_p \quad \text{where } m \geq N \quad (30)$$

$\chi_p$  are the AO and  $C_{ip}$  are coefficients. Without loss of generality the

LCAO form an orthonormal set and

$$\int \chi_p^* \chi_q d\tau = \delta_{pq} \quad (31)$$

When this substitution is made in the Hartree-Fock Equation followed by a multiplication on the left by  $\sum_q^m C_{iq}^* \chi_q^*$  with integration a new expansion is formed

$$\sum_q^m C_{iq}^* \sum_p^m C_{ip} (F_{pq} - S_{pq} \epsilon_i) = 0 \quad (32)$$

$$S_{pq} = \int \chi_q^* \chi_p d\tau = \delta_{pq} \quad (33)$$

and  $F_{pq} = \int \chi_q^* \hat{F} \chi_p d\tau = I_{pq} + \sum_j^2 [2(qj|pj) - (qj|jp)] \quad (34)$

Since the AO are presumed known it is possible to diagonalize the  $\epsilon_{ij}$  matrix and to calculate the integrals.

$$I_{pq} = \int \chi_q^*(a) \hat{H}_K(a) \chi_p(a) d\tau(a) \quad (35)$$

and  $(pq|rs) = \int \chi_p^*(a) \chi_q^*(b) \frac{e^2}{|r_a - r_b|} \chi_r(a) \chi_s(b) d\tau(a) d\tau(b) \quad (36)$

It should be noted that

$$I_i = \sum_q^m C_{iq}^* \sum_p^m C_{ip} \int \chi_q^* \hat{H}_K \chi_p d\tau \quad (37)$$

$$J_{ij} = \sum_q^m C_{iq}^* \sum_p^m C_{ip} \int \chi_q^* J_j \chi_p d\tau \quad (38)$$

and  $K_{ij} = \sum_q^m C_{iq}^* \sum_p^m C_{ip} \int \chi_q^* K_j \chi_p d\tau \quad (39)$

Performing a variational calculation on Equation 32 yields

$$\sum_p^m C_{ip} (F_{pq} - S_{pq} \epsilon_i) = 0 \quad \text{Roothaan Equations} \quad (40)$$

which lead to a Secular Determinant of order m

$$\begin{vmatrix} F_{pq} - S_{pq} \epsilon_i \end{vmatrix} = 0 \quad (41)$$

Equations 37-39 show that the operator  $\hat{F}$  depends explicitly on the  $C_{ip}$ , (see also Equations 64-66). To achieve the best MO which minimizes the molecular energy a set of  $C_{ip}$  is assumed, the matrix  $\|F\|$  is calculated with the aid of Equations 37-39, the Secular Determinant is solved for the N lowest eigenvalues and a new set of  $C_{ip}$  is generated from the Roothaan Equations. This process is iterated until the  $C_{ip}$  are self-consistent. The similarity of this process to that of the Hartree-Fock SCF method has lead to this procedure being called the LCAO-SCF method. If m is made large enough to form a complete set, the  $\phi_i$  generated by the LCAO-SCF method are exactly those determined by the Hartree-Fock SCF method. However the set m is usually truncated in practice to conform with computer limitations. Again this loss in generality is somewhat overcome by the subsequent parametrization.

Most of the molecular properties of interest here are related to the ground and the lowest excited states of these molecules. The excited state properties are primarily associated with " $\pi$ " electrons. All other electrons in such molecules are called " $\sigma$ " electrons.

**Assumption 9:** The  $\pi$ -electrons are delocalized over the whole molecule while the  $\sigma$ -electrons are associated about particular nuclear centers.

For all molecules investigated here the  $\pi$ -electrons MO are constructed from  $2p\pi$  AO. Physical intuition indicates that the delocalized  $\pi$ -electrons are more susceptible than the localized  $\sigma$ -electrons to physical processes such as electronic excitation. For this reason

**Assumption 10:  $\Sigma$ - $\Pi$  Separability.** The wavefunction  $\Psi$  is separable into a product of two functions ( $\Sigma$ ) ( $\Pi$ ) both of which are

antisymmetric with respect to themselves and each other.

Each of these functions is represented by Slater determinants and is normalized to unity.

$$\int (\Sigma)^2 d\tau_\sigma = \int (\Pi)^2 d\tau_\pi = 1 \quad (42)$$

One of the outcomes of these conditions is that Equation 1 yields

$$E_{el} = E_\Sigma + E_\Pi \quad \text{where} \quad (43)$$

$$E_\Sigma = \int (\Sigma)^* \hat{H}_\Sigma (\Sigma) d\tau_\Sigma \quad \text{and} \quad E_\Pi = \int (\Pi)^* \hat{H}_\Pi (\Pi) d\tau_\Pi \quad (44)$$

A further restriction is placed on these functions.

**Assumption 11:** The spin orbitals from which the  $\Sigma$  and  $\Pi$  functions are constructed form a disjunctive set. That is electrons are restricted to one function or the other. Each spin orbital belongs to one set or the other but not to both.

These assumptions become more plausible provided:

**Assumption 12:** The molecules investigated are considered planar.

The molecule is thus pictured as consisting of nuclei and  $\sigma$ -electrons which form a molecular core of planar configuration. This core is enveloped by a  $\pi$ -electron cloud above and below the plane. Foresight about some of the properties of the observables to be calculated restricts the type of AO which form the  $\Sigma$  and  $\Pi$  functions.

**Assumption 13:** The  $\chi_\Sigma$  are symmetric and the  $\chi_\Pi$  are antisymmetric with respect to reflection through the plane of the molecule.

In order to carry out the variational procedures outlined above

**Assumption 14:** The  $\Sigma$  wavefunction must be the same for all states of the molecule.

That is, to carry out SCF procedures or to calculate any observable based only on the properties of the  $\pi$  MO requires that the  $\Sigma$  MO contribute the same aspect to all molecular states. This means that  $E_\Sigma$  in Equation 43 is constant and the LCI SCF procedures affect only  $E_\pi$ .

With these restrictions the Hamiltonian has become

$$\hat{H}_\pi(1,2,\dots,n_\pi) = \sum_i^{n_\pi} \hat{h}_{\text{core}}(i) + \frac{1}{2} \sum_{i \neq j}^{n_\pi, n_\pi} \frac{e^2}{|r_i - r_j|} \quad (45)$$

$$\text{where } \hat{h}_{\text{core}}(i) = -\frac{\hbar^2}{2m_i} \nabla_i^2 - \sum_\alpha^K \frac{Z_\alpha e^2}{|R_\alpha - r_i|} + \hat{V}_\Sigma(r_i) \quad (46)$$

The term  $\hat{V}_\Sigma(r_i)$  represents the repulsion on the  $i$ th  $\pi$ -electron due to the average of the  $\sigma$ -electrons. It is still difficult to actually perform calculations due to the form of the Hamiltonian. This operator still causes analytical problems when applied to specific molecules. To overcome this difficulty the Hamiltonian must be molded into a more tractable form. In addition it would be advantageous to build into it some means for overcoming the lack of generality caused by the above restrictions!

Assumption 15: The Goeppert-Mayer-Sklar (GMS) approximation is used in formulating  $\hat{h}_{\text{core}}$ .

This approximation transforms  $\hat{h}_{\text{core}}$  into a form which has correlations based on physical parameters and is outlined as follows. From Equation 46

$$\hat{V}_\Sigma(r_i) = \left\langle \phi_\Sigma(r_1 \dots r_{n_\Sigma}) \left| \sum_{j=1}^{n_\Sigma} \frac{e^2}{|r_i - r_j|} \right| \phi_\Sigma(r_1 \dots r_{n_\Sigma}) \right\rangle = \int \rho_\Sigma(r) \frac{e^2}{|r - r_i|} dr \quad (47)$$

Thus  $V_\Sigma(r_i)$  acts as an electrostatic potential due to the  $\sigma$  electrons.

It is assumed that

$$\rho_{\Sigma}(r) = \sum_{\alpha=1}^K \rho_{\alpha}(r) \quad (48)$$

so

$$\widehat{V}_{\Sigma}(r_i) = \sum_{\alpha}^K \int \rho_{\alpha}(r) \frac{e^2}{|r-r_i|} dr \quad (49)$$

$$\text{and } \widehat{h}_{\text{core}}(i) = -\frac{\hbar^2}{2m_i} \nabla_i^2 + \sum_{\alpha}^K \int [\rho_{\alpha}(r) - Z_{\alpha} \delta(r-R_{\alpha})] \frac{e^2}{|r-r_i|} dr \quad (50)$$

The term in the brackets is essentially related to the point charge of a given nucleus together with its  $\sigma$ -electrons and is given the symbol  $-Z^{\alpha}$ . If  $\rho_{\alpha}^{\circ}(r)$  is due to all electrons ( $\sigma$  and  $\uparrow\downarrow$ ) belonging to atom  $\alpha$  an identity may be stated:

$$\rho_{\alpha}(r) \equiv \rho_{\alpha}^{\circ}(r) - Z^{\alpha} \tau_{\alpha}(r) \quad (51)$$

with the restrictions

$$\left. \begin{aligned} \rho_{\alpha}^{\circ}(r) &= f(|r-R_{\alpha}|) \\ \int \rho_{\alpha}^{\circ}(r) dr &= Z_{\alpha} \\ \int \tau_{\alpha}(r) dr &= 1 \end{aligned} \right\} \quad (52)$$

In general  $\tau_{\alpha}(r)$  is not spherically symmetric.

$$\begin{aligned} \text{Then } \widehat{h}_{\text{core}}(i) &= -\frac{\hbar^2}{2m_i} \nabla_i^2 + \sum_{\alpha}^K \int [\rho_{\alpha}^{\circ}(r) - Z_{\alpha} \delta(r-R_{\alpha})] \frac{e^2}{|r-r_i|} dr \\ &\quad - \sum_{\alpha}^K Z^{\alpha} \int \tau_{\alpha}(r) \frac{e^2}{|r-r_i|} dr \end{aligned} \quad (53)$$

$$= \widehat{T}(i) + \sum_{\alpha}^K \widehat{U}_{\alpha}(r_i) - \sum_{\alpha}^K Z^{\alpha} \widehat{\tau}_{\alpha}(r_i) \quad (54)$$

When this equation is written in terms of the basis AO

$$\langle \chi_p | \widehat{h}_{\text{core}} | \chi_g \rangle = h_{pg} = T_{pg} + \sum_{\alpha}^K U_{r_g}^{\alpha} - \sum_{\alpha}^K Z^{\alpha} \tau_{p\alpha g\alpha} \quad (55)$$

since

$$\left. \begin{aligned} \tau_{\alpha}(r) &= \chi_{\alpha}^2(r) \\ \widehat{\tau}_{\alpha}(r_i) &= \int \chi_{\alpha}^*(r) \frac{e^2}{|r-r_i|} \chi_{\alpha}(r) dr \\ \langle \chi_p(r_i) | \tau_{\alpha}(r_i) | \chi_g(r_i) \rangle &= \langle \chi_p(r_i) \chi_{\alpha}(r) | \frac{e^2}{|r-r_i|} | \chi_g(r_i) \chi_{\alpha}(r) \rangle \equiv \tau_{p\alpha g\alpha} \end{aligned} \right\} \quad (56)$$

It is possible to explicitly include the effects of molecular substituents such as hydroxyl, amino, or methyl groups in Equation 55. However the molecules investigated in this thesis do not contain substituents other than hydrogen so these terms will not be included. The explicit effects of the hydrogens will also be neglected here.

Intuitively it seems plausible that most of the structural features of molecules are due to nearest neighbor interactions between the atoms which constitute the molecule. For this reason

**Assumption 16:** The tight-binding approximation is applied to the Hamiltonian.

Specifically  $h_{pq} \rightarrow h_{pq}^Q$

where  $Q_{pq} = \delta_{pq} + M_{pq}$

and  $M_{pq} \begin{cases} = 1 & \text{when } p \text{ and } q \text{ are nearest neighbors.} \\ = 0 & \text{otherwise.} \end{cases}$

$M_{pq}$  is known as the molecular "topological matrix." With this restriction

$$h_{pq} = \left[ T_{pp} + U_{pp}^p + \sum_{(k)} U_{pp}^k - \sum_{\alpha} z^{\alpha} \sigma_{p-\alpha} \right] \delta_{pq} + \left[ T_{pq} + U_{pq}^p + U_{pq}^q - \sum_{\alpha} z^{\alpha} \sigma_{p-\alpha} \right] M_{pq} \quad (57)$$

where  $k$  refers to indices of atoms directly bonded to the  $p$ -th  $\alpha$ -atom.

The terms  $\sum_{(k)} U_{pq}^k$  are quite negligible compared to  $U_{pq}^p$  and  $U_{pq}^q$ . If a substitution is made

$$\begin{aligned} A_{pp} &= T_{pp} + U_{pp}^p \\ \text{and} \quad A_{pq} &= T_{pq} + U_{pq}^p + U_{pq}^q \end{aligned} \quad (58)$$

$$\text{then } h_{pq} = \left[ A_{pp} + \sum_{(k)} U_{pp}^k - \sum_{\alpha} Z^{\alpha} \sigma_{p\alpha p\alpha} \right] \delta_{pq} + \left[ A_{pq} - \sum_{\alpha} Z^{\alpha} \sigma_{p\alpha q\alpha} \right] M_{pq} \quad (59)$$

The term  $A_{pp}$  is equivalent to the experimentally determined electron affinity of the p-th  $\uparrow$ -atom. The electron affinity in turn is related to the p-th  $\uparrow$ -atom ionization potential and the coulomb repulsion of two electrons on atom p:

$$A_{pp} \longrightarrow -I_p + Z^p \sigma_{pp} \quad (60)$$

where  $Z^p$  is the effective core charge of the p-th  $\uparrow$ -atom. The term  $A_{pq}$  represents an empirical property of the bond between atoms p and q. Following the Hückel theory nomenclature for such a bond property it is called the resonance integral  $\beta_{pq}$ .

Observation of the Hamiltonian, e.g. Equation 27 or 34, indicates there are a large number of electron repulsion integrals to evaluate. However the number and complexity of such evaluation can be considerably reduced by recalling that AO are being used and that the overlap character of the  $\uparrow$ AO should be very small if they lie on different atoms.

Assumption 17: The MO are constructed from AO for which the Zero

Differential Overlap (ZDO) approximation may be used.

That is:

$$\chi_p(r_i) \chi_q(r_i) = 0 \quad \text{for } p \neq q \quad (61)$$

Thus

$$\langle \chi_p(r_i) \chi_q(r_j) | \frac{e^2}{|r_i - r_j|} | \chi_r(r_i) \chi_s(r_j) \rangle = \langle \chi_p(r_i) \chi_q(r_j) | \frac{e^2}{|r_i - r_j|} | \chi_p(r_i) \chi_q(r_j) \rangle \delta_{pr} \delta_{qs} \quad (62)$$

or

$$\sigma_{pqrs} = \sigma_{pq} \delta_{pr} \delta_{qs} \equiv \sigma_{pq}$$

With this approximation

$$h_{pq} = \left[ -I_p + Z^p \sigma_{pp} + \sum_{(k)} U_{pp}^k - \sum_{\alpha} Z^{\alpha} \sigma_{p\alpha} \right] \delta_{pq} + \beta_{pq} \quad (63)$$



The ZDO approximation may also be applied to the  $\uparrow\uparrow$ -electron repulsion terms in the Hamiltonian. To determine what integrals arise in the actual calculations Equation 29 is the basic equation. Its terms are delineated by multiplying on the left by  $\phi_k$  and integrating. In terms of the AO

$$\langle \phi_k | \hat{F} | \phi_i \rangle = \sum_p C_{kp}^* \sum_q C_{iq} \langle \chi_p | \hat{F} | \chi_q \rangle = \sum_p C_{kp}^* \sum_q C_{iq} [\langle \chi_p | \hat{h}_{core} | \chi_q \rangle + \sum_j \{ 2 \langle \chi_p \phi_j | \frac{e^2}{|r_a - r_b|} | \chi_q \phi_j \rangle - \langle \chi_p \phi_j | \frac{e^2}{|r_a - r_b|} | \phi_j \chi_q \rangle \}] = \quad (64)$$

$$\sum_p C_{kp}^* \sum_q C_{iq} [h_{pq} + \sum_j \{ 2 \sum_r C_{jr}^* \sum_s C_{js} (\langle \chi_p \chi_r | \frac{e^2}{|r_a - r_b|} | \chi_q \chi_s \rangle - \frac{1}{2} \langle \chi_p \chi_r | \frac{e^2}{|r_a - r_b|} | \chi_s \chi_q \rangle \} ]$$

If the substitution  $P_{rs} = 2 \sum_j C_{jr}^* C_{js}$  (65)

is made

$$F_{ki} = \sum_{p,q} C_{kp}^* C_{iq} [h_{pq} + \sum_{r,s} P_{rs} (\sigma_{prqs} - \frac{1}{2} \sigma_{prsq})] \quad (66)$$

The term in the brackets is indentially the  $F_{pq}$  stated in Equation 34.

When ZDO approximation is applied there are two cases:

$$\begin{aligned} \text{Case 1: } p=q \quad F_{pp} &= h_{pp} + \sum_{r \neq p}^m P_{rr} \sigma_{prpr} + 1/2 P_{pp} \sigma_{pppp} \\ \text{Case 2: } p \neq q \quad F_{pq} &= h_{pq} - 1/2 P_{pq} \sigma_{pqpq} \end{aligned} \quad (67)$$

The Hamiltonian is now expressed in terms of quantities such as ionization potentials, electron affinities and coulomb integrals which are the properties of atoms and bonds and should be invariant between molecules. These parameters are somewhat amenable to experimental investigation so their values should be physically reasonable. Once they have been determined the Hartree-Fock operator is determined and the MO are generated. These MO are then used to calculate the observables being examined. Since the operator which generated the MO is due

to a particular set of parameters, any observables calculated must be properties of the molecule under the same conditions.

**Assumption 18:** The parameters and calculated observables are evaluated for molecules in an equilibrium geometry configuration.

The nuclei are thus assumed to be in their most probable position for all calculations. A result of this assumption is that the calculated transitions are vertical. This may not correspond to the 0-0 transition.

These are the assumptions and conditions for making the calculations. Due to the impossibility of analytically solving the Schrodinger Equation exactly except in elementary instances, a formalism has been derived from the quantum mechanical apparatus using a successive set of assumptions. This formalism allows the use of semiempirical parameters to generate integrals associated with molecular properties.

With these assumptions the question still remains: Are these calculations valid? The most succinct answer is that they are valid if they work in predicting observables which correlate quite well with experimental facts. This is the crux of any theoretical investigation.

### III. Format for the Calculations

The calculations were performed using the CDC 3600 computer at Michigan State University. They were controlled with a program conceived and written by Petr Hochmann<sup>4</sup>. The program was designed to be as general and flexible as possible. This is achieved by the program's multiswitch character which allows a variety of one-electron effective Hamiltonians, MO, input parameter forms and outputs to be incorporated or formulated. New formulations for the Hamiltonian or parameters can be inserted at will. Only those procedures and forms used in the calculations for the molecules studied here will be presented. Other expressions are included in reference 4, but they do not constitute a complete set. Any user of the program may introduce procedures with a minimum of effort.

For these calculations the set of AO used was restricted to the  $2p\pi$  orbitals of the atoms contributing to the  $\pi$ -system. All molecules for which calculations were performed were planar conjugated organic. Each atom in these molecules contributes at least one  $\pi$ -electron (recall the effects due to hydrogens are neglected). Thus the number of AO ( $m$ ) comprising the molecular  $\pi$ -system is identical with the number of nuclei ( $k$ ) in the molecule so for the previous equations  $m = k$ .

It is also instructive to note from Equation 51 that  $\tau_\alpha(r)$  is functionally the complement of  $\rho_\alpha(r)$  based on a spherical electronic charge distribution for the neutral atom. Since  $\rho_\alpha(r)$  is due to the  $\sum_\alpha$  charge distribution only,  $\tau_\alpha(r)$  is functionally an AO on the  $\alpha$ -th atom.

With these further restrictions Equation 68 becomes

$$F_{pq} = h_{pq} - \frac{1}{2} P_{pq} \tau_{pq} + \delta_{pq} \sum_r^k P_{rr} \tau_{rp} \quad (69)$$

where

$$h_{pq} = \left[ -I_p + z^p \gamma_{pp} + \sum_{(k)}^k U_{pp} - \sum_r^k z^r \gamma_{rp} \right] \delta_{pq} + \beta_{pq} \quad (70)$$

and

$$P_{pq} = 2 \sum_i^{\infty} C_{ip} C_{iq} \quad (71)$$

The terms are defined:

$I_p$  - the  $\pi$ -electron ionization potential for the p-th  $\pi$ -atom in the  $sp^2\pi$  valence state.

$z^p$  - the effective charge of the core of the p-th  $\pi$ -atom.

$\gamma_{pp}$  - the one-center two-electron repulsion integral on the p-th  $\pi$ -atom.

$\gamma_{pq}$  - the two-center two-electron repulsion integral between  $\pi$ -AO on the p-th and q-th  $\pi$ -atoms.

$U_{pp}^{(k)}$  - the two-center penetration integral between the  $\pi$ -AO on the p-th  $\pi$ -atom and the spherical charge distribution on the k-th  $\pi$ -atom whose total charge is electrically neutral.

$\sum_{(k)}$  - denotes a summation over indices of the  $\pi$ -atoms bonded directly to the p-th  $\pi$ -atom.

$\beta_{pq}$  - the resonance integral between the p-th and the q-th  $\pi$ -atoms.

$P_{pq}$  - for  $p = q$  : the  $\pi$ -electron charge density on the p-th  $\pi$ -atom.

for  $p \neq q$  : the Coulson bond order for the bond between the p-th and the q-th  $\pi$ -atoms.

The calculations were initiated by ascertaining the types of atoms comprising each molecule and their relative positions. Three atomic types were used in these calculations:

- 1)  $sp^2\pi$  hybridized C which contributes one electron to the  $\pi$ -system.
- 2)  $sp^2\pi$  hybridized N which contributes one electron to the  $\pi$ -system (pyridinic type).

- 3)  $sp^2\pi$  hybridized N which contributes two electrons to the  $\pi$ -system (pyrrolic type).

From this topological arrangement a Hückel type calculation was carried out to generate an initial set of MO to be used in the subsequent Hartree-Fock SCF calculations. The number of MO included in a given set was regulated by the number of  $\pi$ -AO contributed by the given molecule. Examination of the Secular Determinant (Equation 41) indicates that the number of MO must be identical with the number of AO comprising the  $\pi$ -electron system,  $i = k$ . The Hartree-Fock calculations were taken over these  $i$  MO,  $\nu$  of which formed a closed shell of  $N = 2\nu$  electrons. By the Aufbau Principle these  $\nu$  MO were the ones of lowest energy leaving  $i$  minus  $\nu$  "virtual" MO. After self-consistency was achieved the following items were calculated:

- Molecular ionization potentials.
- Molecular electron affinities.
- Ground state  $\pi$ -electron charge densities and bond orders.
- Bond lengths in the molecular ground state.
- Ground state molecular permanent dipole moment magnitude intensity and orientation.

A configuration interaction calculation was then carried out using monoexcited configurations. These configurations were formed by promoting an electron from one of the  $\nu$  ground state orbitals to one of the  $i - \nu$  "virtual" orbitals. The following considerations were used in performing the configuration interaction calculations. The MO are arranged in the order  $1, \dots, \nu, \dots, i$ . Specific orbitals are labeled:

$$\begin{array}{ll}
 \text{(filled)} & \text{(unfilled)} \\
 1 \leq I \leq \nu, & \nu < J \leq i \\
 1 \leq K \leq \nu, & \nu < L \leq i
 \end{array}
 \left. \vphantom{\begin{array}{ll} 1 \leq I \leq \nu, \\ 1 \leq K \leq \nu, \end{array}} \right\} \quad (72)$$

To clarify the development of configurations the Slater Determinant, Equation 4, is rewritten:

$$\Psi = \hat{A} \prod_{i=1}^k \phi_i \quad (73)$$

where  $\hat{A}$  is the antisymmetrization operator given by

$$\hat{A} = \frac{1}{\sqrt{k!}} \sum_p (-1)^p \hat{P} \quad (74)$$

For the ground state the Slater Determinant becomes

$$\Psi_0 = \hat{A} \prod_{i=1}^{\nu} \phi_i = |(0)\rangle \quad (75)$$

Upon excitation an electron is annihilated from one of the ground state orbitals and an electron is created in one of the heretofore virtual orbitals. This leads to expressions of the type

$$|(I, J)\rangle = \hat{A} \prod_{i=1}^{I-1} \phi_i \phi_J \prod_{i=I+1}^{\nu} \phi_i \quad (76)$$

However each MO is doubly occupied in the ground state. Since either electron may be excited, excitation is given by the expression

$$\frac{1}{\sqrt{2}} |(2I, 2J)\rangle + \frac{1}{\sqrt{2}} |(2I-1, 2J-1)\rangle = |1, (I, J)\rangle \quad (77)$$

for the singlet excited state and

$$\frac{1}{\sqrt{2}} |(2I, 2J)\rangle - \frac{1}{\sqrt{2}} |(2I-1, 2J-1)\rangle = |3, (I, J)\rangle \quad (78)$$

for the triplet excited state.  $(2I, 2J)$  may be considered as denoting spin  $\alpha$  and  $(2I-1, 2J-1)$  may be considered as denoting spin  $\beta$ . The right hand member of these equations is expressed in the codetor notation (the spin projection quantum number has been specifically omitted in these formulations). In codetor notation the molecular ground state is given

by  $|1, (0)\rangle$  (for an explanation of codetors see reference 3, p. 204).

The matrix used in performing a configuration interaction analysis is composed of elements with the form:

$$\langle 1, (0) | \hat{H} | 1, (0) \rangle \equiv H_0 = \frac{1}{2} \sum_{p,q}^{R,R} P_{pq} (F_{pq} + h_{pq}) \quad (79)$$

$$\langle 1, (0) | \hat{H} | S, (I, J) \rangle = \sqrt{2} [I | J] \delta_{1s} \quad (80)$$

$$\begin{aligned} \langle S, (I, J) | \hat{H} | S', (K, L) \rangle = & \{ [J | L] \delta_{IK} - [I | K] \delta_{JL} - [IJ || KL] \\ & + (3-S)[IK || JL] + H_0 \delta_{IK} \delta_{JL} \} \delta_{SS'} \end{aligned} \quad (81)$$

where

$$\left. \begin{aligned} [J | L] &= \sum_{p,q}^{R,R} C_{Jp}^* F_{pq} C_{Lq} \\ [IJ || KL] &= \sum_{p,q}^{R,R} C_{Ip}^* C_{Jq}^* \gamma_{pq} C_{Kp} C_{Lq} \end{aligned} \right\} \quad (82)$$

After configuration interaction each  $\pi$ -electron wave function for singlet and triplet states is

$$|\Theta_\alpha^S\rangle = A_{(0)}^{1,\alpha} |1, (0)\rangle \delta_{1s} + \sum_{(I,J)} A_{(I,J)}^{S,\alpha} |S, (I, J)\rangle \quad (83)$$

where

$S$  is the multiplicity of the state.

$\alpha$  is the sequence number for the state.

$A_{(0)}^{1,\alpha}$  and  $A_{(I,J)}^{S,\alpha}$  are the configuration interaction coefficients.

$\sum_{(I,J)}$  denotes summation over all monoexcited configurations included in the configuration interaction.

After this limited configuration interaction analysis the following items were calculated:

- f) Ground to singlet excited state transition energies, oscillator strengths and transition moment magnitudes and

orientations.

- g) Ground to triplet excited state transition energies.
- h) Lowest triplet to higher triplet excited state transition energies, oscillator strengths and transition moment magnitudes and orientations.
- i) Excited state  $\pi$ -electron charge densities and bond orders.
- j) Excited state interatomic bond lengths.
- k) Excited state molecular permanent dipole moment magnitudes and orientation.

Formulas in the codetor basis for the transition momenta are given in Reference 4. The excited state permanent dipole moments, charge densities, and bond lengths were calculated from first and second order density matrices. These matrices are also formulated in Reference 4 in the codetor basis.

In order to have confidence in the validity of these calculations it was felt that as many observables should be calculated for as many molecules with as little parametrization as possible. These observables could then be checked against the corresponding experimental values. If the calculations were of general utility there should be fairly good agreement between these quantities. The procedure was to choose a small set of "test" molecules, vary the parameters utilized in Equations 69 and 70 until the calculated observables agreed as well as possible with the known experimental values and then to use these parameters in calculations for a large group of similar molecules. This variation of parameters is called "parameter optimization". If the calculations on the large group evoked any major discrepancies the parameters were reoptimized until good agreement was reached.



Optimization was achieved in three steps. It was first performed for the hydrocarbons by Hochmann, et al.<sup>5</sup> The next step was to optimize the calculations for molecules containing pyridinic type nitrogens. The test molecules for this series were pyridine, pyrazine, and 1,5 naphthyridine. Finally optimization was carried out for molecules containing pyrrolic type nitrogens using the test molecules of pyrrole, carbazole, and imidazole. The test molecules were chosen on the basis of the amount of experimental data available, the range a particular quantity had from one molecule to another, and the number of different experimental quantities available for a particular molecule. The optimized parameters were then used for calculations of the indoles. The scheme was to use the parameters optimized in previous procedures to perform calculations on the molecules of interest here. Hopefully the results of these latter calculations would not reflect any bias in parameter optimization.

Unfortunately it is evident that there is not much experimental data available for nitrogen heterocyclics to use for optimization-especially when compared with the data available for hydrocarbons. Thus there were fewer optimization checks which could be made for the Nitrogen heterocyclics. When optimization had proceeded to the point that parameter adjustments adversely affected one observable more than another the arbitrary choice was made to optimize the singlet transition energies as well as possible. The other observables were optimized but their optimization was of secondary importance. Although technically feasible, optimization was not attempted for molecules containing nearest neighbor, i.e. contiguous nitrogens. Lack of time was the principal reason for this omission.

The final values and equations used in evaluating the parameters are listed in Table 1. It must be emphasized that this set of parameters may be superseded at any time by an improved set which uses a different group of constants or, more probably, new formulations. The efficacy of this parametrization is indicated in Table 2 which compares the experimental and calculated results for the nitrogen heterocyclic test molecules. Overall the calculations vs. experimental data correlation is remarkably good considering the breadth of comparisons being attempted. This gives confidence for proceeding to perform correlations and predictions of the indoles. However any calculated results must be tempered with caution since there is no absolute guarantee for their accuracy.

Table 1. Semiempirical Parameters,

Note:  $N_I$  denotes Pyridinic type Nitrogen  
 $N_{II}$  denotes Pyrrolic type Nitrogen

Type	Atom(s)	Value	Units
$I_p$	C	9.84	eV
	$N_I$	12.57	
	$N_{II}$	20.40	
$Z^p$	C	1	e
	$N_I$	1	
	$N_{II}$	2	
$\sigma_{pp}$	C	11.97	eV
	$N_I$	15.44	
	$N_{II}$	15.44	
$\beta_{pq}$	C-C	$-2.42(2.76068-1.26033 R_{CC})$ $R_{CC}=1.517-0.180 P_{CC}$	eV Å
	C- $N_I$	$-2.40(2.44950-1.08333 R_{CN_I})$ $R_{CN_I}=1.458-0.180 P_{CN_I}$	
	C- $N_{II}$	$-2.31(2.50597-1.12554 R_{CN_{II}})$ $R_{CN_{II}}=1.458-0.180 P_{CN_{II}}$	

Note:  $N_I - N_{II}$  was not parameterized since they aren't nearest neighbors.

Table 1 (cont'd.)

Type	Atom(s)	Value	Units
$\beta_{pq}$	C-C	$6.91-3.99(R_{CC}-1.397)$ for $R_{CC} \leq 2.0$ $\frac{1}{2}e^2/(R_{CC}^2+2.00070) + 1/(R_{CC}+0.0)$ for $R_{CC} > 2.0$	eV R in Å
	C-N <sub>I</sub>	$7.51-3.99(R_{CN_I}-1.338)$ for $R_{CN_I} \leq 2.0$ $\frac{1}{2}e^2/(R_{CN_I}^2+1.68114) + 1/(R_{CN_I}^2+0.01389)$ for $R_{CN_I} > 2.0$	
	C-N <sub>II</sub>	$5.69-3.99(R_{CN_{II}}-1.338)$ for $R_{CN_{II}} \leq 2.0$ $\frac{1}{2}e^2/(R_{CN_{II}}^2+1.68114) + 1/(R_{CN_{II}}^2+0.01389)$ for $R_{CN_{II}} > 2.0$	
	N <sub>I</sub> -N <sub>I</sub>	$\frac{1}{2}e^2/(R_{N_I N_I}^2+1.17872) + 1/(R_{N_I N_I}^2+0.0)$	
	N <sub>I</sub> -N <sub>II</sub>	$\frac{1}{2}e^2/(R_{N_I N_{II}}^2+1.17872) + 1/(R_{N_I N_{II}}^2+0.0)$	
	N <sub>II</sub> -N <sub>II</sub>	$\frac{1}{2}e^2/(R_{N_{II} N_{II}}^2+1.17872) + 1/(R_{N_{II} N_{II}}^2+0.0)$	
Note: N-N must be $>2.0$ Å apart since they can only be nonnearest neighbors. $R_{pq}$ take the corresponding values shown for $R_{pq}$ in $\beta_{pq}$ if they are nearest neighbors, otherwise they are the geometrical $R_{pq}$ .			
$U_{pq}^{(k)}$	C-C	$0.07(-183.005+131.714 R_{CC})$ $R_{CC}=1.517-0.180 P_{CC}$	eV Å
	C-N <sub>I</sub>	$0.03(-248.760+186.667 R_{CN_I})$ $R_{CN_I}=1.458-0.180 P_{CN_I}$	
	C-N <sub>II</sub>	$0.03(-248.760+186.667 R_{CN_{II}})$ $R_{CN_{II}}=1.458-0.180 P_{CN_{II}}$	
	N <sub>I</sub> -C	$0.14(-52.520+40 R_{N_I C})$ $R_{N_I C}=1.458-0.180 P_{N_I C}$	
	N <sub>II</sub> -C	$0.14(-52.520+40 R_{N_{II} C})$ $R_{N_{II} C}=1.458-0.180 P_{N_{II} C}$	

Table 2. Comparison of Experimental and Calculated Values for Test Molecules.

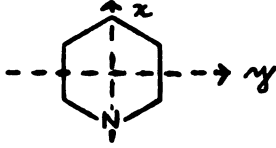
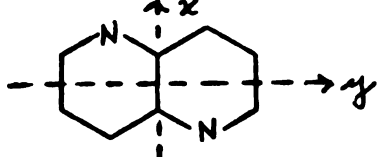
Pyridine			
			
Quantity	Units	Experimental Value	Calc. Value
Bond length C-C	Å	1.39, 1.40	1.40
" " C-N		1.34	1.34
Ionization Potential (1)	eV	9.23, 9.26	9.28
" " (2)		9.31, 9.28	
" " (2)		9.51 ?	9.62
Transition Energy (1)	Å	2511, 2516	2562
" " (2)		1980, 1976	1967
" " (3)		1754, 1782	1795
Transition Angle (1)	degrees from	90	90
" " (2)	x axis	0	0
" " (3)		90	90
Oscillator Strength (1)		0.032	0.009
" " (2)		0.122	0.048
" " (3)		0.660	1.111
1,5 - Naphthyridine			
			
Transition Energy (1)	Å	3080	3063
" " (2)		2571	2500
" " (3)		2060	2017
Oscillator Strength (1)		0.13	0.063
" " (2)		0.094	0.154
" " (3)		1.08	2.026

Table 2 (cont'd.)

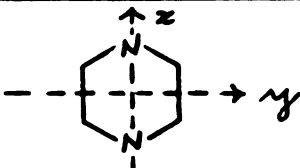
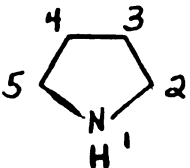
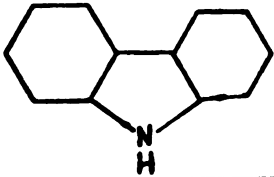
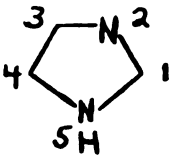
Pyrazine 			
Quantity	Units	Experimental Value	Calc. Value
Bond length C-C	A	1.378	1.399
" " C-N		1.334	1.337
Ionization Potential (1)	eV	9.36, 9.27, 9.29	9.32
" " (2)		9.51 ?, 10.11	10.03
Transition Energy (1)	A	2601, 2610, 2580, 2600	2580
" " (2)		1943, 1965, 1966, 1970	1975
" " (3)		1811, 1846	1794
Transition Angle (1)	degrees from	90	90
" " (2)	x axis	0	0
" " (3)		90	90
Oscillator Strength (1)		0.08	0.036
" " (2)		0.119	0.104
" " (3)		-	1.018
Pyrrole 			
Bond Length 1-2	A	1.42, 1.383	1.354
" " 2-3		1.35, 1.371	1.388
" " 3-4		1.44, 1.429	1.408
Ionization Potential (1)	eV	8.20	7.75
Transition Energy (1)	A	2075, 2110, 2113, 2360	2078
" " (2)		1829	1984 weak
" " (3)		1725, 1747, 1717	1791
" " (4)			1734

Table 2 (Cont'd.)

Carbazole			
			
Quantity	Units	Experimental Value	Calc. Value
Transition Energy (1)	A	3397, 3367, 3258,	3357
" " (2)		3259, 3306, 3368	
" " (3)		2933, 2938, 2931,	2914
" " (3)		2890, 2907, 2912	
Oscillator Strength (1)		2550, 2572	2729
" " (2)		0.04	0.07
" " (3)		0.16	0.13
" " (3)		0.25	0.18
Imidazole			
			
Bond Length 1-2	A	1.33	1.33
" " 2-3		1.38	1.35
" " 3-4		1.36	1.39
" " 4-5		1.37	1.35
" " 5-1		1.35	1.35
Transition Energy (1)	A	2065	2082

Notes: 1) All transitions and oscillator strengths are of the singlet type.

2) When more than one experimental value is listed, all values have been reported in the literature.

3) Numbers in parentheses denote the sequence number of the observable ordered from lower to higher energy.

## CHAPTER III

### EXPERIMENTAL PROCEDURES

Although there have been a variety of experimental investigations made of the indoles there still remain a large amount of data to be amassed. Advances in experimental techniques allow investigations of hitherto unstudied properties as well as duplication of prior studies made under less stringent conditions. In this investigation an assault was made on the mountain of untapped data. Since indole and to a lesser extent purine have been most extensively studied. Our experimental investigations were concentrated primarily on the aza-indoles and in particular benzimidazole. In the following paragraphs are stated the apparatus, techniques, and materials utilized. The results of these experimental ventures are incorporated in the appropriate discussion section of each molecules's spectral properties.

#### I. Vapor Absorption Spectra.

All vapor absorption spectra were run on a Cary 15. Wavelength calibration was achieved by observing the position of the various  $H_g$  emission lines from a low pressure mercury arc. These lines were recorded at the slowest scan speed and most expanded wavelength scale ( $10 \text{ \AA}/17 \text{ mm}$ ) available. All vapor absorption spectra obtained for the purpose of determining absorption peak positions were recorded under identical conditions as the mercury emission lines. Wavelength corrections based on these lines were then applied to the absorption spectra. Wavelengths to five significant figures were read on the expanded wavelength scale.



The spectra were taken using a modified 10 cm absorption cell with quartz windows. The modification consisted of attaching a vacuum stopcock to the only opening of the absorption cell. A ball joint fitting was installed on the exhaust end of the stopcock for attachment to a vacuum line or to a second vacuum stopcock which in turn was attached to a vacuum line. The modified cell was wrapped with nichrome wire which was secured with silicone cement. The wire was also wound around the inlet to the cell and extended to the stopcock itself. The ends of the nichrome wire were attached to a Variac. When spectra were to be obtained a few milligrams of the molecule to be studied were introduced directly into the cell. A vacuum of about  $3 \times 10^{-6}$  Torr was obtained in the vacuum line and the stopcock closed. The Variac was slowly turned up until a spectrum could be obtained with most peaks occurring at 2/3 full scale on the normal OD scale setting. The nichrome wire was wrapped such that there were more turns at the ends than in the center of the cell barrel. This insured that more heat was available at the quartz windows which retarded crystallization of the sample on the windows. No fogging, crystallization or clouding of the windows was ever noted during the course of these experiments. All vapor absorption spectra were taken with ambient air in the reference compartment. The instrument sensitivity was increased as much as possible consonant with a tolerable signal-to-noise ratio. This allowed a very narrow split width to be used (0.01 mm or less) which in turn increased the spectral resolution as much as possible. With this setup it was possible to resolve spectral features lying  $3 \text{ cm}^{-1}$  from each other at  $35000 \text{ cm}^{-1}$ .

All molecules for which vapor absorption spectra were run were also subjected to an investigation of the temperature-dependent behavior of

spectral features. This was accomplished by placing a few milligrams of the molecule under investigation in a reservoir sidearm off the exhaust side of the cell stopcock, evacuating this sidearm, opening the cell stopcock to evacuate the cell to  $3 \times 10^{-6}$  Torr, closing the stopcock closest the vacuum line, allowing the material to equilibrate for a few minutes at room temperature and then closing the cell stopcock. Depending on the vapor pressure of the molecule under investigation, there was supposedly a low but unknown concentration of molecules in the vapor phase trapped in the absorption cell. Absorption spectra were taken at a successive series of temperatures as controlled by the Variac. Temperature equilibration was attained at each Variac setting before the spectrum was run. The first spectrum in a temperature series was run when the first spectral features appeared using the expanded OD scale. Spectra were then recorded at successively higher temperatures with the final run usually taken at a temperature of about 150°C.

## II. Solution Absorption Spectra.

The solution absorption spectra were also run with the Cary 15. In all cases 1 cm pathlength cells were used and the reference cell always contained the solvent alone. However when low temperature spectra were recorded the reference was the solvent at room temperature.

## III. Emission Spectra

All fluorescence and phosphorescence spectra were obtained with the apparatus illustrated in Figure 3. A 1000 W xenon high pressure lamp was used as the excitation light source.

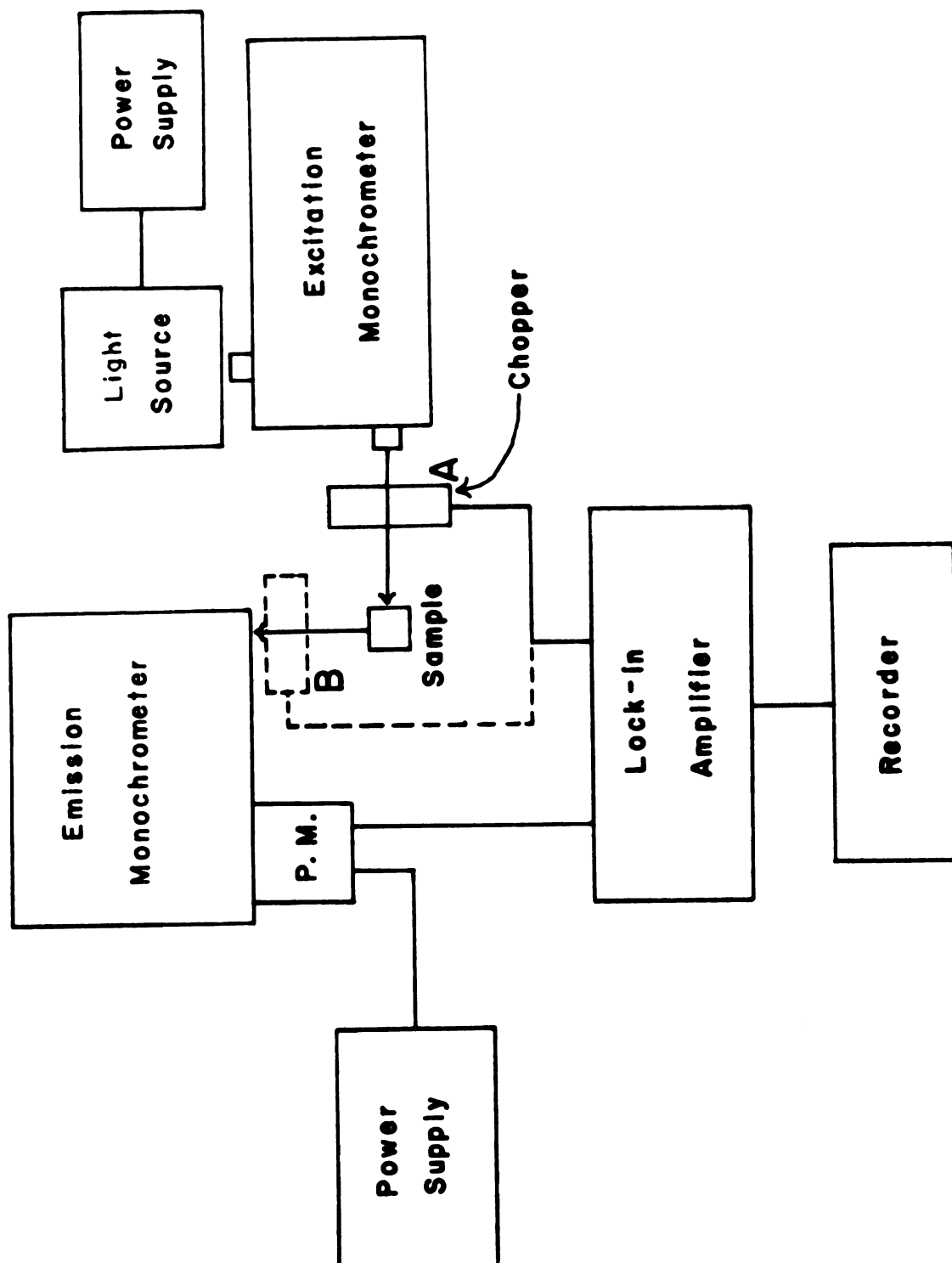


Figure 3. Luminescence Apparatus.

The lamp's voltage was generated by a Christie power supply. Excitation wavelengths were selected by a B&L 10 cm grating blazed at 3000 Å in a B&L 500 mm monochrometer. UV bandpass filters were often used to eliminate any stray light which was passed by the excitation monochrometer. The excitation illumination was focused on the sample whose emission was detected at a right angle relative to excitation. The emission monochrometer was a Spex 1700-II which utilized a 10 cm B&L grating blazed at 5000 Å. The emission spectrum was detected by an EMI 9558QB photomultiplier tube. The tube's high voltage was maintained by a Fluke 412B power supply which was normally operated at 1100 V. Signals from the detected emission were fed to a PAR HR-8 Lock-in Amplifier whose reference was provided by a light chopper. This chopper was located at position A when fluorescence alone was being studied or at position B when both fluorescence and phosphorescence were to be analyzed. Finally the amplified emission signal was displayed on a Bristol's 12 in strip-chart recorder. All spectra reported here are uncorrected for source, monochrometer, or photomultiplier tube response variation with wavelength.

Some of the solution samples were degassed prior to their use in luminescence studies. This procedure consisted of attaching the sample tube together with a closed stopcock to the vacuum line, freezing the tube with liquid nitrogen, opening the stopcock to evacuate the tube above the frozen sample to a pressure of about  $3 \times 10^{-6}$  Torr, closing the stopcock, allowing the sample to thaw, refreezing, evacuating the tube and continuing this freeze-thaw cycling until the vacuum line ionization gauge did not quiver when the stopcock was opened after a freeze. The tube was then sealed off and used in the experiment.

#### IV. Solvents

Following is a list of the solvents used in this study and the method of purification for each.

1. Water. Only doubly-distilled water was used.
2. Ethanol. 200 proof ethanol was placed in a flask and distilled through a 1 m vacuum jacket column. The distillation rate was adjusted such that a very slow rate (about 5 drops per minute) was maintained. Distillation continued until the benzene-alcohol azeotrope was no longer present as determined by an absorption spectrum of the distilled alcohol in a 10 cm cell. That is, the characteristic benzene UV absorption spectrum was no longer apparent. Ethanol was then distilled and used as needed.
3. Ethyl ether. Commercial anhydrous ethyl ether was refluxed over sodium ribbon. The ether was distilled through a 1 m column and used as needed.
4. 3-methyl pentane. A modified version of the purification method of Potts<sup>6</sup> was used. Phillips Pure Grade 3-methylpentane (3MP) was shaken for 30 minutes with a 50:50 mixture of concentrated sulfuric acid and concentrated nitric acid. It was then shaken 3 times for 30 minutes each with concentrated sulfuric acid. This was followed with several shakings using sodium carbonate solutions until the CO<sub>2</sub> production ceased. The 3MP was then shaken several times with water until the water remained clear compared to the initial yellow color it attained with the first shaking. After storing the 3MP overnight over anhydrous calcium sulfate it was placed in a flask and sodium ribbon was added. It was refluxed through a vacuum jacketed 1 m column and distilled for use as needed. Passing the distillate through a 1 m column of activated

Silica Gel did not alter its absorption characteristics so this step was not required in the purification process.

V. Experimentally Studied Molecules.

The means of purification is described below for each molecule. Any changes in the UV absorption spectra after a purification step was cause to perform another step.

1. Indole. - purchased from Aldrich was recrystallized once from an alcohol-water mixture and subsequently recrystallized twice from petroleum ether. The resultant compound formed white shimmering plates.
2. 7-azaindole. - purchased from K & K Chemical Co. was recrystallized twice from cyclohexane and formed white blocky crystals.
3. Benzimidazole. - was purchased from Aldrich and recrystallized three times from hot water. It was then vacuum sublimed slowly for two days. The material which had sublimed to the cold finger was then analyzed by mass spectrometry. No heavier compounds were detected and all lower molecular weight peaks could be accounted for by benzimidazole subgroups. The purified material was white and formed needlelike crystals when recrystallized from water.
4. 4-azabenzimidazole. - purchased from Aldrich was dissolved in ethanol in an Erlenmeyer flask. This solution was placed on a hot plate and the ethanol was allowed to boil off. Further heating forced sublimation of 4-azabenzimidazole onto the side of the flask leaving a dark brown residue on the bottom. The sublimate was carefully scraped from the side and the process was repeated three times. The resultant product formed very long white needles.
5. Indazole. - purchased from Aldrich was recrystallized three times from water. The product formed white plates.

6. Benzotriazole. - purchased from Matheson Coleman & Bell was recrystallized three times from water with the resultant product forming long white needles.
7. Purine. - purchased from Aldrich was not subjected to any further purification procedures.

## CHAPTER IV

### ANALYSIS OF SPECTRAL DATA FOR EACH MOLECULE

This chapter will be devoted to a discussion of the theoretical and experimental UV spectral data available for indole, the azaindoles and purine. Theoretical and experimental results performed by the author will be incorporated in this discussion. These data will be correlated to provide a unified picture of how the changes occurring in the electronic structure are related to spectral features. The perturbing influence of environmental factors are powerful probes of these structures so much use will be made of them. Each molecule will be discussed in turn with data correlation being limited to just that molecule. Finally general predictions of spectral occurrences under heretofore unstudied conditions will also be made based on the analysis of the available data. The overall aim is to accumulate enough experience to make as valid statements as possible about the electronic structures of these molecules.

#### INDOLE

##### I. Vapor Absorption Spectra.

The vapor absorption spectrum of indole has been obtained by Hollas<sup>7</sup> and by El-Bayoumi, et. al.<sup>8</sup> Hollas assigns the  ${}^1L_b$  0-0 transition at  $35233.2\text{ cm}^{-1}$  while El-Bayoumi, et. al. assign it at  $35263\text{ cm}^{-1}$ . Our observations place it at  $35261\text{ cm}^{-1}$ . Since Hollas' experimental conditions were more exacting than ours we will assign the  ${}^1L_b$  0-0 transition at  $35233.2\text{ cm}^{-1}$ . Indeed, when we make this correction in our data we can reproduce most of Hollas' data although we also see structural features at higher and lower energies than he reports.



The lower energy features may be attributed to "hot bands" since we obtained our data at higher temperatures than Hollas did. Observation of the vapor spectra (Figure 4) indicates a region of absorption which is rich in sharp vibrational structure (the long  $\lambda$  region). This region seems to be superposed on a broad band absorption which has diffuse character. Its maximum occurs at a shorter  $\lambda$  than that of the structured absorption. If one invokes knowledge about the absorption spectrum of naphthalene which is isoelectronic with indole and uses the Platt notation<sup>9</sup> for absorption band monomenclature, it appears that there are two absorption bands. The  ${}^1L_b \leftarrow {}^1A$  band has sharp vibrational structure while the  ${}^1L_a \leftarrow {}^1A$  is broad and has diffuse structure.

Although Hollas did not mention the  ${}^1L_a \leftarrow {}^1A$  transition, El-Bayoumi, et. al. assigned the  ${}^1L_a$  0-0 at  $36000\text{ cm}^{-1}$  in the vapor by observing the fluorescence and assuming a mirror image relationship between fluorescence and absorption. That is, one observes room temperature fluorescence in solution and locates its 0-0 position relative to its maximum. The assumptions were made that this emission is from the  ${}^1L_a$  state and that the separation of maximum and 0-0 are the same in absorption as it is in fluorescence in solution. In this connection Konev<sup>10a</sup> did a similar fluorescence-absorption analysis in cyclohexane at  $-196^\circ\text{C}$ . He determined the  ${}^1L_b$  0-0 to be at  $34,820\text{ cm}^{-1}$  and the  ${}^1L_a$  0-0 at  $34,800\text{ cm}^{-1}$ . His method of analysis consisted of finding matching peaks in absorption and fluorescence spectra, assigning these to the  ${}^1L_b$  or  ${}^1L_a$  transitions, and concluding that the 0-0 transition is midway between these peaks. It should be pointed out that El-Bayoumi, et. al. assign the  ${}^1L_a$  0-0 transition energetically above the  ${}^1L_b$  0-0 transition while Konev reverses their order but places them such that they almost coincide.

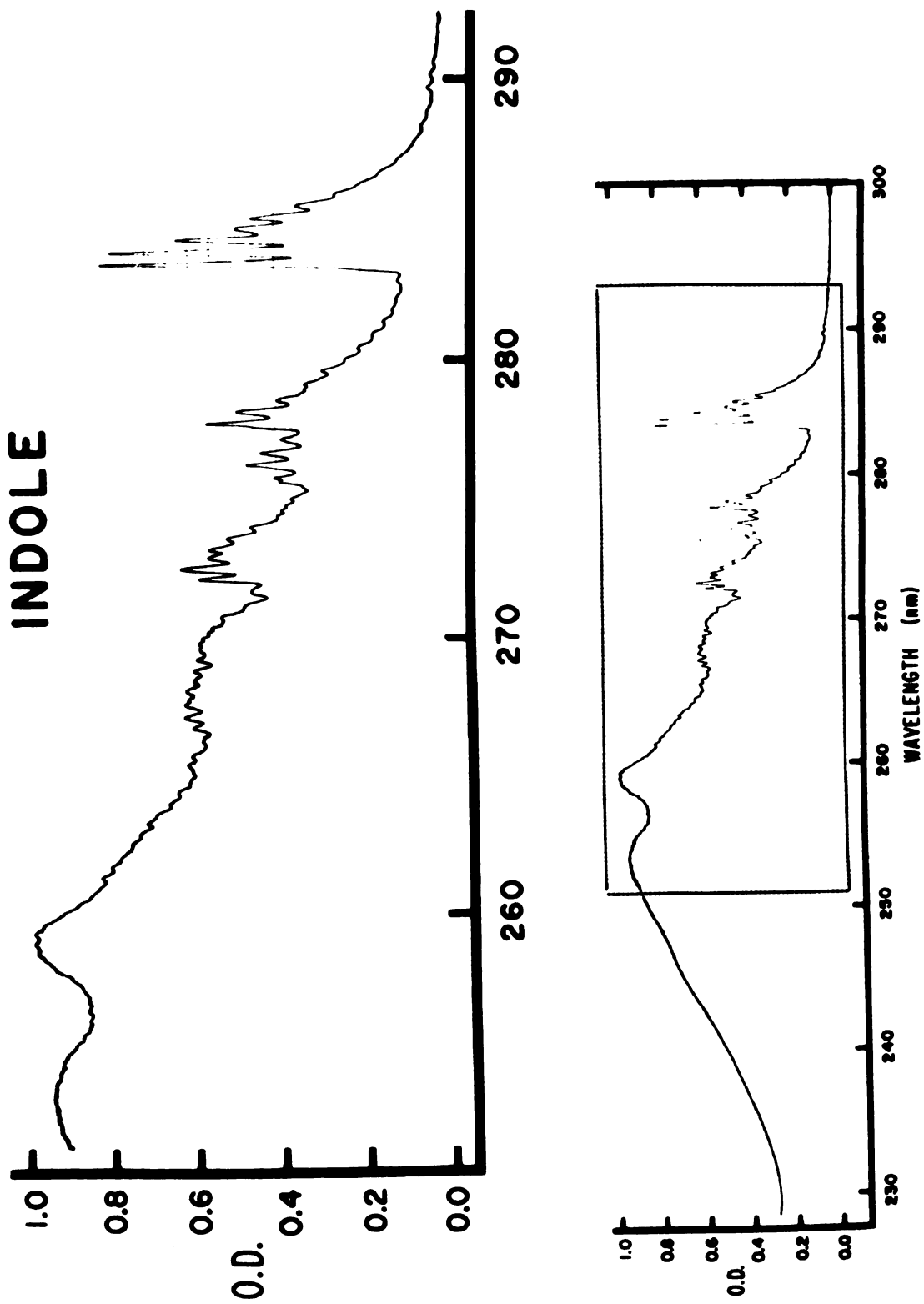


Figure 4. Indole Vapor Absorption Spectrum.

These  $^1L_a$  0-0 assignments should be considered as quite tenuous. There is no guarantee that the vibrational contributions to the absorption and emission transitions will be the same, i.e. the expressions for the absorption and emission moments may not contain the same functional vibronic character. This is especially true since these analyses were taken from solution data and solvent-solute interactions are evident but not accounted for in any specific manner. In addition it appears likely that these transitions are not from single electronic states. The discussion in the Fluorescence section for indole will amplify this assertion. Again solvents may differentially perturb one state versus another and attempts at correlating absorption and emission spectra may be hazardous.

An analysis of the vibrational structure of this vapor spectrum is difficult to carry out. A normal coordinate analysis has not been performed and appears to be quite formidable since this molecule (as well as all others included in this study) exhibits only planar symmetry. The overlap of two distinct electronic transitions also complicates such an analysis. Both transitions contain vibrational structure which carries over to the neighboring transition thus forming a complex vibrational pattern. However, visual clues such as groups of sharp vibrational peaks offer suggestions for the assignment of vibronic progressions or sequences. If one assumes the  $^1L_b$  0-0 transition (2834 Å<sup>•</sup> on Figure 4) as the beginning of a sequence, another sequence apparently begins at 2777 Å<sup>•</sup> or about 725 cm<sup>-1</sup> above the first sequence. Using this 725 cm<sup>-1</sup> vibrational energy as a fundamental and successively looking to the blue by this amount one can observe further sequences beginning at 2722, 2668, 2618, 2570 and 2522 Å<sup>•</sup>. Hollas also found this

sequence pattern and his analysis indicated this energy was most probably attributable to a benzene ring vibration. In addition one may observe the two diffuse peaks at 2534 and 2590 Å which presumably belong to the  ${}^1L_a$  transition. The energy separation for these peaks is about  $875\text{ cm}^{-1}$ . Moving to the red by successive energy increments of this amount one would place vibrations of the  ${}^1L_a$  of the transition at 2648, 2711, 2778, and possibly 2850. The spectrum of Figure 4 indicates this is to be a plausible assignment. In addition another vibrational member of this transition at 2462 Å is evident and is  $875\text{ cm}^{-1}$  to the blue of the broad peak at 2534 Å. Thus these assignments are consistent. A consequence of this analysis is the indication that one member of the  ${}^1L_a$  transition (at 2850 Å) lies beneath the  ${}^1L_b$  0-0 transition (2834 Å) both energetically and in intensity.

To further investigate this spectrum it was decided that a "hot band" analysis should be performed; that is, a study of the relative vibrational peak heights as a function of temperature. The results are shown in Figure 5 and are quite surprising. The most striking fact is the growth of the  ${}^1L_a$  absorption relative to the  ${}^1L_b$  absorption as the temperature is increased. To our knowledge this phenomenon has not been reported before. It cannot be explained simply on the basis of a change in the vapor-solid equilibrium since any change in this equilibrium should result in similar alterations for both transitions according to Beer's Law. It is obvious that the  ${}^1L_a$  transition is becoming more allowed as the higher vibrational levels of the ground state become more populated. A plausible explanation of this phenomenon is that the  ${}^1L_a \leftarrow {}^1A$  transition "borrows" its intensity from another electronic state via vibronic coupling. The state from which it steals intensity is

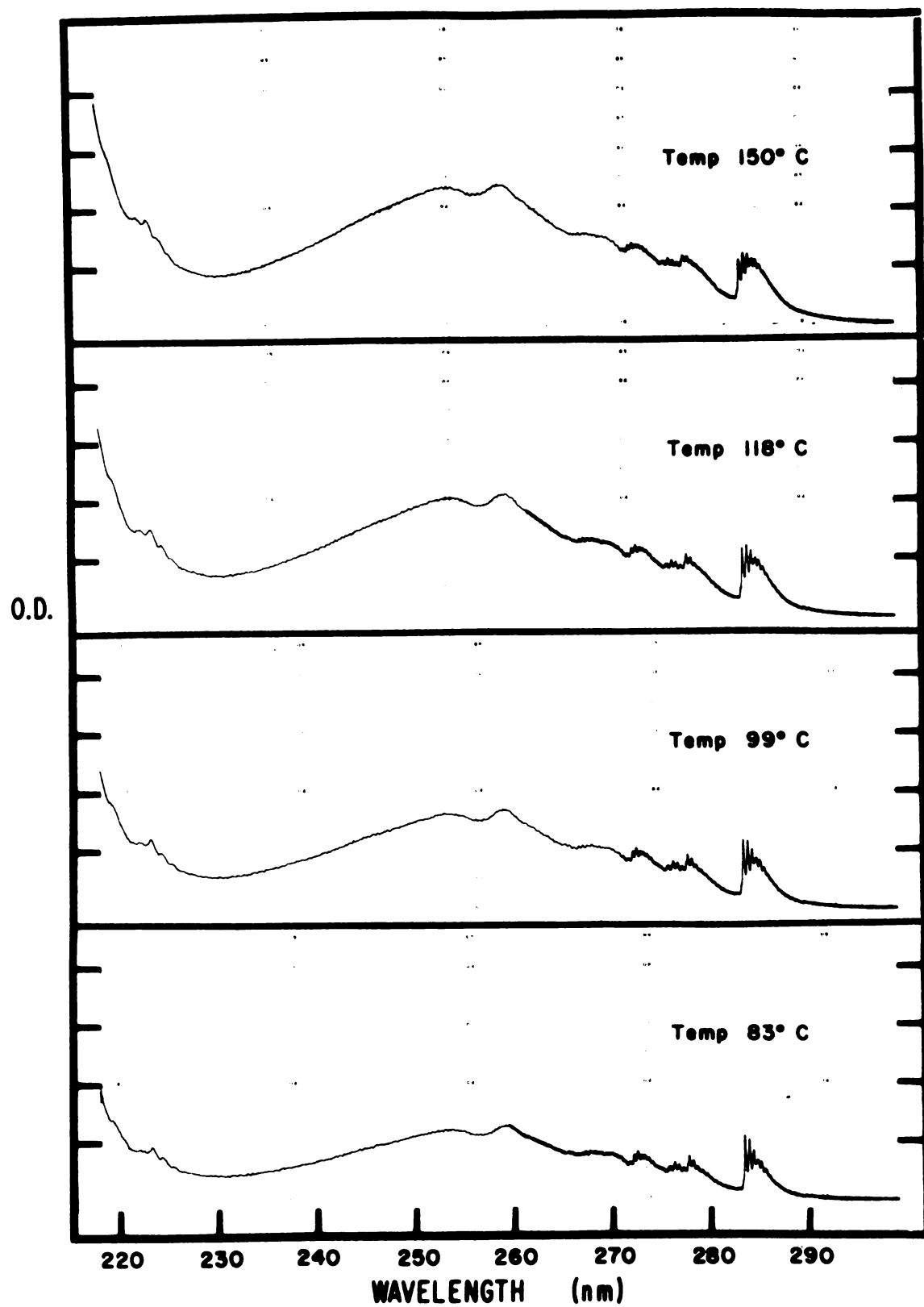


Figure 5. Indole Vapor Absorption Spectra as a Function of Temperature.

apparently at a higher energy than the  ${}^1L_a$  state since the  ${}^1L_b \leftarrow {}^1A$  transition does not appear to lose intensity. The next higher transition ( ${}^1B_b \leftarrow {}^1A$ ) also exhibits an intensity increase as the temperature is raised. If the intensity stealing is from a still higher state vibronic coupling may be a general trait encompassing several electronic states. This coupling mechanism is not unlikely due to indole's lack of symmetry.

It was also reported that naphthalene (isoelectronic with indole) displayed an anomalous  ${}^1L_b \leftarrow {}^1A$  transition. This transition was found to consist of two sets of bands with one set 10 times as intense as the second. A surprising fact was that the former set was forbidden and the latter set was allowed from symmetry arguments. Again vibronic mixing was invoked to explain this phenomenon.<sup>11</sup> These findings when compared with those observed for indole led us to study the vapor absorption spectrum of naphthalene at the temperature extremes employed in the indole study. Again we found an enhancement of the  ${}^1L_a$  intensity relative to that for the  ${}^1L_b$  transition although these results were more ambiguous than those for indole. Thus this vibronic coupling mechanism may be more ubiquitous than previously thought.

The hot band analysis of the (presumed) sequence beginning with the  ${}^1L_b$  0-0 transition (2834 Å) indicated that indeed these  ${}^1L_b$  vibronic transitions are superposed on a member of the  ${}^1L_a$  transition. This was indicated by the fact that the whole intensity envelope of this sequence slowly increased as the temperature was raised. This correlated quite well with the intensity increase observed for the  ${}^1L_a$  transition with temperature. A possible explanation for these results is that a diffuse, low-intensity sequence belonging to the  ${}^1L_a \leftarrow {}^1A$  transition underlies this  ${}^1L_b$  0-0 sequence. The anomalous intensity behavior as a function of temperature of the  ${}^1L_b$  0-0

sequence could be caused by intensity changes of hot bands belonging to a diffuse  ${}^1L_a$  0-0 sequence. This implies that the  ${}^1L_a$  0-0 transition is energetically close to the  ${}^1L_b$  0-0 transition. Support for the definite assignments of the  ${}^1L_a$  and  ${}^1L_b$  0-0 transitions would come if a correlation of IR data with the vapor absorption spectrum were made. Such a correlation has proven to be difficult.<sup>7</sup>

## II. Polarization Measurements of Fluorescence Excitation

By analogy with naphthalene the  ${}^1L_b$  and  ${}^1L_a$  transitions are expected to be long axis and short axis polarized respectively and both transitions should occur in the plane of the molecule. Several experimental observations have been carried out attempting to assess the relative direction of transition polarizations in indole. It should be noted that no crystal absorption measurements have been reported yet.

The first experiments were done by Weber<sup>12</sup> on  $2 \times 10^{-4}M$  propylene glycol solutions at  $-70^\circ C$ . His technique was to run a polarization excitation spectrum of indole fluorescence which was observed at 340 nm. He found two polarization maxima at 270 and 298 nm and a minimum at 290 nm. The minimum had a positive polarization value however. These features were ascribed to two superposed transitions in the excitation spectrum, namely the  ${}^1L_a$  and  ${}^1L_b$  transitions. One of these transitions had a "negative polarization" relative to the other and accounted for the polarization minimum observed at 290 nm. This transition was ascribed as  ${}^1L_b$ .

Zimmermann and colleagues<sup>13,14</sup> did fluorescence polarization excitation measurements on ethanol solutions at  $-180^\circ C$ . (no concentrations reported) with results similar to those of Weber. They gave no interpretations of their results other than stating that two

transitions were responsible for the observed polarization spectra and that the 0-0 bands for the  $^1L_a$  and  $^1L_b$  transitions are at  $34,000\text{ cm}^{-1}$  (294 nm) and  $34,500\text{ cm}^{-1}$  (290 nm) respectively.

Konev and coworkers<sup>10b,15,16</sup> did another set of fluorescence polarization excitation experiments with tryptophan imbedded in stretched polyvinyl alcohol films at room temperature. This technique was employed to preferentially orient the molecules in-plane and along a preferred axis in that plane. The fluorescence was observed at 330 nm. Their results also were interpreted as a superposition of the  $^1L_b$  transition on the  $^1L_a$  transition with  $^1L_b$  transition maximum at 289 nm. They also state that these results indicate the " $^1L_b$  oscillator is oriented at almost a right angle to the  $^1L_a$  oscillator".

Song and Kurtin<sup>17</sup> also did fluorescence polarization excitation experiments on  $10^{-5}\text{M}$  indole in 9:1 glycerol-methanol at 263°K. They monitored the fluorescence at 345 nm and observed minima in the polarization excitation spectrum at 240 and 293 nm. The 293 nm minimum was attributed to the  $^1L_b$  0-0 transition superposed on the  $^1L_a$  transition with  $^1L_a$  state emitting at the monitored wavelength. They interpret their polarization excitation data as reflecting the  $^1L_a$  and  $^1L_b$  transition to be 90° relative to each other. (However, I believe their data doesn't warrant such a strong statement).

Finally Zuclich<sup>18</sup> performed magnetophotoselection experiments on  $10^{-2}\text{M}$  skatole in ethanol solutions at 77°K. That is, an EPR signal was monitored as a function of polarized exciting light rotated relative the permanent magnetic field impressed on the sample. He interpreted the data to indicate the first two transitions were perpendicular to each other.



An analysis of these polarization data reveal two features: First the  ${}^1L_b$  transition is superposed on the  ${}^1L_a$  transition. Thus there are some components of the  ${}^1L_a$  transition at lower as well as higher energies than the  ${}^1L_b$  transition. However it should be remembered that these data were taken in polar media which red-shifts the  ${}^1L_a$  transition more than the  ${}^1L_b$  transition as will be shown in the following section. Second it is premature to assert that the  ${}^1L_a$  and  ${}^1L_b$  transitions are perpendicular to each other. If they were perpendicular some negative values for polarization should be manifested when the  ${}^1L_b \leftarrow {}^1A$  transition is excited. This effect is no doubt partially masked by the overlap of the  ${}^1L_a$  and  ${}^1L_b$  transitions.

### III. Solution Absorption Spectra

The most general feature of the absorption spectra in solution is the loss of much of the vibrational structure seen in the vapor spectrum. The general features of the spectrum remain in hydrocarbon solvents but they are much more diffuse. In polar solvents the spectra are further blurred. The oscillator strength also tends to decrease slightly as the solvent polarity increases.<sup>19,20</sup>

Chignell and Gratzner<sup>20</sup> analyzed the absorption spectrum of indole by adding small amounts of H-bonding solvent to isooctane solutions ( $2.5 \times 10^{-4} M$ ) and observed the pattern shown in Figure 6. They separated this pattern into two effects: that due to H-bonding alone<sup>21</sup> and that due to solute-solvent interactions other than hydrogen bonding. These results are summarized in Table 3a. Water is a notable exception to their analysis; a blue shift of  $150 \text{ cm}^{-1}$  was observed. They showed that all solvents listed but water follow the McRae Equation<sup>22</sup> which takes into account the dipole-induced dipole interactions between

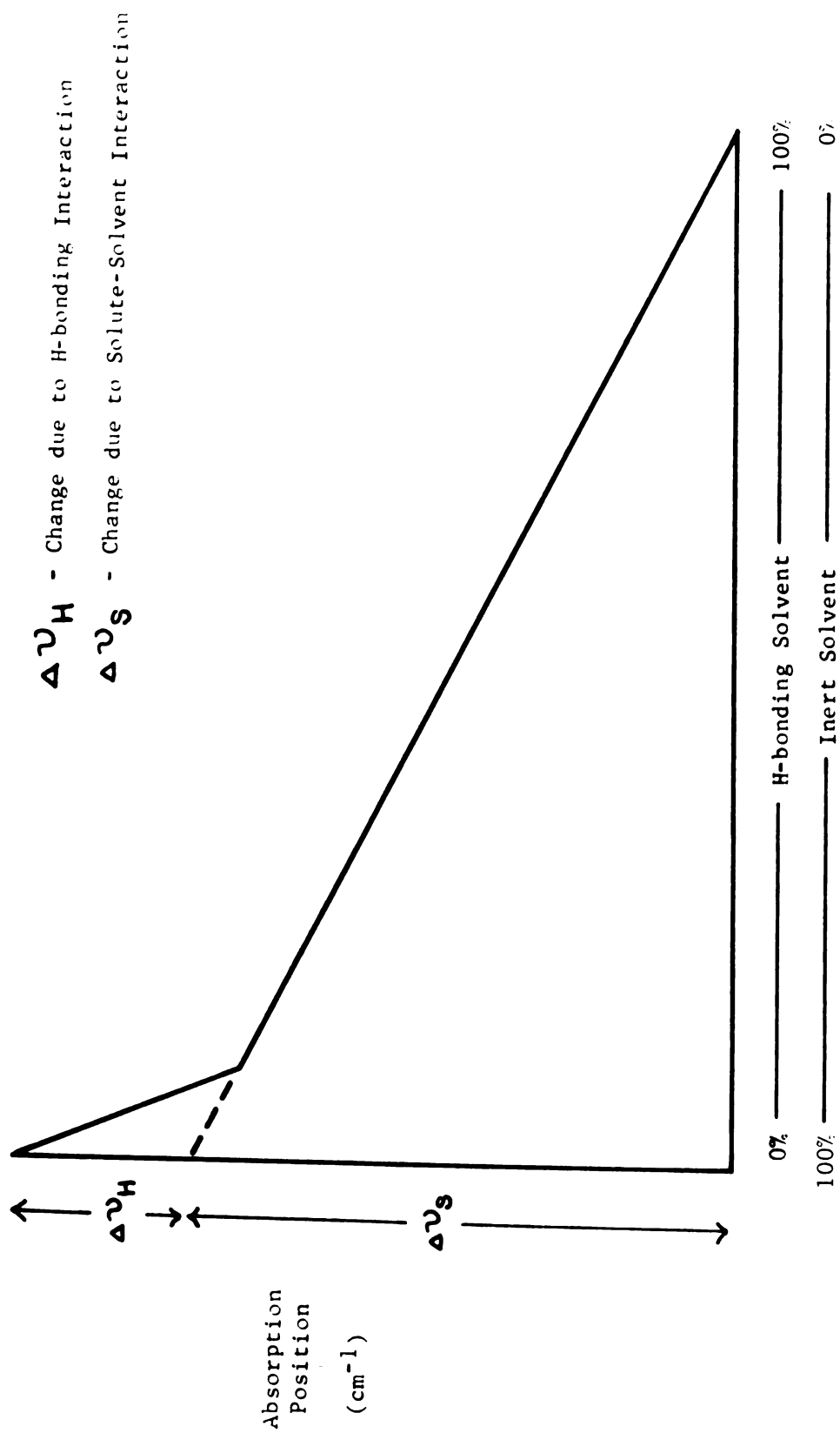


Figure 6. Solvent Effects on the Absorption Spectrum of Indole (after Chignell and Gratzer<sup>20</sup>).

Table 3a. Solvent Effects on Indole Absorption.

	$\Delta \nu_H^* (\text{cm}^{-1})$	$\Delta \nu_S (\text{cm}^{-1})$	$\Delta \nu_{\text{Total}} (\text{cm}^{-1})$
Isooctane	-	-329.0	-329.0
Isopropyl Alcohol	-102	-338.0	-431.0
Ethyl Ether	-104	-347.6	-433.0
Ethanol	-112	-343.0	-441.0
Dioxane	-122	-305.9	-451.0
Isobutyl Alcohol	-130	-327.9	-459.0
Water	+150	?	?

\* these values are relative to isooctane

Table 3b. Indole: Comparable Maxima in 2 Solvents.

Methylcyclohexane			EtOH	
(A)	$\text{cm}^{-1}$	(EtOH - MCH)	(A)	$\text{cm}^{-1}$
2610.6	38305	-737	S 2661.8	37568
2662.9	37553	-677	2711.8	36876
S 2714.1	36845			
S 2766.5	36147	-77	2772.4	36070
2791.8	35819	-29	2794.1	35790
S 2804.1	35662			
2871.2	34829	-50	2875.3	34779

S=shoulder

solute and solvent.

Thus the excited state stabilization observed in most H-bonding solvents is due to the sum of two effects. One effect is caused by the inherent polar nature of such solvents and is explicitly considered in the interactions formulated by the McRae Equation. That is, the transition moment and the excited state permanent dipole moment interact with the solvent dipoles. If the excited state permanent dipole moment is larger than the ground state permanent dipole moment the net effect is a transition red-shift since the solvation energy for the solute has increased. The data in Table 3a indicate this effect accounts for 3/4 of the stabilization energy. The other 1/4 is due to H-bonding. For this effect the pyrrolic nitrogen's proton is hydrogen-bonded with a solvent molecule. The electronic charge on the pyrrolic nitrogen decreases as a result of excitations as will be shown later; thus the pyrrolic hydrogen becomes more acidic and the hydrogen bond more stable in the excited state. This will contribute to the observed red shifts.

El-Bayoumi, et.al.<sup>8</sup> also presented data which can be analyzed for solvent shifts. In this case an attempt was made to analyze both the  ${}^1L_b$  and the  ${}^1L_a$  transitions by observing the shifts of the lowest energy vibronic  ${}^1L_b$  transition and the maximum in the  ${}^1L_a$  transition. They showed that the observed red shifts for the  ${}^1L_a$  transition was larger than for the  ${}^1L_b$  transition. Konev and coworkers<sup>24</sup> also observed the stronger red-shift of the  ${}^1L_a$  transition (max at 276 nm) than the  ${}^1L_b$  transition (279 and 287 nm) when n-butanol was added to hexane.

Another possible solute-solvent interaction is between an acidic hydrogen of the solvent (or a proton) with the  $\pi$ -electron charge density

at the pyrrolic nitrogen. Such an interaction would cause a blue shift of both the  ${}^1L_a$  and  ${}^1L_b$  transitions since the charge density at that position decreases for both the  ${}^1L_a$  and  ${}^1L_b$  states. This explains the blue shift observed in acidic media which will be discussed later as well as the observed shift in water.

Table 3b lists data which I obtained in a polar and a nonpolar solvent. In this case the corresponding vibronic bands were tabulated and compared. Again the bands belonging to the  ${}^1L$  transition are red-shifted much more than those belonging to the  ${}^1L_b^a$  transition when one shifts from a hydrocarbon to an H-bonding solvent. The spectrum in the polar solvent also displays less vibrational structure than that in a nonpolar solvent as was intimated in the opening paragraph of this section. Finally the vibronic species associated with each electronic transition are not shifted the same distance. This indicates that the solvent differentially affects the vibronic species, i.e. the solvent-solute interaction during excitation exhibit different couplings which depend on the vibronic transition member.

Solvent effects on the absorption spectrum of indole lead to the following conclusions: 1. The pyrrolic nitrogen should exhibit a large  $\pi$ -electronic charge density in the ground state. 2. This charge density decreases in the excited states making the pyrrolic hydrogen more acidic, particularly in the  ${}^1L_a$  state. 3. The  ${}^1L_a$  and  ${}^1L_b$  state permanent dipole moments should be greater than the ground state permanent dipole moment; this is especially true for the  ${}^1L_a$  state.

#### IV. Fluorescence Spectra.

Probably the most studied UV spectral characteristic of indole is its fluorescence. There are a number of interesting aspects which are in current controversy.

The most striking characteristics of the fluorescence is that it appears to emanate from two excited states; that is, the  $^1L_a$  and  $^1L_b$  states. The most convincing evidence for this trait comes from polarization data. The first evidence and interpretation was by Zimmerman's group.<sup>13,14</sup> They found that by exciting at 275 nm, which is mostly the  $^1L_a \leftarrow ^1A$  transition, the fluorescence polarization was 0.13 at 290 nm. The polarization spectrum then rose rather sharply to 0.30 at 340 nm where it leveled off. Konev's group observed the same effect in polyvinyl alcohol films<sup>15</sup> ( $P = 0.10$  to  $0.25$ ). Since they had measured the fluorescence quantum yields as a function of exciting wavelength from 250 nm to 300 nm and observed no change they reasoned that a redistribution of excitation energy occurred before fluorescence took place. Subsequent experiments showed that fluorescence depolarization as an increasing function of solute concentration was higher at longer fluorescent wavelengths than at shorter wavelengths.<sup>25</sup> This again is indicative of emission from different states. Finally Song and Kurtin<sup>17</sup> did further experiments to gain more evidence for this dual emission process. When they excited at 285 nm, which is rich in  $^1L_b \leftarrow ^1A$  transition character, they observed a maximum fluorescence polarization at short wavelengths followed by a sharp decrease and tailing off of polarization at longer wavelengths. Upon excitation at 265 nm the opposite result was obtained, namely that polarization spectrum observed by Zimmermann and by Konev. Others<sup>26</sup> have also excited at 290 nm ( $^1L_b$  rich) and seen the high polarization at short wavelengths with a subsequent tailing off at long wavelengths. These experiments were all done in a variety of polar and nonpolar solvents at low temperatures and indicate that the emission observed at short

wavelengths is due to the  ${}^1L_b \leftarrow {}^1A$  transition while that a longer wavelength is due to the  ${}^1L_a \leftarrow {}^1A$  transition.

Another phenomenon which occurs in the fluorescence spectrum is the extensive solvent effect on the shape and position of the spectrum. This phenomenon is somewhat related to both the analysis immediately above and that in the absorption spectra section since the two emissions appear to have quite different solvation properties. It was noted by Konev<sup>24</sup> that in n-hexane the fluorescence spectrum at room temperature was not the anticipated mirror image of the absorption spectrum. The relative intensities were quite dissimilar. As small amounts of n-butanol were added the vibrational structure was lost and the  ${}^1L_a$  transition underwent much more of a Stokes' shift than the  ${}^1L_b$  transition. Eventually the  ${}^1L_b$  transition disappeared as more butanol was added and only a broad fluorescence band with its maximum at 330 nm was all that remained. They reasoned<sup>10c</sup> that solvent relaxation processes caused the long wavelength emission and that the broad structureless band was due to successively catching the emission at different stages of solvent relaxation. Thus emission at the longest wavelength should have a comparatively long  $\tau_F$  since it was only seen after solvent relaxation had occurred. Mataga, et. al.<sup>27</sup> observed a similar shift and loss of vibrational structure when ethanol was added to n-hexane. In this case the fluorescence maximum shift was from 300 to 335 nm. They attributed the shift to solvent "stabilization" of the  ${}^1L_a$  state relative to that of the  ${}^1L_b$  state. This occurred because the increase in the dipole moment as a result of excitation was greater for the  ${}^1L_a$  state than for the  ${}^1L_b$  state. Selective stabilization of the  ${}^1L_a$  state compared with the  ${}^1L_b$  state occurs when a higher dielectric constant

solvent is used. They reported that preliminary measurements of  $\tau_F$  at different positions on the fluorescence spectrum show two decays with that due to the  ${}^1L_a \rightarrow {}^1A$  transition having the shortest component. This however is opposite what one would expect from Konev's reasoning.

There have been several results of fluorescence spectra published using various solvent conditions. Typical results are shown in Table 4. In general it is observed that polar solvents destroy the vibrational structure of fluorescence and cause a red shift. Several explanations of these results have been proposed and the main ones will be outlined below. The effects can be thought to occur as a result of three phenomena which are not mutually exclusive: 1) the influence of the dielectric properties of the solvent on the excited state of the solute. 2) H-bonding between solute and solvent, and 3) solvent relaxation during the lifetime of the solute's excited state. There is no question that whatever effect(s) cause the observed changes, such effects take place after the molecule has been excited. This is borne out by the negligible effect of different solvents on the absorption spectra. Moreover, viscous polar solvents which don't have a chance to interact with the excited solute molecules exhibit little red shift in emission.

There were several other observations made which weren't included in Table 4. It was reported that there was lower fluorescence intensity in water and in benzene than in cyclohexane, dioxane or ethanol, that fluorescence was quenched in chloroform and in carbon tetrachloride, and that acetone alone or as 1% in a cyclohexane or water solution quenches fluorescence.<sup>12</sup> When solvents having the same dielectric constant but divergent viscosities were used (propylene glycol and methanol) the fluorescence yield in the viscous solvent was 1.2 times that in the



Table 4, Indole Emission in Various Solvents,

Solvent	Temp.	pH	Conc.	Indole	N-Methyl Indole	3-diMethyl Indole	Ref
n-hexane	20°C		$5 \times 10^{-6} \text{M}$	288,299.5		322	24
n-pentane	20°C		$5 \times 10^{-5} \text{M}$	289	295	304	30
benzene	RT		$4.7 \times 10^{-5} \text{M}$	305			28
ether	20°C		$5 \times 10^{-5} \text{M}$	303	311		30
p-dioxane	20°C		$5 \times 10^{-5} \text{M}$	310	318		30
n-butanol	20°C		$5 \times 10^{-5} \text{M}$	326	328	345	30
E P A	77°K		$10^{-5} \text{M}$	325			17
ethanol	RT		$10^{-4} \text{M}$	335			27
ethylene glycol	RT			335			12
propylene glycol	RT		$5 \times 10^{-5} \text{M}$	$\tau_f = 3.9 \text{ n sec}$			32
H <sub>2</sub> O	20°C		$5 \times 10^{-6} \text{M}$	342		380	24
H <sub>2</sub> O	RT			$f = 0.1$ $\phi_f = 0.40$			33
H <sub>2</sub> O	RT		$3 \times 10^{-3} \text{M}$	$\tau_f = 4.1 \text{ n sec}$			34
H <sub>2</sub> O	RT			$\phi_f = 0.23$	$\phi_f = 0.38$		35
H <sub>2</sub> O	RT	1.7		$\tau_f = 2.7 \text{ n sec}$			40
H <sub>2</sub> O	RT	15		None	None		40
				400			
glycerol	RT			$\phi_f = 0.145$			26
1:1 ethylene glycol: H <sub>2</sub> O	77°K			346			34
				310			
1:1 ethylene glycol: H <sub>2</sub> O	RT			$\phi_f = 0.6$			34
				350			

nonviscous one. The respective lifetimes were 3.9 and 3.1 n sec<sup>32</sup> indicating the quenching process in this case was due to internal conversion.

Stryer had proposed an H-bonding mechanism to explain the quantum yield ratios in D<sub>2</sub>O and H<sub>2</sub>O solvents, i.e.  $\phi_F(D_2O)/\phi_F(H_2O)$ . This ratio was 1.29 for indole and 1.09 for n-methylindole<sup>45</sup>. He asserted that an excited state proton exchange reaction, which was responsible for the lower quantum yields in H<sub>2</sub>O, is faster in H<sub>2</sub>O than in D<sub>2</sub>O. However the proton-exchange mechanism cannot explain the data for tryptophan vs. n-methyltryptophan where a sizeable isotope effect was observed in both cases<sup>34</sup>.

A controversy was evoked when Walker, et. al. proposed their exciplex theory to explain the observed fluorescence shift in polar solvents.<sup>30,44</sup> They observed the same red shifts in the fluorescence spectra of indole, 1-methylindole and 1,3-dimethylindole when small quantities added were so small that the dielectric constant change could not explain the spectral shifts. However, highly localized concentrations of the polar solvent around each solute molecule could significantly alter the local dielectric environment.<sup>20</sup> But Lumry's group found no correlations between the observed shift and the dielectric constant of the polar solvent used. The only trend one could see was that polar-protic solvents shifted the spectrum more than polar-nonprotic solvents. They ruled out H-bonding since the red shifts occurred for n-methyl indoles as well as indole. Using kinetic arguments and plotting a long wavelength "second fluorescence band" vs. concentration of polar solvent Walker, et. al. invoked an "Exciplex" between the excited solute molecule and polar solvent molecules to

explain the red shift. This was thought to be a reaction between the excited solute and specific solvent molecules. For polar-nonprotic solvents their exciplex stoichiometry was determined to be 1:1 and for polar-protic solvents it was 1:2 solute:solvent molecules. This "second fluorescence band" was their exciplex emission. It has some charge-transfer character with the indoles acting as donors and the solvent acting as an acceptor. Indirect evidence supporting this view was that the observed loss of fluorescence intensity was proportional to the dielectric constant of the polar solvent.<sup>30</sup> Thus the loss could be explained by a partial ionization mechanism.

Exciplex formation as an explanation of the spectral data was challenged by Chopin and Wharton<sup>29</sup> for two reasons: the Walker, et.al. data showed 1) the rate constant for exciplex formation in polar-protic solvents to be 100-600 times that in polar-nonprotic solvents, and 2) the rate constant for exciplex formation for indole to be 10-15 times that for N-methyl indole in alcoholic solutions.<sup>29</sup> Furthermore Chopin and Wharton observed fluorescence in 1:1 isopentane:3-methylpentane from room temperature down to the glass transition temperature of the solvent. At that point the fluorescence was quenched and intense phosphorescence appeared. However, if minute traces of water were present the fluorescence quenching was not complete below the glass transition temperature. If butanol were added to the IP:3MP mixture the spectrum showed vibrational loss, red shifting and a fluorescence intensity decrease at room temperature as Walker, et. al. had reported. At 77°K both fluorescence and phosphorescence were present with both seeming "to be superpositions of 2 emissions". They explained their results as well as those of Lumry and coworkers on the basis of a

phototautomerism to 2 H indole. Their scheme involved some intricate kinetics with emission only occurring from an excited 2 H indole molecule complexed with a solvent molecule and not from a 2 H indole molecule alone. No reason was given why emission wouldn't come from an uncomplexed molecule. In addition no rationale was given for the polar-nonprotic solvents-induced red shift.

Another challenge to the exciplex formation came from Eisinger and Navon who observed the fluorescence of indole and N-methylindoles as a function of temperature in a 1:1 ethylene glycol-water solvent.<sup>34</sup> They found: 1) as the temperature is decreased the spectrum moves to the blue and acquires structure with most of this change occurring around the glass transition temperature of the solvent (this effect was also reported in ethanol, iso-butanol, glycerol, and in polyvinyl alcohol<sup>46</sup>), 2)  $\phi_F$  decreases at higher temperatures but most of this decrease takes place at temperatures above those at which the spectral shifts occur and 3) a solvent isotope effect on the quantum yield is seen for all molecules in deuterated solvents but this effect vanishes after  $\phi_F$  has leveled off as the temperature is lowered. Probably the most important evidence against the exciplex formulation was the lack of an isosbestic point formation as the spectral shifts were taking place which indicates that a unique excited solute-solvent interaction doesn't occur. Eisinger and Navon interpreted the spectral shifts as due to progressive nondescript solvent reorientation effects. They interpreted the quenching to be due to the potential surfaces of the ground and excited states lying closer to each other after solvent reorientation had occurred thus allowing tunnelling mechanisms to be more efficient than before reorientation. Finally, using kinetic

arguments they reasoned that the isotope effect was due to solvent perturbations (not including H-bonding) affecting the tunnelling mechanisms. These mechanism are manifested by  $k_{\text{non-radiative}}$ . This kinetic term was found to be proportional to  $e^{-E_a/RT}$ .  $E_a$  was not found to be dependent on the isotope but the proportionality constant was which further strengthens the perturbation argument.

All the above data show that the dipolar interaction between the excited molecule and the solvent, as well as H-bonding, contribute to the spectral shifts, quenching and lifetimes seen in the indoles. However, dynamic solvent cage effects also have an important role in the ultimate fate of the excitation energy. The magnitudes of these effects are different for the  ${}^1L_a$  and  ${}^1L_b$  states. Only after cognizance and elucidation is made of these states' interplay with themselves and their environment will the fundamental significance of solvent effects be more fully understood.

An examination of Table 4 also shows that the cation and anion species of indole exhibit different fluorescent properties than the neutral molecule. No fluorescence has been reported from the cation, i.e. total fluorescence quenching occurs at low pH. This is undoubtedly due to a change in the non-radiative transition rate, possibly the intersystem crossing rate. The anion however does emit although its fluorescence is weaker and at longer wavelengths than the neutral species. Presumably the long wavelength emission is related to an influence of the negative charge on the excited  $\pi$ -electron system. For the anion this charge resides on the pyrrolic nitrogen whose proton has been removed. Long wavelength emission is also observed for neutral methyl indoles. Again the methyl can exhibit an electron inductive

effect. Thus there is a correlation between the extra electronic charge and the long wavelength emission.

Finally attention must be drawn to some unique results observed for a particular set of indoles. Bridges and William did some fairly extensive measurements on the effects of pH on the fluorescence of indoles and substituted indoles.<sup>40</sup> Their results are summarized in Table 5. They noted that of all the methyl indoles, hydroxy indoles, and indole itself only 5-hydroxy indole showed fluorescence in acid solutions. In addition 5-methoxy and 5-phenoxy indole exhibited similar fluorescence in acid solutions. However it was much weaker than the fluorescence in neutral or basic solutions. It didn't occur at 77°K. (It should also be noted here that indole did fluoresce at 77°K in ETOH + KOH at pH's where quenching occurred at room temperature; ~pH 11.) No solvent dependence was observed and the absorption spectrum wasn't affected much by the pH change. Thus it was thought that some excited state reaction or rearrangement was responsible for this emission. This hypothesis was further substantiated by the observation that the emission was at a longer wavelength than either the neutral molecule or anion emission which indicates energy is lost in the reaction or rearrangement.

All these fluorescence spectra data show that there is a configurational change of the molecule before emission occurs. The type and amount of change is dictated by the solvent and its effects on the excited solute molecule. The spectral features therefore are a reflection of the environment as well as of the uniqueness of that molecule. Vapor phase fluorescence spectra would delineate the inherent molecular characteristics. In addition these spectra would add information about the

Table 5. Effect of pH on Fluorescence of Indoles (Reference 40).

Molecule	Emitter	(abs) $\lambda_{\max}$	(fluor) $\lambda_{\max}$	$\phi_f$	$pK_a$	pH range of max fluor	Stokes' shift ( $\text{cm}^{-1}$ )
Indole and 5-Me indole	Cation	269	-	-	1.7	-	-
	Neutral	270	355	0.46	14	3.3-11.0	8870
	Anion	280	400	0.145	-	17.4	10710
N-methyl indole	<del>D</del> cation	280	-	-	1.6	-	-
	Cation	280	-	-	2.5	-	-
	Neutral	282	350	0.47	-	4.3-16	7000
5-methoxy indole	Cation	$\sim 293$	-	-	-	-	-
	Cation	$\sim 293$	520	0.01	-	-0.7	15430
	(Excited)						
	Neutral	$\sim 292$	388	0.46	-	2.1-10.4	5070
	Anion	$\sim 298$	402	0.105	-	17.4	8230

apparent dual emission, i.e. whether it occurs in the vapor phase. Also a study of methyl substituted derivatives of indole could yield interesting information regarding dual emission.

#### V. Phosphorescence Spectra.

It was surprising to find that indole phosphorescence had not been investigated too extensively. Heckman<sup>47</sup> reported the indole phosphorescence spectrum in EPA and attempted to make a vibrational analysis of it. He reported three vibrational sequences with  $795\text{ cm}^{-1}$ ,  $1235\text{ cm}^{-1}$ , and  $1585\text{ cm}^{-1}$  as fundamental components. Another report<sup>14</sup> stated there were vibrational sequences of  $800\text{ cm}^{-1}$ ,  $1200\text{ cm}^{-1}$  and  $1600\text{ cm}^{-1}$ .

Those who have reported spectral results have seen three peaks at 405, 430, and 455 nm with inflections at 417, 425, and 445 nm regardless of solvent. The phosphorescence has been studied in EPA,<sup>17,47</sup> polyvinyl alcohol film,<sup>15</sup> ethanol,<sup>7</sup> 2:1 ethanol:ether,<sup>48</sup> 9:1 methanol:ethanol,<sup>49</sup> 1:1 methylcyclopentane:methylcyclohexane,<sup>29</sup> 1:1 isopentane:3-methylpentane,<sup>29</sup> butanol,<sup>15</sup> and glycerol.<sup>15</sup> The nonspecificity of solvent effect on phosphorescent emission is in direct contrast to the observations of fluorescence.

Reported values of phosphorescence lifetimes are: 2.4 sec in the hydrocarbon solvents,<sup>29</sup>  $6.0 \pm 0.2$  sec in the EPA,<sup>17</sup>  $6.3 \pm 0.02$  sec in the 2:1 ethanol:ether,<sup>48</sup> 7 sec in polyvinyl alcohol film.<sup>15</sup> The phosphorescence to fluorescence ratio  $\phi_p/\phi_f$  is also solvent sensitive.<sup>29,48</sup>

The effect of the status of the pyrrolic nitrogen's hydrogen on phosphorescence intensity was discussed by Konev and coworkers.<sup>10d</sup> They found that in hexane there was a large amount of phosphorescence and little fluorescence; in methanol, ethanol, butanol, or ethylene glycol there were about equal quantities of fluorescence and phosphorescence;



but in 0.1M NaOH the phosphorescence was practically nonexistent. This indicates that the nitrogen's hydrogen is needed in the indole structure for phosphorescence to occur but for the indole anion, phosphorescence either does not occur or is very weak.

Probably the most interesting and informative data is that using polarization techniques. In all reported cases both excitation and phosphorescent emission polarization studies show that the triplet transition moment is primarily out-of-plane as opposed to the moments of singlet transitions. The emitting triplet is probably the  $^3L_a$  state<sup>52</sup> and there is an in-plane component of the phosphorescence transition which lies parallel to the  $^1L_b$  transition moment.

Polarized phosphorescence spectral studies<sup>14,15,17</sup> excited at wavelengths corresponding to the  $^1L_a$  and  $^1L_b$  transitions supports the contention that the  $^3L_a$  state is the emitting triplet. Song and Kurtin,<sup>17</sup> using Raman and IR literature data, correlated the  $650 \pm 100 \text{ cm}^{-1}$  sequence observed in the phosphorescence spectrum with either in-plane skeletal distortion of the ring, out-of-plane C-H bending or possibly N-H bending. The  $1600 \pm 100 \text{ cm}^{-1}$  sequence could be correlated with a ring stretching mode. They also suggested that spin orbit coupling occurs between the  $^3L_a$  state and the  $^1L_b$ ,  $^1B_b$  and other states arising from  $\sigma\pi^*$  and  $\pi\sigma^*$  transitions.

The question arises whether the  $^3L_b$  state is involved in the phosphorescence, i.e. that dual triplet emission is occurring similar to dual singlet emission. This could explain the structure observed in the phosphorescence polarization spectrum.<sup>15,17</sup> In the phosphorescence polarization spectrum of indazole, two vibrational sequences with perpendicular transition moments relative to each other was suggested.<sup>14</sup>

This seems to us to be a further indication for dual triplet emission. Emission studies at very low temperatures (4°K) and as a function of temperature could resolve this problem.

#### VI. Theoretical Calculations.

The results of these calculations are shown in Table 6 and Figure 7. An assignment of the two lowest singlet transitions was made after considering the excited state's permanent dipole moments, the transition moment orientations and the oscillator strengths. Naphthalene was again used as the model for this assignment. Thus the  $^1L_b$  state was expected to have the lower permanent dipole moment and the  $^1L_b$  transition was expected to be preferentially oriented along the y-axis and have the weaker oscillator strength compared with the  $^1L_a$  state and transition. These three criteria all agree with the calculated prediction that indole's first singlet transition is to the  $^1L_a$  state. The first two transitions are calculated to lie energetically close to each other. The actual calculated values do not coincide exactly with the 0-0 transition values experimentally determined. However they do not differ by more than 0.1 eV which is remarkable predictive agreement for the calculations. One should recall that the calculations are for vertical transitions and the 0-0 transitions may not belong to this class. The transition moments are not calculated to be parallel to either of the geometrical coordinate axes. The first two excited state permanent dipole moments are much larger than the ground state permanent dipole moment. Both excited states are also predicted to have molecular internuclear distances somewhat larger than the ground state internuclear distances. The first two singlet triplet transition energies are

Table 6. Calculation Results for Indole,

Trans. Energy (cm <sup>-1</sup> )	Trans. Energy (nm)	Trans. Moment (Debyes)	Trans. Polar (deg. from x-axis *)	f
35457	282.0	0.559	0.88	0.120
36912	270.9	0.478	-54.46	0.092
47023	212.7	0.732	-80.70	0.273
49319	202.8	0.904	63.47	0.437
Molecular State		Perm. Dipole Moment (Debyes)	Perm. Moment Polar. (deg. from x-axis*)	
Ground		3.93	-34.91	
1st Excited		7.44	-68.91	
2nd Excited		6.63	-47.40	

\* See Figure 7

Figure 7. Calculated Charge Densities and Bond Lengths for Indole.

Legend:

Numbers at each atomic position denote  $\pi$ -electron charge densities in electron units.

Numbers at each bond denote bond lengths in Angstroms.

The top number corresponds to the ground state.

The middle number corresponds to the first excited singlet state ( $^1L_a$ ).

The bottom number corresponds to the second excited singlet state ( $^1L_b$ ).

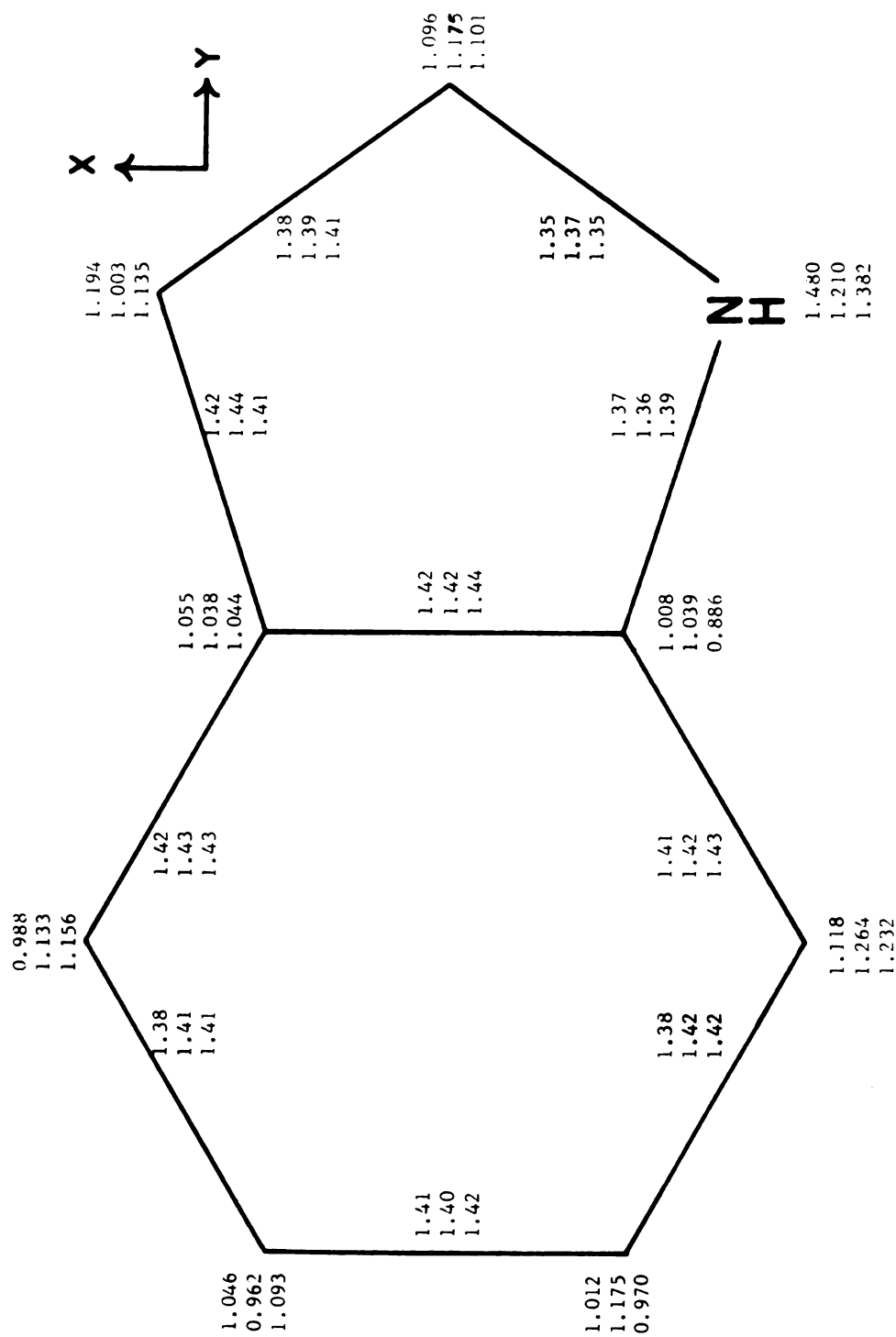


Figure 7.

calculated to be at 529 and 395 nm. However since the test molecules were not optimally parameterized for singlet-triplet transition energy correlations, little credence is given to these values. The ionization potential and electron affinity are calculated to be 7.0 and 1.8 eV respectively. The charge density calculations show that the pyrrolic nitrogen's acidity is  ${}^1L_a > {}^1L_b > \text{ground state}$ .

## VII. Correlations and Summary.

The value of our computations lies in the consistency between calculated values and experimental data. In this section we shall compare our calculations with experiments.

1. The calculations predict the vertical energies of the  ${}^1L_a$  and  ${}^1L_b$  states to be very close with the  ${}^1L_a$  state energetically lower. Vapor absorption spectra indicate that the 0-0 energies of the  ${}^1L_a$  and  ${}^1L_b$  transitions are close. It is difficult to choose which state is energetically lower. In polar media the  ${}^1L_a$  state lies energetically below the  ${}^1L_b$  state. The closeness of the  ${}^1L_a$  and  ${}^1L_b$  energies is consistent with the possibility of dual emission proposed experimentally.
2. The calculations predict the angle between the  ${}^1L_a$  and  ${}^1L_b$  transition moment vectors to be  $55^\circ$  and that neither moment parallels the x or y axes. Experimentally these transition moments are oriented at a relatively large acute angle to each other. The  ${}^1L_b$  transition moment is predominantly oriented along the longer axis of the molecule which is consistent with the calculations.
3. The calculations predict the first two singlet excited states have much larger permanent dipole moments than the ground state with the  ${}^1L_a$  state having the larger of the two. This correlates very well with the experimental results for absorption and emission. The polar

solvents red-shift the  ${}^1L_a$  absorption more than the  ${}^1L_b$  absorption as predicted. These solvents also red-shift fluorescent emission from the  ${}^1L_a$  state much more than from the  ${}^1L_b$  state. In fact the permanent dipole moment change is so large that the fluorescence red-shift is quite pronounced. This effect is both predicted and experimentally observed.

4. The calculations predict that the acidity of the pyrrolic hydrogen has the order  ${}^1L_a > {}^1L_b > {}^1A$ . This is due to the decreased charge density on the pyrrolic nitrogen as a result of excitation. The decrease is more apparent for the  ${}^1L_a$  state than for the  ${}^1L_b$  state. Thus the energy of the H-bond between the pyrrolic hydrogen and a solvent molecule would be larger in the  ${}^1L_a$  state than in the  ${}^1L_b$  and ground state. A larger red shift is therefore expected for the  ${}^1L_a$  state due to H-bonding effects. This is consistent with the observed red shifts in H-bonding solvents.

5. The calculated charge densities at the pyrrolic nitrogen also agree with the ground state  $\pi$ -electron stabilization mechanism proposed to explain the effect of water on indole's absorption. The pyrrolic nitrogen's  $\pi$ -electron charge density is calculated to be much larger than that of any other atom. It also undergoes a larger decrease upon excitation. So a solvent proton could stabilize the ground state electron system at the pyrrolic nitrogen to a larger extent than the  ${}^1L_a$  or the  ${}^1L_b$  states. This would cause an absorption blue-shift. The spectrum of indole in ethanol in the presence of small amounts of  $H_2SO_4$  exhibits a  $260\text{ cm}^{-1}$  blue-shift of the  ${}^1L_a \leftarrow {}^1A$  transition and a  $140\text{ cm}^{-1}$  blue-shift of the  ${}^1L_b \leftarrow {}^1A$  transition.<sup>58</sup> This is the expected result if an acidic proton stabilizes the ground state and this

stabilization affects the  $^1L_a$  transition more than the  $^1L_b$  transition.

6. A further correlation of calculated charge densities and experimental observations was provided by the ground state reactivity studies of Hinman and Lang.<sup>53</sup> They found that in indole's ground state the 3 position was quite basic. This was quite evident compared with the basicity of the 2 position. All these correlative data lend validity to the calculated predictions of the charge densities.

Acids and bases particularly affect the excited singlet states. In an acidic medium the fluorescence is quenched by some radiationless transition process. In basic media the fluorescence yield is somewhat reduced (no pun intended) and its emission is at a lower energy than in a neutral medium. Obviously more spectroscopic data must be obtained to understand the processes which these pH effects provoke.

Probably the most provocative aspect of the indole spectra is the possibility of dual emission from the singlet and triplet states. Very few molecules have been thought to exhibit such properties. Their existence is quite unique and indicates open communication between the excited states. If this process occurs one might expect to observe fluorescent lifetimes with different values depending on where the lifetime was monitored in the spectrum. Although we have made some preliminary attempts to find this dual fluorescent decay we have not been successful yet. Likewise a close reexamination of phosphorescence decay is also warranted to see if a dual decay exists.

The problem of two closely spaced excited electronic states is a very intriguing problem both experimentally and theoretically. A study where one can vary such spacing and look for changes in absorption and emission properties could be quite revealing. Substituted methylindoles



seem to be such a potential series of molecules which should be studied.

These data show that indole is a unique molecule spectroscopically. The significance, if any, of this uniqueness to biology is unknown and discussion of this significance will be deferred to the final chapter.

## INDAZOLE

### I. Vapor Absorption Spectra.

The vapor absorption spectrum of indazole is shown in Figure 8. There are two electronic transition bands evident: one rich in vibrational structure centered at 285 nm and the other with diffuse vibrational structure centered at 245 nm. In contrast to the analogous bands for indole, these bands are quite well separated and exhibit little overlap. They are tentatively assigned the  ${}^1L_b \leftarrow {}^1A$  and the  ${}^1L_a \leftarrow {}^1A$  transitions respectively. The  ${}^1L_a$  0-0 transition remains unassigned but the  ${}^1L_b$  0-0 transition is assigned at  $34770\text{ cm}^{-1}$  ( $2897\text{ \AA}$ ). Other vibrational sequences in the  ${}^1L_b \leftarrow {}^1A$  transition begin at 2836, 2787, and  $2731\text{ \AA}$  with an average energy separation between sequences of  $692\text{ cm}^{-1}$ . Another sequence to the red of the  ${}^1L_b$  0-0 transition apparently begins at  $2950\text{ \AA}$  and is denoted as a "primed" sequence. Its origin remains a mystery. Again a normal coordinate analysis of the  ${}^1L_b$  transition vibrational structure has not been carried out. The  ${}^1L_a$  transition vibrational groups lie at 2570, 2516, 2446, and  $2395\text{ \AA}$  with a mean energy separation between these groups of  $945\text{ cm}^{-1}$ .

A hot band analysis was also performed with this molecule. The results are shown in Figure 9. Normal results were obtained for the  ${}^1L_b$  transition confirming the 0-0 position at  $34470\text{ cm}^{-1}$ . However

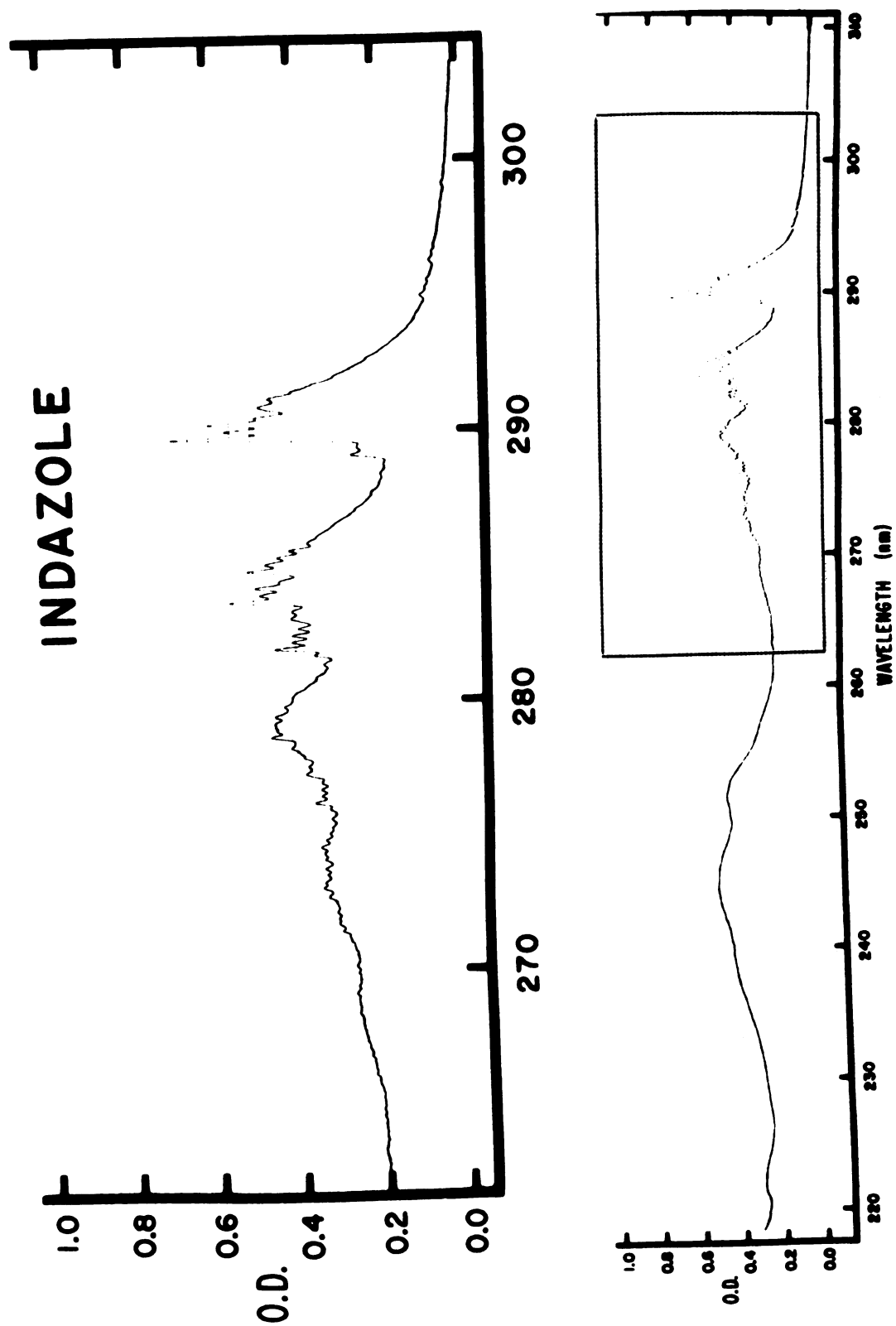


Figure 8. Indazole Vapor Absorption Spectrum.

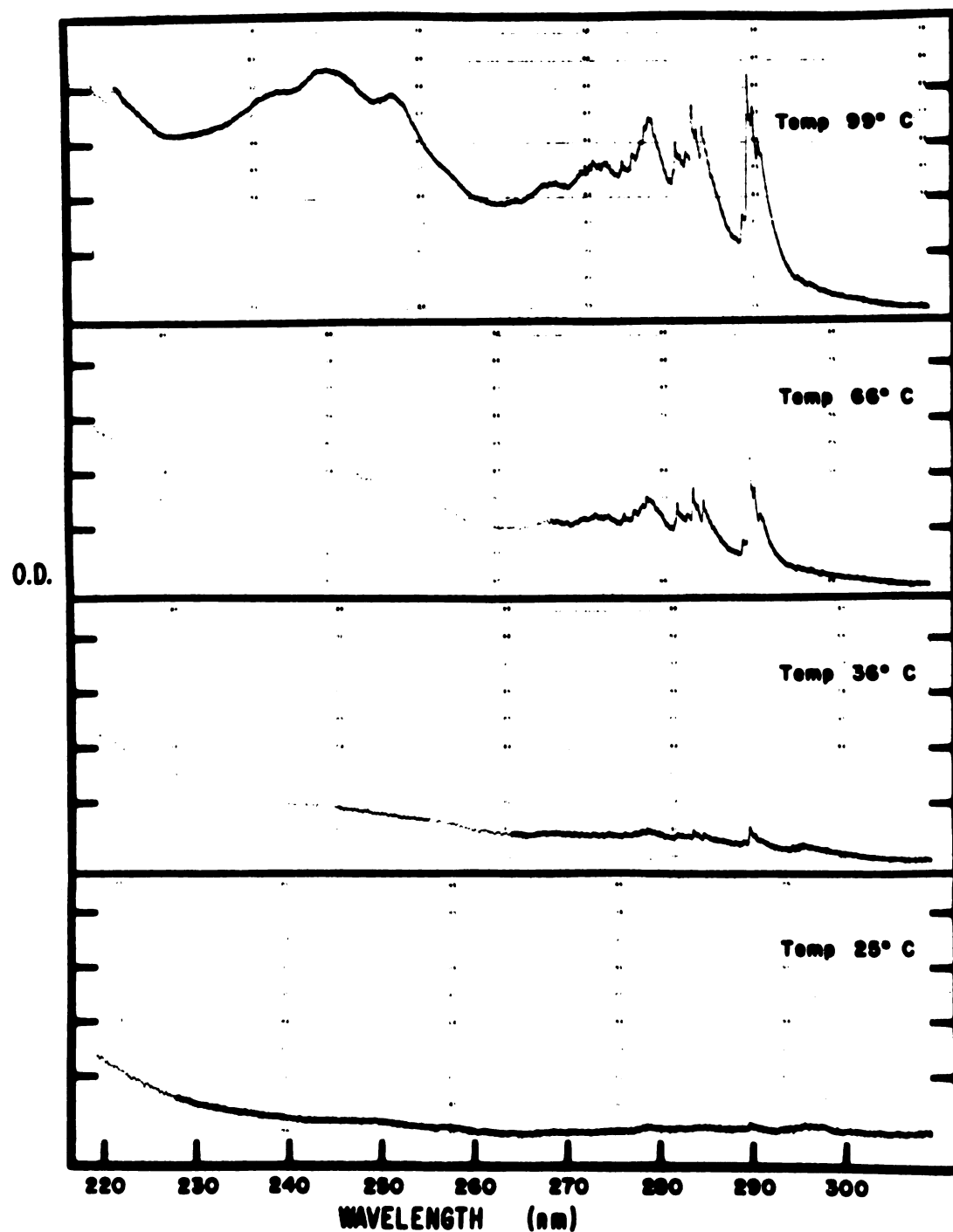


Figure 9. Indazole Vapor Absorption Spectra as a Function of Temperature.

again the  $^1L_a$  transition oscillator strength grew more rapidly than that of the  $^1L_b$  transition. A transition borrowing mechanism involving vibronic coupling may be invoked to explain this phenomenon. This molecule also has limited symmetry in the ground state so vibronic coupling may again be significant.

## II. Polarization Measurements of Fluorescence Excitation.

The only excitation polarization measurements reported were performed by Schutt and Zimmermann<sup>14</sup> in ethanol at  $-180^\circ\text{C}$ . Their results were quite expected. Monitoring at 310 nm they observed a negative polarization from 240 to 260 nm. This polarization then rapidly became positive and gradually leveled off toward a high positive value at 300 nm. The data strongly suggests that fluorescence is only emitted from the  $^1L_b$  state. The negative polarization at the shorter wavelengths corresponds with excitation into the  $^1L_a$  state while positive polarizations at the longer wavelengths corresponds with excitation into the  $^1L_b$  state. The fact that the positive polarization does not plateau before 300 nm indicates that there is still some  $^1L_a$  transition character down to about 290 nm. The polarization values at their extremes were 0.42 at 300 nm and -0.10 at 240 to 260 nm. The high positive polarization correlates well with the statement that fluorescent emission is from the  $^1L_b$  state. However the fact that the negative polarization does not approach -0.3 suggests that the  $^1L_a$  and  $^1L_b$  transition oscillators are not at right angles with each other. They probably do lie at a rather large acute angle though.

## III. Solution Absorption Spectra.

Table 7 is a compilation of all the available absorption as well as emission data for the azaindoles with the exception of purine.

Table 7. Solvent Effects on Azaindole Spectra.

		Vapor	Hydrocarbon	Ether	Ethanol	Water	Acid	Base	Phosphorescence
Indazole (2-aza)	Abs	245, 284, 290(58)	250, 291, 295(14)		254, 288(55) 255, 294, 298(14)	290(71) 250, 284, 297(54)	260, 302(14) 253, 291, 302(54)	300(71)	
	Fluor				327(54) 320(14)	322(54) 310(71)	370(54) 358(71)	365(71)	420, 450(14) Cation: 450, 480(14)
Benzimidazole (3-aza)	Abs	238, 272, 277(58)	242, 274, 280(58) 242, 274, 280(56) 243, 274, 280(56)	244, 274, 281(58)	244, 272, 279(58) 242, 270, 279(14)	243, 271, 277(58) 242, 271, 277(54) 244, 271(57)	241, 266, 273(56) 240, 267, 273(54) 240, 266, 270(14)	242, 271, 277(56) 250, 274(57)	
	Fluor		282, 292, 298(58)	283, 292, 301(58)	281, 291, 297(58) 294(14)	281, 290, 298(58) 310(54)	370(58) 365(54)	300(58) 310(71)	374, 398, 420(58) Cation: 390, 420(14)
4-azaindole	Abs					292(54)	327(54)		
	Fluor				380(54)	417(54)	420(54)		
5-azaindole	Abs					265, 273(54)	268, 293(54)		
	Fluor				352(54)	404(54)	405(54)		
6-azaindole	Abs					260, 291(54)	261, 319(54)		
	Fluor				390(54)	392(54)	387(54)		
7-azaindole	Abs	282, 288(58) 269, 288(8)	286, 292(59) 277, 293(8)	287, 294(59) 293(8)	290, 296(59) 295(8)	288, 295(59) 290(54)	290, 305(59) 293(54)		
	Fluor		330(59)	346(59)	368(59) 375(54)	390(59) 391(54)	438(59) 438(54)		
Benzotriazole (2,3-diaza)	Abs	242, 272, 279(58)	248, 282(14) 248, 278(57)		257, 274(55) 263, 278(14)	275(71) 265(54)	275(71) 275(54)		
	Fluor				350(54) 320(14)	350(54) 350(71)	390(54) 383(71)	338(71)	420, 440(14) Cation: 430, 460, (14)
4-azabenzimidazole (3,4-diaza)	Abs	236, 277, 283(58)	243, 282(57)			244, 282(57) 280(54)	231, 282(57) 295(54)	265, 289(57)	
	Fluor				345(54)	320(54)	330(54)		
5-azabenzimidazole	Abs					275(54)	265(54)		
	Fluor				360(54)	355(54)	350(54)		

All wavelengths are expressed in nm.  
References are denoted by parentheses ( ).

Indazole does not exhibit an absorption spectrum in hydrocarbon solvents much different than that in the vapor other than being somewhat more diffuse. However in ethanol the spectrum is red-shifted, with the  ${}^1L_a$  transition red-shifted more than the  ${}^1L_b$  transition ( $800\text{ cm}^{-1}$  vs.  $400\text{ cm}^{-1}$ ). In water there appears to be slight blue-shift compared to the spectrum in ethanol. Interpretation of this data follows the same tact as for indole. The  ${}^1L_a$  state permanent dipole moment is probably larger than that of the  ${}^1L_b$  state and both are larger than that of the ground state. Ethanol stabilizes the  ${}^1L_a$  state more than the  ${}^1L_b$  state through dipole-dipole interactions. In addition it can further stabilize the  ${}^1L_a$  state more than the  ${}^1L_b$  state through H-bonding provided the pyrrolic nitrogen's acidity follows the same trend as in indole. If the latter assertion is true, water could interact via its hydrogen proton with the  $\pi$ -electronic charge centered on the pyrrolic nitrogen causing a spectral blue-shift.

When absorption is done in an acidic solution the resultant cation spectrum has a demonstrable red-shift. Although the acidic proton is stabilizing the pyrrolic nitrogen's  $\pi$ -electron charge it also must be interacting elsewhere in the molecule to cause this red-shift. The most likely place would be at the  $\pi$ -electron charge on the pyridinic nitrogen. This stabilization would occur if the excited states' charge density exceeded that of the ground state. Since the  ${}^1L_b$  transition is red-shifted more than the  ${}^1L_a$  transition, our reasoning predicts that the pyridinic nitrogen's charge density is more in the  ${}^1L_b$  state than in the  ${}^1L_a$  state. The charge density changes at the pyridinic nitrogen must be more than those at the pyrrolic nitrogen since the effects are antagonistic and a red-shift is observed. In

a basic medium the resultant anion also shows a red-shift. This is not surprising since the Coulombic attraction between the pyrrolic hydrogen's proton and the  $\pi$ -electron charge and the residual negative charge after the proton is extracted. It then takes less energy to excite the electronic system. The anion also exhibits an apparent merging of the two absorption transition bands. The  $^1L_a$  transition loses intensity and appears to form a high energy shoulder to the now broad  $^1L_b$  transition. Thus the anion has a different spectrum than either the neutral or cation species.

These absorption spectra indicate that the replacement of a carbon with a pyridinic nitrogen introduces new factors which must be considered when one interprets these spectra, particularly solvent perturbations.

#### IV. Fluorescence Spectra.

The relative red and blue solvent shifts of the fluorescence spectra parallel those solvent shifts observed in the absorption spectra. Fluorescence with some vibrational structure is exhibited by the neutral molecule. The Stokes' shift of this emission in polar solvents is not as large as that for indole. This indicates that the lowest excited state permanent dipole moment doesn't differ much from the ground state permanent dipole moment. In addition the excited state stabilization due to H-bonding does not manifest itself greatly in a Stokes' shift contribution. Fluorescence polarization shows that emission is from only the  $^1L_b$  state.<sup>14</sup> This is an expected result since the  $^1L_a$  and  $^1L_b$  transitions are well separated.

In contrast with the results for indole, the cation of indazole fluoresces. Its emission is somewhat broader with less vibrational structure than the neutral species. The red-shift of the cation

emission from the neutral molecule correlates well with the supposition that the acidic proton stabilizes the  $^1L_b$  excited state at the pyridinic nitrogen position. Only the  $^1L_b$  state emits and our absorption spectra analysis predicted the pyridinic nitrogen charge density to be greatest for that state. It seems reasonable to conclude that the cation is formed through an interaction of the acidic proton with the lone pair electrons of the pyridinic nitrogen.

The anion also fluoresces. Its emission is slightly to the red of the cation's fluorescence and is broad and vibrationally structureless. As for indole this emission is probably due to an influence of the pyrrolic nitrogen's residual negative charge on the excited  $\pi$  electron system.

#### V. Phosphorescence Spectra.

The only phosphorescence spectra published for any of the azaindoles excluding purine has been that of Schutt and Zimmermann<sup>14</sup> in ethanol at  $-180^\circ\text{C}$ . For indazole they obtained spectra for both the neutral and cation species. The neutral molecule displays peaks at 422, 452, and 481 nm and inflections at 437, 467, and 500 nm. The cation's spectra is red shifted and displays peaks at 446, 481, and 508 nm and inflections at 461 and 550 nm. Phosphorescence excitation polarizations were negative for both  $^1L_b$  and  $^1L_a$  excitations. This yields the expected interpretation that the phosphorescent transition(s) is polarized out-of-plane. The emission polarization measurements, though expectedly negative, surprisingly showed spectral structure. As stated before, Schutt and Zimmermann interpreted this to indicate phosphorescent emission from two different triplet states. These are presumably the  $^3L_a$  and the  $^3L_b$  states. Since excitation was to the



$^1L_b$  state the emission polarization spectra could be interpreted as showing that the phosphorescence peaks corresponded with emission from the  $^3L_b$  state and the inflections with emission from the  $^3L_a$  state (the more negative polarizations corresponded with the phosphorescence peaks and the more positive polarizations with the inflections). If phosphorescence is indeed emitted simultaneously from two states the  $^3L_a$  and  $^3L_b$  state overlap is quite coincidental. This is especially true when one considers the separation between the  $^1L_a$  and  $^1L_b$  states.

The vibrational structure of the cation phosphorescence was more diffuse than that of the neutral species but the essential features, polarizations and data interpretations were the same.

#### VI. Correlations and Summary.

Indazole exhibits an observable energy separation of the  $^1L_a$  and the  $^1L_b$  state. Apparently these two lowest transition moments form an acute angle with each other and lie in the plane of the molecular nuclei. The  $^1L_b \rightarrow ^1A$  transition has the lowest energy. Fluorescence then only emanates from this lower state. The fluorescence spectra has vibronic structure which is difficult to correlate with the corresponding absorption spectrum. Thus one must view correlations between absorption and fluorescence vibronic structure as somewhat temerarious. Since the anion absorption shows a merging of the  $^1L_a$  and  $^1L_b$  bands, emission polarization studies may show dual fluorescent emission similar to that noted for indole.

The absorption and fluorescence data also show that solvent perturbations can yield knowledge about the electronic structure of this

molecule. For indazole it appears that the acidity of the pyrrolic nitrogen is  ${}^1L_a > {}^1L_b > \text{ground state}$  and the basicity of the pyridinic nitrogen is  ${}^1L_b > {}^1L_a > \text{ground state}$ . In addition the permanent dipole moment magnitudes appear to follow the trend  ${}^1L_a > {}^1L_b > \text{ground state}$ .

## BENZIMIDAZOLE

### I. Vapor Absorption Spectra.

One report has been published of the benzimidazole vapor absorption spectrum.<sup>23</sup> Our results were quite similar to those reported by Gordon and Yang with the exception that we obtained more structure to the red and to the blue of their spectrum. We also scanned the  ${}^1L_a$  region of the spectrum. Our spectrum is shown in Figure 10. The  ${}^1L_b \leftarrow {}^1A$  and  ${}^1L_a \leftarrow {}^1A$  transitions are well separated and are centered at 275 and 240 nm respectively. The  ${}^1L_b$  0-0 transition occurs at  $36023\text{ cm}^{-1}$  ( $2772\text{ \AA}$ ) and the  ${}^1L_a$  0-0 transition remains unassigned. Again the  ${}^1L_b$  transition is characterized by the richness of vibrational structure while the  ${}^1L_a$  transition is much broader and has very diffuse vibrational contributions. The mean separation of vibrational groups in the  ${}^1L_a$  transition is  $1064\text{ cm}^{-1}$ . These groups occur at 2266, 2320, 2381, and  $2439\text{ \AA}$ . Vibrational sequences other than the 0-0 sequence for the  ${}^1L_b$  transition begin at 2561, 2610, 2661, and  $2715\text{ \AA}$ . The mean separation between these sequences is  $743\text{ cm}^{-1}$ . An interesting phenomenon was observed in the two lowest energy sequences of the  ${}^1L_b$  transition. The higher energy members of these sequences are actually doublets. There is about an  $11\text{ cm}^{-1}$  separation between the individual peaks comprising each doublet (the higher energy peak of the first member in the  ${}^1L_b$  transition lowest energy sequence was chosen as the  ${}^1L_b$  0-0). The origin of

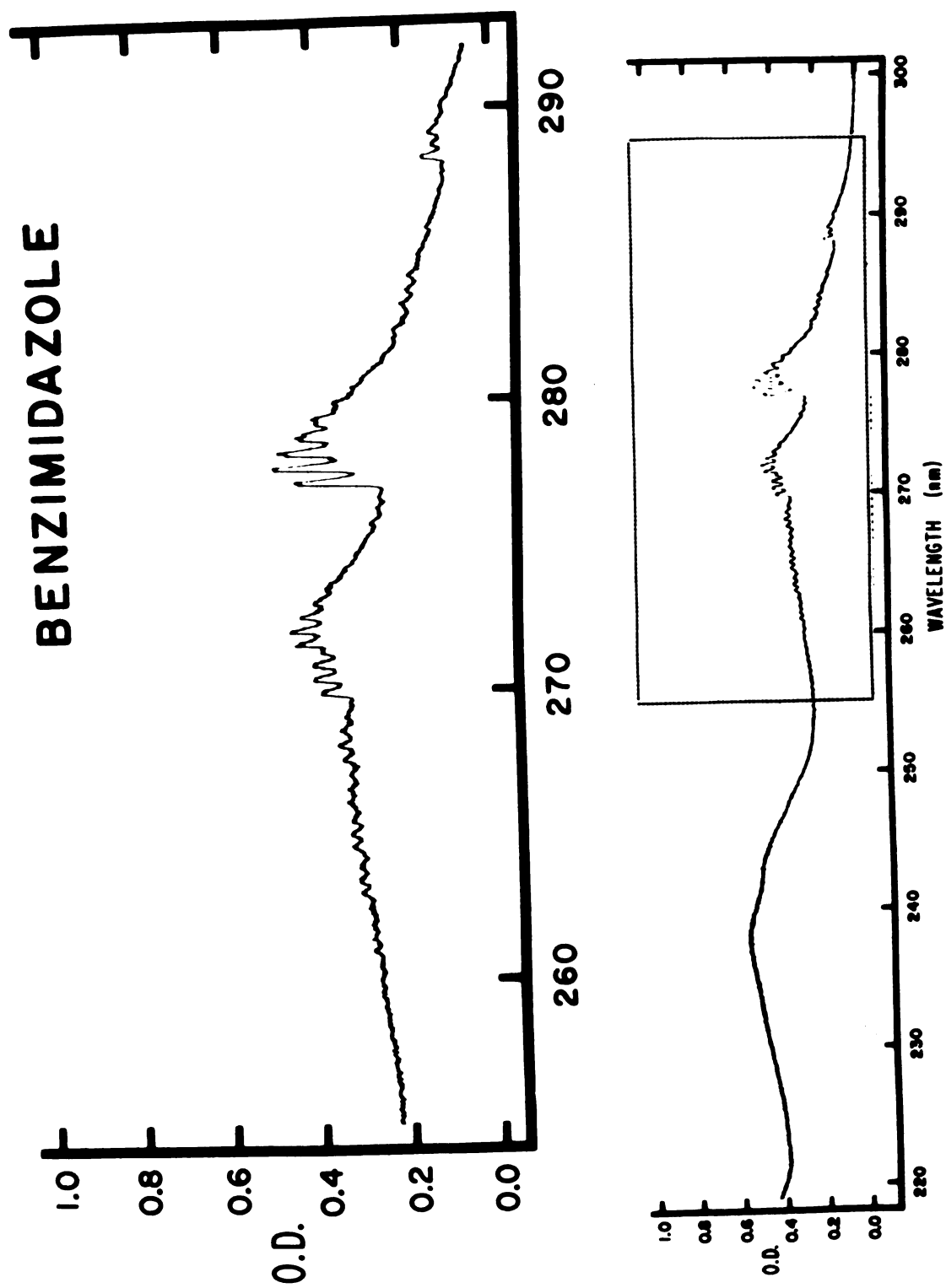


Figure 10. Benzimidazole Vapor Absorption Spectrum.

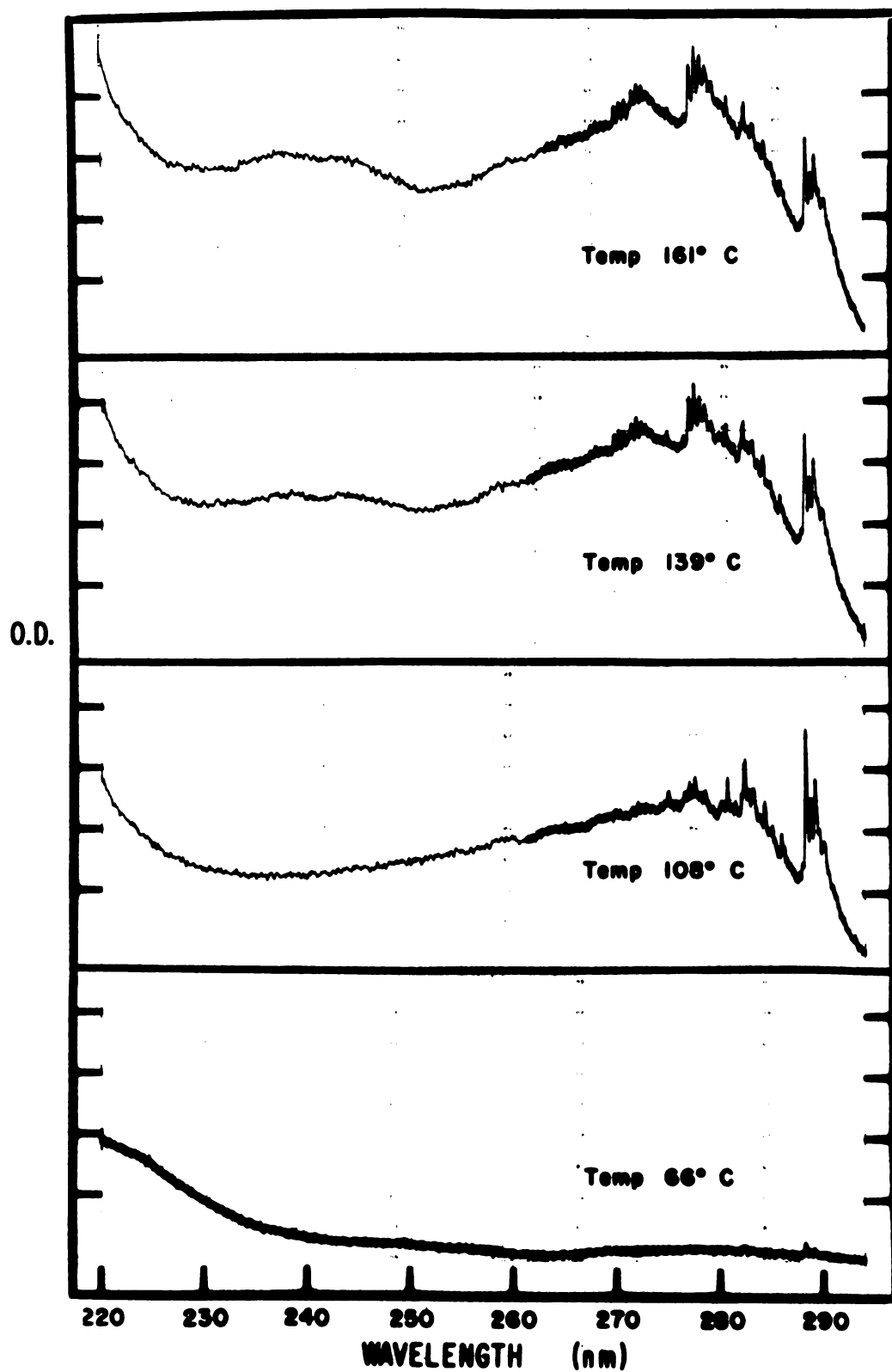


Figure 11. Benzimidazole Vapor Absorption Spectra as a Function of Temperature.

these doublets remains unexplained.

Vapor spectra of benzimidazole at different temperatures were obtained. The results are shown in Figure 11. Again the oscillator strength of the  $^1L_a$  transition increases relative to that of the  $^1L_b$  transition. A vibronic coupling mechanism may be invoked to cause the presumed transition stealing. In addition another curious effect was noted. The first sequence to appear in this analysis occurs  $1377\text{ cm}^{-1}$  to the red of the  $^1L_b$  0-0 transition. This sequence is subsequently overwhelmed by the oscillator strength of the  $^1L_b$  transition as the temperature is increased. It is also present in the "concentrated" vapor absorption spectra but only appears as minor peaks in the  $^1L_b$  0-0 transition sequence. However in polar and nonpolar solvents all vestiges of this sequence are absent. Thus it does not seem that this sequence is due to a solute impurity since this substance should also absorb in dilute solution.

## II. Polarization Measurements of Fluorescence Excitation.

Excitation polarization measurements for benzimidazole were reported by Schutt and Zimmermann<sup>14</sup> in ethanol at  $-180^\circ\text{C}$  and reproduced in our laboratory. The polarization values were slightly negative from 240 to 250 nm, rapidly became increasingly positive to 270 nm and then gradually became more positive to 280 nm. The final polarization value was 0.45. These data show that fluorescent emission emanates from the  $^1L_b$  state and that the  $^1L_a$  transition moment is oriented at an acute angle to the  $^1L_b$  transition moment. This angle is not  $90^\circ$ . In fact our investigations indicate that the angle between transition moments is about  $56^\circ$ . The gradual increase in polarization values from 270 to 280 nm is indicative of some  $^1L_a$  transition character in this

predominantly  ${}^1L_b$  transition portion of the spectrum.

Fluorescence excitation polarization measurements were also made for the benzimidazole cation.<sup>14</sup> Results similar to those described above were obtained so the same interpretations as stated above are sufficient to explain these data.

### III. Solution Absorption Spectra.

The data in Table 7 are again useful for this discussion. Hydrocarbon solvents tend to diffuse the absorption spectrum of benzimidazole relative to the vapor absorption spectrum. In addition there is a slight red-shift in these solvents which can be attributed to dispersive forces.<sup>22</sup> The spectrum in ether shows a further slight red-shift with the  ${}^1L_a$  transition red-shifted more than the  ${}^1L_b$  transition. Since ether can H-bond with the hydrogen on the pyrrolic nitrogen this observation probably means that the pyrrolic nitrogen's  $\pi$ -electronic charge density follows the pattern ground state  $>{}^1L_b > {}^1L_a$ .

In both methanol and ethanol there is a slight blue-shift of the  ${}^1L_b$  transition relative to the spectrum in ether. A slight blue-shift for the  ${}^1L_a$  transition was observed in ethanol compared to ether. These shifts cannot be interpreted in terms of the dipole-dipole interaction since the permanent dipole moment increases to some extent as a result of excitation to either the  ${}^1L_a$  or  ${}^1L_b$  states. This is supported by the red shift observed for both transition bands in going from vapor to hydrocarbon solvent. This shift is due to dipole-induced dipole interactions. The increase of the  ${}^1L_a$  state permanent dipole moment in benzimidazole is probably much smaller than that in indole. The observed blue-shift must be due to another mechanism which more than compensates for the small dipolar interaction red-shift. In addition

the mechanism must compensate for the red-shift produced by solvent H-bonding with the pyrrolic nitrogen's hydrogen which should not differ appreciably from that observed in ether. The mechanism probably involves the influence of the solvent proton on the pyridinic nitrogen's  $\pi$ -electronic charge density. The pyridinic nitrogen's charge density must therefore be smaller in the excited states than in the ground state. This would lead to solvent stabilization of the ground state compared to the  ${}^1L_b$  or  ${}^1L_a$  states giving rise to a blue-shift. When water was utilized as a solvent a further slight blue-shift of both the  ${}^1L_a$  and the  ${}^1L_b$  transitions was observed when compared with the spectra obtained in the alcohols. This further strengthens the contention that there is a stabilizing interaction between a solvent proton and the solute pyridinic  $\pi$ -electronic charge. The further blue-shift only reflects the relative acidity of the water proton compared with the alcoholic proton.

Although it is difficult to make an exact assessment of the relative shifts it appears that the  ${}^1L_b$  transition blue-shifts more than the  ${}^1L_a$  transition when varying the solvent from ether to alcohol to water. One must recall that the shifts are the result of several modes of interaction, namely, dipole-dipole interaction, H-bonding involving the pyrrolic hydrogen and that involving the pyridine nitrogen. Individual effects can be cause antagonistic shifts. Thus only qualitative statements can be made: The dipole-dipole interactions cause red shifts of both bands with the  ${}^1L_a$  transition shifted to a slightly larger extent (3MP vs. vapor spectra). H-bonding with the pyrrolic hydrogen causes a red shift (ether vs. 3MP spectra) indicating that the hydrogen is slightly more acidic in the  ${}^1L_a$  and  ${}^1L_b$  states.

The acidity is greater in the  ${}^1L_a$  state. H-bonding with the pyridinic nitrogen causes a blue shift (alcohol vs. ether) indicating a smaller charge density at the pyridinic nitrogen in both the  ${}^1L_a$  and  ${}^1L_b$  states. The smaller blue shifts for water vs. alcohol (relative to alcohol vs. ether) is a reflection of a greater dipole-dipole interaction red shift in the more polar solvent. The smaller blue shifts (relative to ether) for the  ${}^1L_a$  state is a reflection of a larger dipole moment for that state compared with the moment of the  ${}^1L_b$  state. One may conclude then that the pyrrolic nitrogen charge density pattern is  ${}^1A > {}^1L_b > {}^1L_a$  and the  $\pi$ -electron pattern for the pyridinic nitrogen is  ${}^1A > {}^1L_a > {}^1L_b$ .

In acidic media a still further blue-shift is observed for the  ${}^1L_a$  and  ${}^1L_b$  transitions. The  ${}^1L_b$  transition again shifts more than the  ${}^1L_a$  transition. The same explanations as proposed above fit these data. The benzimidazole cation also exhibits an oscillator strength diminution of the  ${}^1L_a$  transition compared with the results obtained in the previously discussed solvents. The  ${}^1L_b$  transition oscillator strength remained visibly unaffected. It is tempting to link this result with the anomalous vapor phase  ${}^1L_a$  transition oscillator strength alterations which were temperature induced. Such spectral similarities should not go unnoticed and a vibronic stealing mechanism should at least be contemplated. However it must be pointed out that the cation is in some respects a different species from the neutral molecule.

The anion of benzimidazole exhibits a radically different absorption spectrum than the spectra previously discussed. This spectrum together with those of the cation and neutral species are shown in Figure 12. The anion spectrum is quite similar to that reported for indazole. The  ${}^1L_a$  transition is less intense and apparently merges with the  ${}^1L_b$



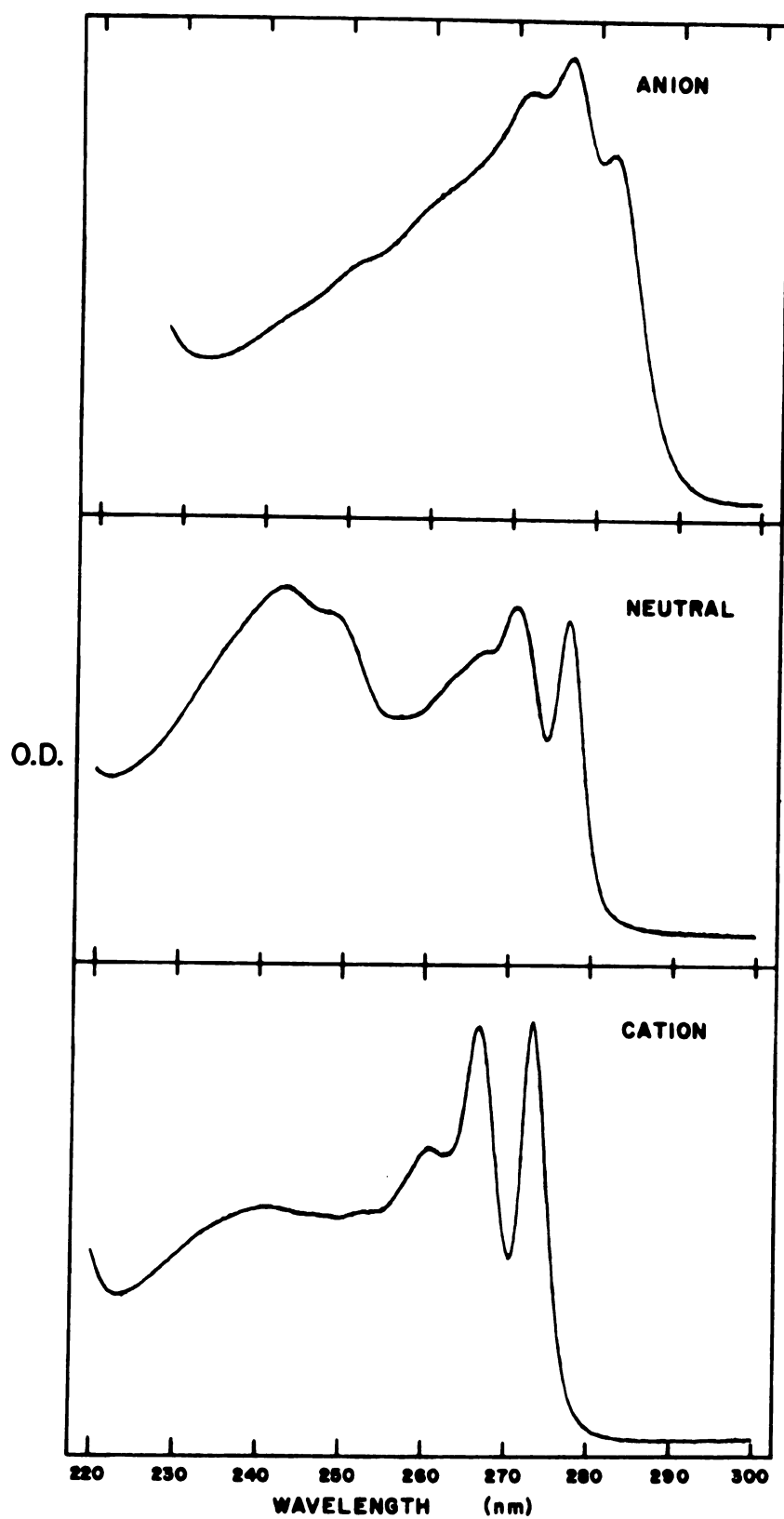


Figure 12. Benzimidazole Absorption Spectra in Basic, Neutral and Acidic Solution.

transition. In turn the  ${}^1L_b$  transition vibrational structure differs from its analogues in the other media. Both transitions exhibit the expected red-shift which has been purported for the previous molecules to be a result of the anion negative charge on the  $\pi$ -electron structure. The resultant Coulombic repulsion presumably causes some destabilization of the  $\pi$ -electron structure which is manifested as a red-shift. The different spectral profile of the anion probably reflects the fact that this species differs somewhat from the neutral molecule and cation.

#### IV. Fluorescence Spectra.

Benzimidazole fluorescence exhibits some vibrational structure. It also exhibits a relatively small Stokes' shift which indicates that the emitting excited state is not solvent-stabilized to any extent compared with the ground state. Thus the emitting state (probably  ${}^1L_b$ ) permanent dipole moment is not much larger than the ground state's moment. This correlates well with the interpretation proffered for the relative shifts observed in various solvents.

The solvent-induced shifts in the fluorescence spectra parallel those shifts observed in the absorption spectra for 3-methylpentane, ether, alcohol and water. The spectrum in water at room temperature is shown in Figure 13 together with spectra obtained in basic and acidic media. Again it is noted that the fluorescence is species specific.

Emission polarization data<sup>14</sup> in alcohol at  $-180^\circ\text{C}$  verified that the  ${}^1L_b$  state fluoresces in the neutral molecule. A slightly negative flat polarization resulted when excitation was monitored at 240 nm which is in the  ${}^1L_a$  transition band. However the results were somewhat different for the cation. Excitation at 265 nm, which is predominantly comprised of the  ${}^1L_b$  transition, resulted in a polarization

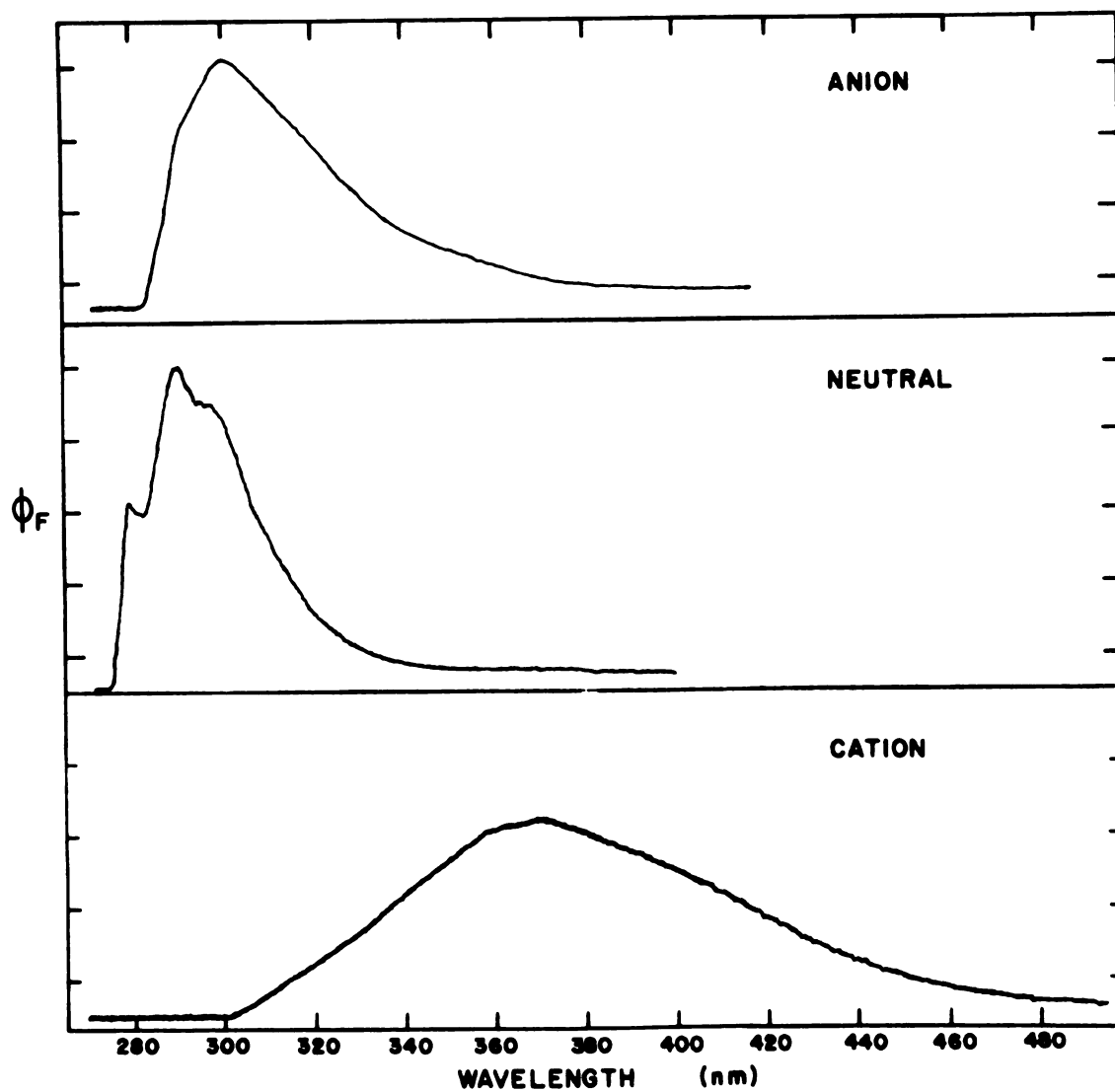


Figure 13. Benzimidazole Fluorescence Spectra in Basic, Neutral and Acidic Solution.

spectrum which was initially flat and positive at shorter fluorescent wavelengths but became less positive toward longer wavelengths. My data at room temperature show only a broad fluorescence peak at 370 nm for the cation. This suggests that Schutt and Zimmermann have not obtained spectra for the cation at all! They probably were making observations with the neutral species.

#### V. Phosphorescence Spectra.

The phosphorescence spectrum in ethanol at 77°K was obtained in our laboratory is shown in Figure 14. It differs from the spectrum reported by Schutt and Zimmermann.<sup>14</sup> The phosphorescence 0-0 occurs at 374 nm. Other peaks appear at 386, 394, 398, and 420 nm. Inflections appear at 407, 414, 425, and 440 nm. Polarization data were obtained by Schutt and Zimmermann and show that the phosphorescence is polarized predominantly out-of-plane relative to the molecular topology. When they excited at 279 nm (the  $^1L_b$  transition) the emission polarization was slightly negative from 250 to 280 nm. These data strongly suggest that the phosphorescence transition oscillator is not oriented exactly perpendicular to the molecular plane but instead lies at some acute angle to this plane.

The cation emission reported by Schutt and Zimmermann was remarkably similar to phosphorescence from the neutral molecule. The general appearance, peak and inflection positions, emission polarization and excitation polarization were hardly distinguishable between these species. This is surprising since both the absorption and fluorescence spectra exhibited a blue-shift. They probably were performing measurements on the neutral molecule so no differences should be seen.

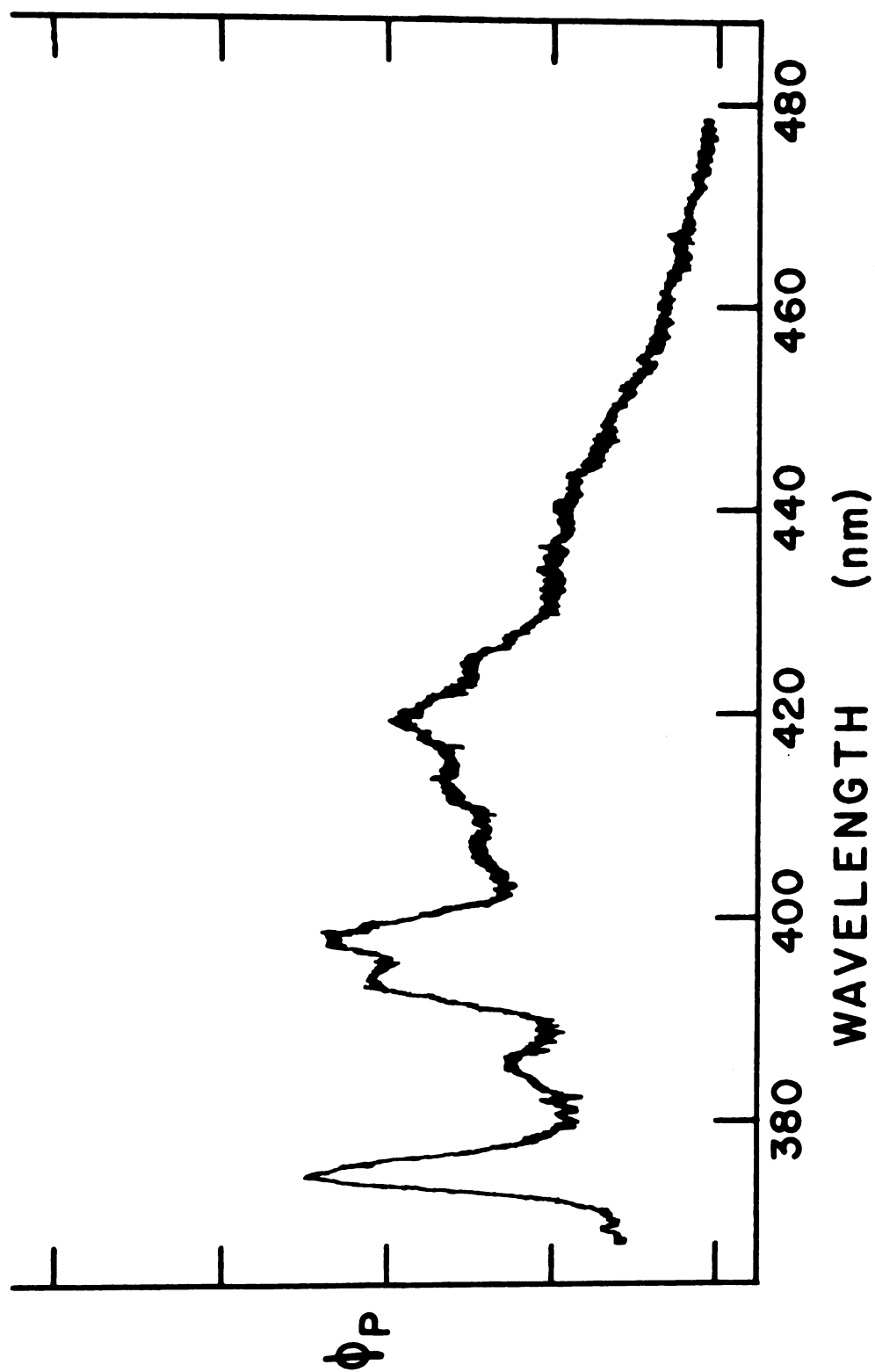


Figure 14. Benzimidazole Phosphorescence in Ethanol at 77° K.

## VI. Theoretical Calculations.

Results of these calculations are shown in Table 8 and Figure 15. Using the criteria of permanent dipole moment magnitudes, transition moment orientations and oscillator strengths the first excited state was assigned as  ${}^1L_b$  and the second excited state as  ${}^1L_a$ . Of these criteria the transition moment orientation was of little use since both moments were oriented at approximately the same angle from the principal axes. The orientation of these transition moment axes is neither parallel to the principal axes nor at right angles to each other. These two lowest singlet transitions are calculated to be energetically close to each other. However it should be recalled that accuracy to within 0.1 eV is considered quite good. The ionization potential and electron affinity are calculated to be 7.2 eV and 1.8 eV respectively. Both excited states are predicted to have larger internuclear distances than the ground state. Charge density results predict the pyrrolic nitrogen's acidity is  ${}^1L_a > {}^1L_b > \text{ground state}$  and the pyridinic nitrogen's basicity is calculated to be  $\text{ground state} > {}^1L_b > {}^1L_a$ .

## VII. Correlations and Summary.

The solution and vapor absorption spectra analysis, polarization data and the computational results all correlate to assign the  ${}^1L_b \leftarrow {}^1A$  transition below the  ${}^1L_a \leftarrow {}^1A$  transition. The energy separation between these transitions is not definitely established. Certainly the main spectral features of each transition are well separated except possibly for the anion. However the polarization data suggest there is some  ${}^1L_a$  transition character at least down to 275 nm in solution. The calculations also predict a small transition energy separation.

Table 8. Calculation Results for the Azaindoles.

Benzimidazole				
Trans. Energy ( $\text{cm}^{-1}$ )	Trans. Energy (nm)	Trans. Moment (Debyes)	Trans. Polar (deg. from x-axis*)	f
36094	277.0	0.420	32	0.069
37424	267.2	0.620	-40	0.156
48019	208.2	1.048	89	0.572
49637	201.5	0.539	31	0.156
4-azaindole				
34788	287.4	0.513	13	0.099
36418	274.6	0.535	-62	0.113
47464	210.7	0.965	-72	0.480
49394	202.4	0.746	48	0.298
5-azaindole				
35790	279.4	0.579	- 9	0.130
36914	270.9	0.406	-53	0.066
47065	212.5	0.670	-88	0.229
49082	203.7	0.941	62	0.472
6-azaindole				
35245	283.7	0.585	0.10	0.131
37373	267.6	0.420	-45	0.071
46975	212.9	0.601	-74	0.184
49994	200.2	0.512	41	0.142
7-azaindole				
34955	286.1	0.551	- 9	0.115
36268	275.7	0.483	-77	0.092
47936	208.6	0.813	-69	0.344
49078	203.8	0.705	53	0.264

\* The x-axis parallels the short axis of the molecule.

Table 8 (cont'd.)

Trans. Energy ( $\text{cm}^{-1}$ )	Trans. Energy (nm)	Trans. Moment (Debyes)	Trans. Polar (deg. from x-axis*)	f
4-azabenzimidazole				
35568	281.2	0.468	52	0.085
37131	269.3	0.590	-43	0.140
48483	206.3	1.177	-78	0.729
49701	201.2	0.614	30	0.203
5-azabenzimidazole				
36565	273.5	0.318	34	0.040
37330	267.9	0.639	-35	0.165
47972	208.4	0.991	78	0.511
49727	201.1	0.485	34	0.127

\* The x-axis parallels the short axis of the molecule.



Table 8 (cont'd.)

Benzimidazole		
Molecular State	Perm. Dipole Moment	Perm. Moment Polar. (deg. from x-axis*)
Ground	4.14	-34
1st Excited	5.50	-58
2nd Excited	8.28	-54
7-azaindole		
Ground	3.57	-36
1st Excited	8.92	-71
2nd Excited	5.25	-46

\*The x-axis parallels the short axis of the molecule.

Figure 15. Calculated Charge Densities and Bond Lengths for Benzimidazole.

Legend:

Numbers at each atomic position denote  $\pi$ -electron charge densities in electron units.

Numbers at each bond denote bond lengths in Angstroms.

The top number corresponds to the ground state.

The middle number corresponds to the first excited singlet state ( $^1L_b$ ).

The bottom number corresponds to the second excited singlet state ( $^1L_a$ ).

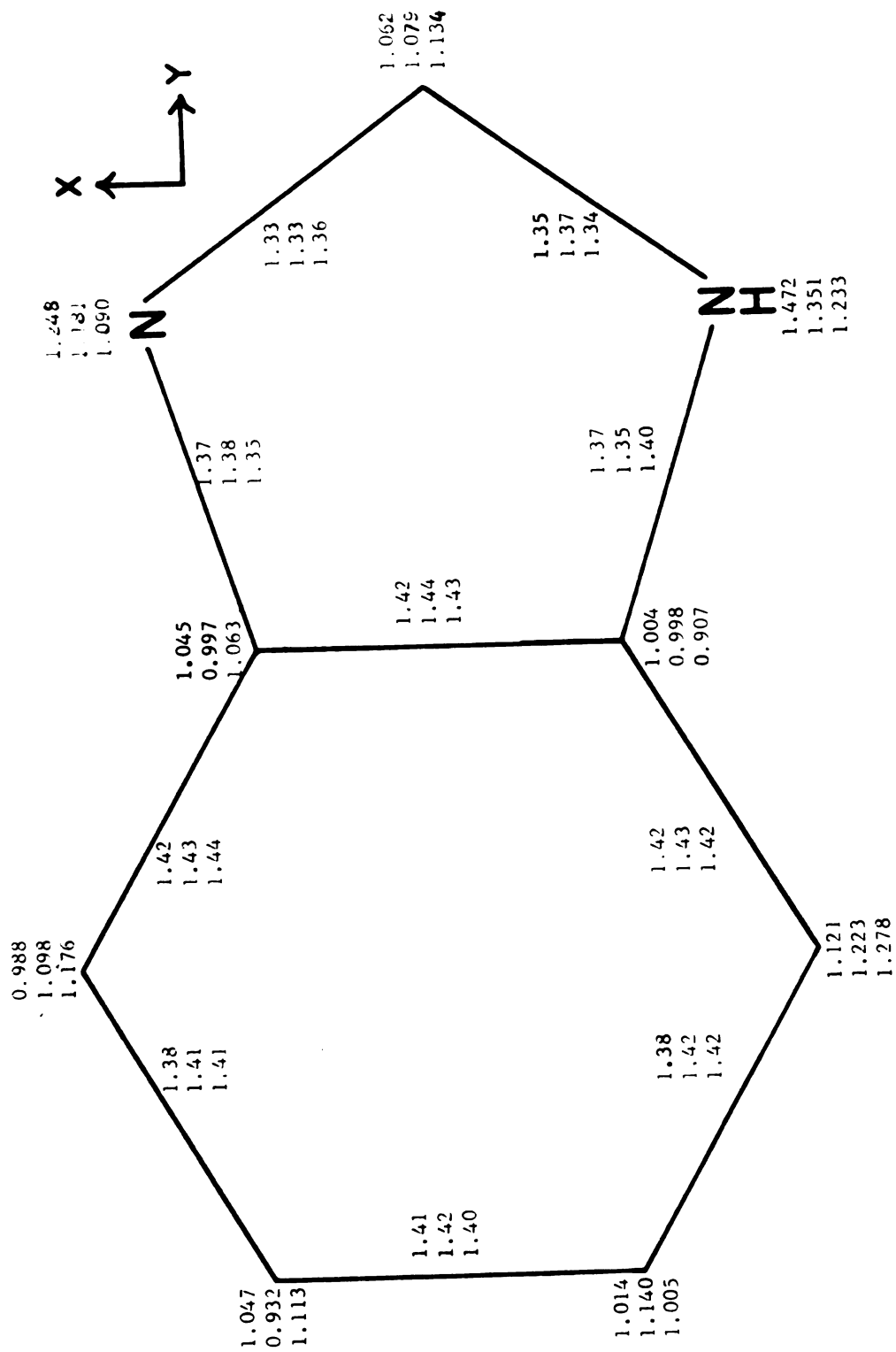


Figure 15.

The two lowest singlet transition moments are not oriented at right angles to each other and neither one lies parallel to either of the principal axes of Figure 15. The calculated angle between these moments is  $70^\circ$  and an analysis of the polarization data indicates the angle is  $56^\circ$ . This is a remarkably good correlation considering the difficulties involved in obtaining each value. These results are not surprising when one considers the lack of symmetry this molecule possesses. The polarization data indicate that the phosphorescence transition moment is primarily out-of-plane but not perpendicular to it.

Fluorescence emanates from the  $^1L_b$  state for the neutral molecule. This fact is exemplified by the polarization data. For the charged species it is difficult to make such positive statements. The acidity of the pyrrolic hydrogen follow the order  $^1L_a > ^1L_b > ^1A$  which is consistent with the  $\pi$ -electron charge density values calculated at the pyrrolic nitrogen. In addition the calculated prediction of the pyridinic nitrogen basicity being more in the ground state than in the excited states correlates well with the solvent shifts. The basicity follows the order ground state  $> ^1L_b > ^1L_a$ .

The calculated permanent dipole moments also correlate well with the observed solvent shifts. The permanent dipole moment magnitudes are  $^1L_a > ^1L_b > \text{ground state}$ . Thus in polar solvents the  $^1L_a$  transition is predicted to red-shift more than the  $^1L_b$  transition. The observed red-shift in going from vapor to 3MP and in going from 3MP to ether correlates with the pyrrolic nitrogen  $\pi$ -electron charge density being lower in the excited states than in the ground state. The observed absorption and fluorescence shifts in alcohol, water and acidic media correlate with the calculations when the dipolar interaction vs. proton-

$\pi$ -electron interaction are both taken into consideration. Thus the solvent protons interact with the pyridinic and possibly the pyrrolic nitrogens'  $\pi$ -electronic charge to cause a blue-shift. This is opposed by the dipole-dipole interactions which tend to red-shift the  $^1L_a$  transition more than the  $^1L_b$  transition. The result is a blue-shift of both transitions with the  $^1L_b$  transition blue-shifted more than the  $^1L_a$  transition. Since the pyridinic nitrogen contains a lone pair of electrons it seems reasonable to assume that most of the proton- $\pi$ -electron interaction occurs at this site.

Benzimidazole also exhibited the fact that vibronic energy spacings were not identical between homologous members in absorption and emission spectra. This again supports the view that quantitative correlations between absorption and fluorescence spectra are tenuous. The relatively small Stokes' shift between absorption and fluorescence correlates with the small difference between the permanent dipole moments of the ground and emitting  $^1L_b$  state. This adds credence to our ability to predict Stokes' shifts based on calculated permanent dipole moments. Finally the anomalous behavior of the vapor absorption data as a function of temperature evoke our ubiquitous vibronic coupling scheme as a possible explanation.

#### 4-AZAINDOLE

##### I. Absorption and Fluorescence Spectra.

The few data which have been reported for these spectra are tabulated in Table 7. One can see that the absorption spectrum of the cation is red-shifted compared with the spectrum of the neutral molecule in water. The fluorescence data exhibit a definite red-shift when comparing the water spectrum with that in ethanol. There also seems to be a further slight red-shift when the cation is formed. All these

fluorescence spectra are at longer wavelengths than those of the azaindoles previously discussed. These spectral positions are reminiscent of those observed in indole.

## II. Theoretical Calculations.

The results of these calculations are shown in Table 8. Based on the transition moment orientations and the oscillator strengths the first and second excited states remain unassigned. The first two transitions lie energetically fairly close and their transition moments are mutually oriented about  $90^\circ$  to each other according to the predictions. Neither moment is calculated to be parallel to a primary molecular axis. Permanent dipole moments and charge densities were not computed for this molecule except for the ground state. The ionization potential and electron affinity were calculated to be 7.1 eV and 1.7 eV respectively.

## III. Correlations and Summary.

Since the amount of experimental data is so scarce any correlations would be more speculative than even I would consider.

### 5-AZAINDOLE

## I. Absorption and Fluorescence Spectra.

Table 7 again shows a paucity of data for this molecule. There seems to be a red-shift of the absorption spectrum of the cation relative to the absorption spectrum of the neutral species. A moderate Stokes' shift is noted in ethanol, water, and acid. The water fluorescence is red-shifted relative to the ethanol emission and the cation is apparently slightly further red-shifted.

## II. Theoretical Calculations.

The results are again shown in Table 8. The transition moment orientations and the oscillator strengths both agree with the assignment

of  $^1L_a$  as the first singlet excited state and  $^1L_b$  as the second singlet excited state. These two states are predicted to lie energetically quite close to each other. Their transition moments are calculated to lie about  $45^\circ$  from each other and neither moment parallels a molecular principal axis. The ionization potential and electron affinity are predicted to be 7.1 eV and 1.8 eV respectively. Neither the excited state permanent dipole moments nor  $\pi$ -electron charge densities were calculated.

### III. Correlations and Summary.

Again the scarcity of experimental data eliminates any correlative conclusions.

## 6-AZAINDOLE

### I. Absorption and Fluorescence Spectra.

Table 7 depressingly again shows a dreadful dearth of data. There is an apparent red-shift of the cation absorption when compared with absorption by the neutral species. A very large Stokes' shift is noted for this molecule in polar solvents. There is a slight absorption spectrum red-shift from ethanol to water and a slight blue-shift from water to acid. The large Stokes' shift is very suggestive of a quite large emitting state permanent dipole moment.

### II. Theoretical Calculations.

Table 8 again shows the results of these calculations. Based on the transition moment orientations and the oscillator strengths the energetically lowest singlet excited state is assigned as  $^1L_a$  and the next excited state as  $^1L_b$ . Their energetic separation is not large. The two transition moments are predicted to lie about  $45^\circ$  relative to each other. Neither moment is calculated to lie parallel to a

primary molecular axis. The excited state permanent dipole moments and their  $\pi$ -electron charge densities were not calculated. The ionization potential and electron affinity are respectively predicted to be 7.1 eV and 1.8 eV.

### III. Correlations and Summary.

Due to the absence of data again correlations will not be attempted.

## 7-AZAINDOLE

### I. Vapor Absorption Spectra.

Figure 16 shows the vapor absorption spectrum of 7-azaindole. This spectrum is quite similar to the vapor spectrum of indole. The  ${}^1L_a \leftarrow {}^1A$  and  ${}^1L_b \leftarrow {}^1A$  transition envelopes significantly overlap each other. Rich vibrational structure characterizes the  ${}^1L_b$  transition while the  ${}^1L_a$  transition has broad diffuse structure. The transition overlap appears to be worse for 7-azaindole than for indole; that is a visual separation of these two transitions is more difficult to perform for 7-azaindole than for indole. Due to this more apparent transition merging it seems likely that the  ${}^1L_a$  0-0 transition is energetically below the  ${}^1L_b$  0-0 transition. The only report in the literature assigned the  ${}^1L_b$  0-0 at  $34676\text{ cm}^{-1}$  ( $2883\text{ \AA}$ ) and the  ${}^1L_a$  0-0 at  $34414\text{ cm}^{-1}$  ( $2905\text{ \AA}$ ).<sup>8</sup> The method used by these authors to assign the  ${}^1L_a$  0-0 was discussed in the indole Vapor Absorption Spectra section together with my comments about the applicability of this method. Our analysis places the  ${}^1L_b$  0-0 at  $34636\text{ cm}^{-1}$  ( $2888\text{ \AA}$ ) and leaves the  ${}^1L_a$  0-0 unassigned since I believe no suitable procedure has been discovered for making the latter assignment.

The 7-azaindole vapor spectrum exhibited an effect similar to one noted for benzimidazole: the three lowest energy sequences in the  ${}^1L_b$



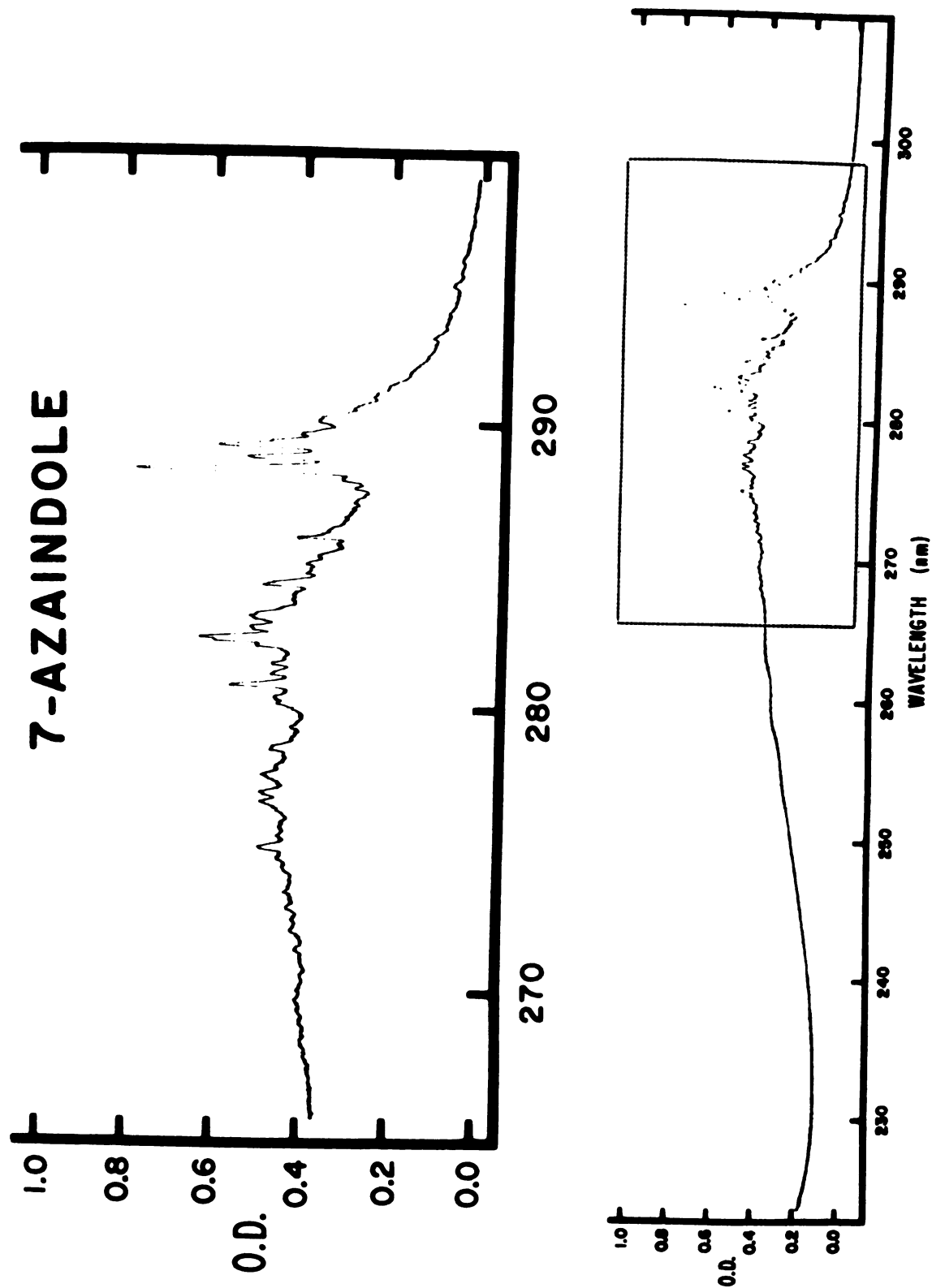


Figure 16. 7-Azaindole Vapor Absorption Spectrum.

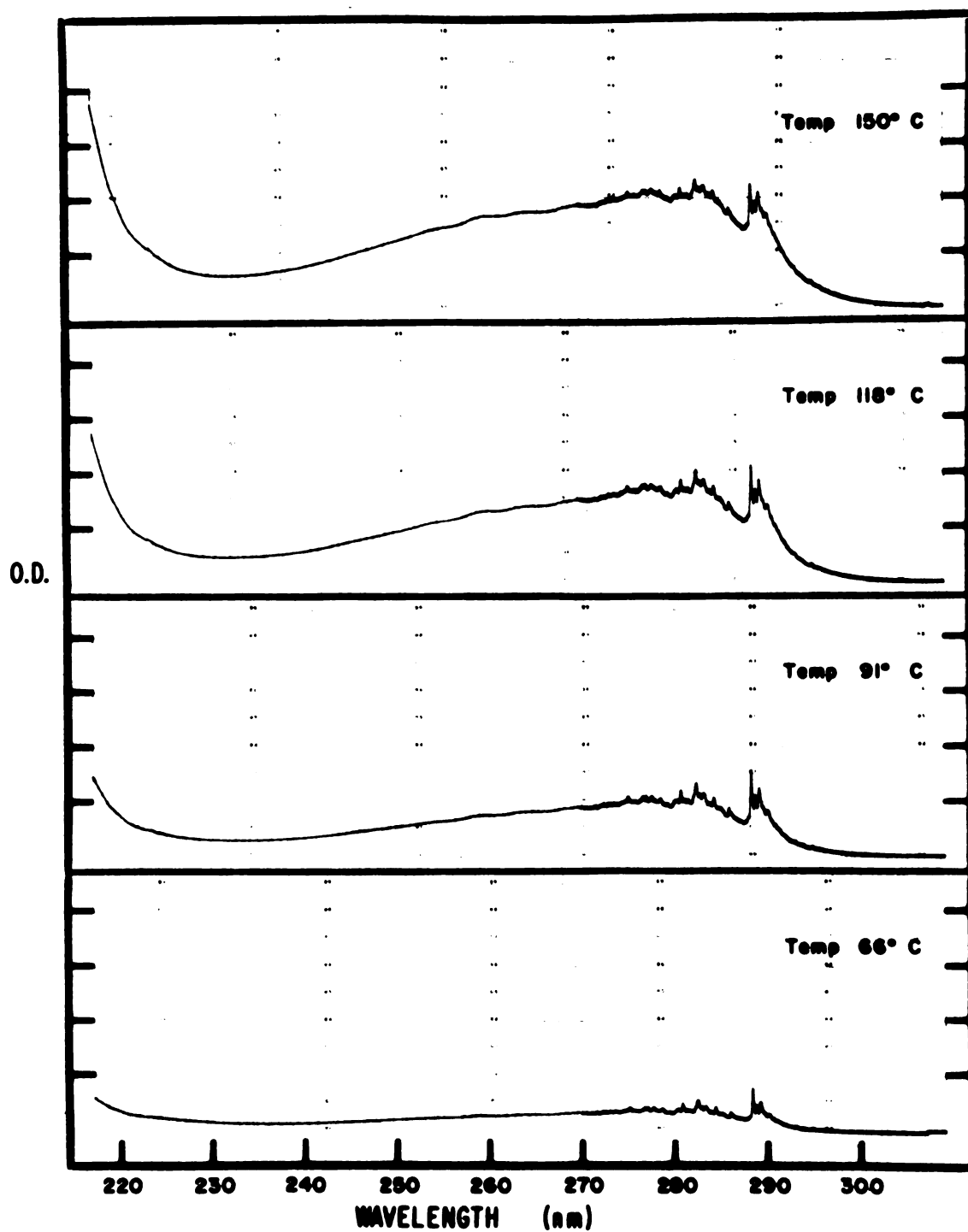


Figure 17. 7-Azaindole Vapor Absorption Spectra as a Function of Temperature.

transition contained doublets for the high energy members of these sequences. The separation between individual peaks comprising each doublet varied but for the  ${}^1L_b$  0-0 sequence the average separation was  $5\text{ cm}^{-1}$ . For this sequence the higher energy peak of the highest energy member was chosen as the  ${}^1L_b$  0-0 transition. Again the origin of these doublets remains unexplained. A reasonably consistent sequence progression (separation of sequences) was noted for the  ${}^1L_b$  and  ${}^1L_a$  transitions. For the  ${}^1L_b$  transition the energy separation is  $706\text{ cm}^{-1}$  which places the beginning of sequences at 2719, 2772, 2826 Å as well as 2888 Å for the 0-0 sequence. The  ${}^1L_a$  transition vibrational group separation is  $723\text{ cm}^{-1}$  with groups occurring at 2545, 2591, 2641, and 2693 Å. There undoubtedly are other groups at lower energies but their topography is masked by the superimposed  ${}^1L_b$  transition. Thus it is difficult to judge that a  ${}^1L_a$  transition sequence lies energetically below the  ${}^1L_b$  0-0 sequence.

A series of vapor spectra were taken as a function of temperature and are shown in Figure 17. A hot band analysis confirmed the  ${}^1L_b$  0-0 transition at  $34636\text{ cm}^{-1}$ . In addition the  ${}^1L_a$  transition oscillator strength increased with temperature relative to the  ${}^1L_b$  transition oscillator strength. Again we are confronted with this anomalous transition behavior. It seems natural to invoke the coupling mechanism between vibronic states to explain the anomaly. The mechanism could cause the  ${}^1L_a$  transition to become more "allowed" through intensity borrowing from another transition.

## II. Solution Absorption Spectra.

The data in Table 7 provide the information used in this discussion. In 3-methylpentane the absorption spectrum is again more diffuse

and has lost much of the vibrational character evident in the vapor phase. There is also a slight red-shift of both the  ${}^1L_a$  and  ${}^1L_b$  transition in this solvent. This shift is probably due to the dispersive forces manifested in solvents.<sup>22</sup> In ether both transitions are further red-shifted. This is indicative of an effect caused by H-bonding, probably at the pyrrolic nitrogen. The red-shifts indicate that this nitrogen is more acidic in the excited than in the ground states.

The spectral shifts observed in ethanol, water, and acidic media are much more puzzling. In ethanol both transitions are further red-shifted. The  ${}^1L_a$  transition is shifted more than the  ${}^1L_b$  transition but both shifts are comparatively slight. There are now three different interactions which must be taken into account. The first interaction is H-bonding which occurs at the pyridinic as well as the pyrrolic nitrogen. The H-bonding effect involving the pyrrolic hydrogen should not differ significantly from that observed in ether solution. The further red shift observed when comparing the spectra in ethanol to that in ether is therefore attributed to the pyridinic nitrogen solvent H-bonding. A second possible interaction is the effect of an acidic proton on the  $\pi$ -electron charge which resides at the pyrrolic and pyridinic nitrogens. Although this interaction may also occur at other nuclear centers the effects of these interactions will not be as pronounced as the effects at the nitrogens. The spectral shifts produced by this interaction will be the same at the pyridinic nitrogen as that produced by H-bonding at this nitrogen. However at the pyrrolic nitrogen the solvent proton  $\pi$ -electron interaction will produce a spectral shift opposite that due to H-bonding at this nitrogen. The third interaction consists of the solvent dipole's effect on the

permanent dipole of the solute molecule's ground and excited states. The red shifts observed in going from vapor to hydrocarbon solvents indicate that the permanent dipole moment increases as a result of excitation to the  ${}^1L_a$  and  ${}^1L_b$  states. This is particularly true for excitation to the  ${}^1L_a$  state. One would therefore expect that the dipole-dipole interaction in polar solvents causes a red shift. The observed shifts in ethanol are probably predominantly due to the dipolar interactions. Since the  ${}^1L_a$  transition is shifted more than the  ${}^1L_b$  transition the permanent dipole moments would then follow the trend  ${}^1L_a > {}^1L_b > \text{ground state}$ . The small observed shifts in going from ether to alcohol can be explained in terms of an increased dipole-dipole interaction in the more polar ethanol.

In water the  ${}^1L_a$  and  ${}^1L_b$  transitions are blue-shifted relative to the spectrum in alcohol. The  ${}^1L_a$  transition is shifted more than the  ${}^1L_b$  transition. These shifts are probably due to the higher acidity of the water proton compared with the acidity of ethanol. This causes a blue shift as a result of a solvent hydrogen interaction with the  $\pi$ -electron charge density at the pyrrolic nitrogen. Dipole-dipole interactions would cause a larger red shift in the more polar water compared with the spectrum in ethanol. Thus the magnitude of the blue shift must exceed such red shifts.

Although the water proton induced a blue-shift the spectrum in an acid medium displayed a red-shift. It seems to indicate there are two loci for solvent proton interactions which provide antagonistic spectra shifts. The likely position for the interaction causing the blue-shift is at the pyrrolic nitrogen. The  $\pi$ -electronic charge there was hypothesized to be less in the ground than in the excited states to explain

the ether induced red-shift via H-bonding. Thus a solvent proton- $\pi$ -electron interaction at this nitrogen would be manifested as a blue-shift. The red-shift observed in an acidic medium could be due to an interaction at the pyridinic nitrogen. This scheme necessitates the excited states  $\pi$ -electron density to exceed the ground state density at the pyridinic nitrogen.

A curious aspect of this analysis is the blue-shift observation in water compared with ethanol and acid. Similar shifts were observed for indazole. The small red-shift observed in ethanol relative to ether is probably due to the dominance of the dipolar interactions as well as aza-nitrogen H-bonding over the blue-shift produced by the proton- $\pi$ -electron interaction at the pyrrolic nitrogen. In water the slightly more acidic proton interacts preferentially with the  $\pi$ -electronic charge at the pyrrolic nitrogen to cause the blue-shift. This effect dominates the other effects causing a blue shift relative to ethanol. When the medium becomes acidic the protons interact with the pyridinic nitrogen  $\pi$ -electronic charge. In addition there are dipole-dipole interactions with the net result of a red-shift.

The fact that subtle changes in solvent acidity cause drastic differences in the solvent induced spectral shifts indicates that this molecule possesses an unusual spectral instability toward solvent protons. Further evidence of the increased acidity of the pyrrolic hydrogen as a result of excitation is manifested by the excited state proton tautomerization which was reported to occur for 7-azaindole.<sup>59</sup>

### III. Fluorescence Spectra.

In all solvents the 7-azaindole fluorescence was broad band and exhibited some vibrational structure especially at low temperatures.

There was a large Stokes' shift observed in all solvents which indicates that the emitting state permanent dipole moment is much larger than the ground state permanent dipole moment. The emitting state is assigned as  $^1L_a$  on the basis of the vapor absorption data. The fluorescence is progressively red-shifted through the solvent sequence 3-methylpentane, ether, ethanol, water and acid. Although fluorescence was sought in a basic solvent none was observed. This means that efficient quenching via some radiationless route occurs for the anion. The emission in acid is probably due to fluorescence from the cation whose emitting state is stabilized at the pyridinic nitrogen by the protons. However the other solvents are ordered by increasing dipole moment. This indicates that the progressive Stokes' shifts are primarily induced by dipolar interactions. The emission in water is red-shifted relative to the ethanol spectrum while the absorption is slightly blue-shifted. This dissimilarity further emphasizes the predominant importance of the dipole-dipole relaxation effects in the Stokes' shifts. This reflects the large disparity between the emitting and ground state permanent dipole moments in 7-azaindole.

As mentioned in the prior section 7-azaindole exhibits a unique photo-induced proton tautomerization which leads to emission from a new species. This fluorescence occurs at 480 nm in 3-methylpentane or ethanol and is broad band. It exhibits some vibrational structure at low temperatures. This emission is not observed in dilute ether solutions nor in water. The lack of fluorescence in water remains unexplained. The green emission presumably occurs when a hydrogen atom is attached to pyridinic nitrogen and one is removed from the pyrrolic

nitrogen leading to an electronic rearrangement in the molecule. This phenomenon is quite unusual and demonstrates the unique electronic structure and reactivity of this molecule's excited state.

#### IV. Theoretical Calculations.

Results of these calculations are shown in Table 8 and Figure 18. The permanent dipole moment magnitudes, transition moment orientations and oscillator strengths all predict the lowest singlet excited state is  $^1L_b$ . These transition moments do not parallel a primary molecular axis and are predicted to lie at a  $70^\circ$  angle to each other. The permanent dipole moment of the  $^1L_a$  state is calculated to have a much larger magnitude than the moment of the ground state. The two transitions are predicted to be energetically close to each other. For the pyrrolic nitrogen the acidity follows the trend  $^1L_a > ^1L_b > \text{ground state}$ . For the pyridinic nitrogen the basicity follows the trend  $^1L_a > ^1L_b > \text{ground state}$ . The charge density difference is quite sizeable between the ground and  $^1L_a$  states at the pyrrolic nitrogen. This difference is much larger than between the ground and  $^1L_b$  states at the pyrrolic nitrogen as well as between the ground and either the  $^1L_a$  or the  $^1L_b$  states at the pyridinic nitrogen. The internuclear distances do not vary appreciably between the ground and either excited state. Finally the ionization potential and electron affinity are calculated to be 7.1 eV and 1.8 eV respectively.

#### V. Correlations and Summary.

The calculations predict and the vapor absorption data allude to the  $^1L_a \leftarrow ^1A$  transition lying energetically below the  $^1L_b \leftarrow ^1A$  transition. Fluorescence of the solvated molecule emanates from the  $^1L_a$  state. The transition moments of the  $^1L_a$  and  $^1L_b$  states are probably oriented at an



Figure 18. Calculated Charge Densities and Bond Lengths for 7-Azaindole.

Legend:

Numbers at each atomic position denote  $\pi$ -electron charge densities in electron units.

Numbers at each bond denote bond lengths in Angstroms.

The top number corresponds to the ground state.

The middle number corresponds to the first excited singlet state ( $^1L_a$ ).

The bottom number corresponds to the second excited singlet state ( $^1L_b$ ).

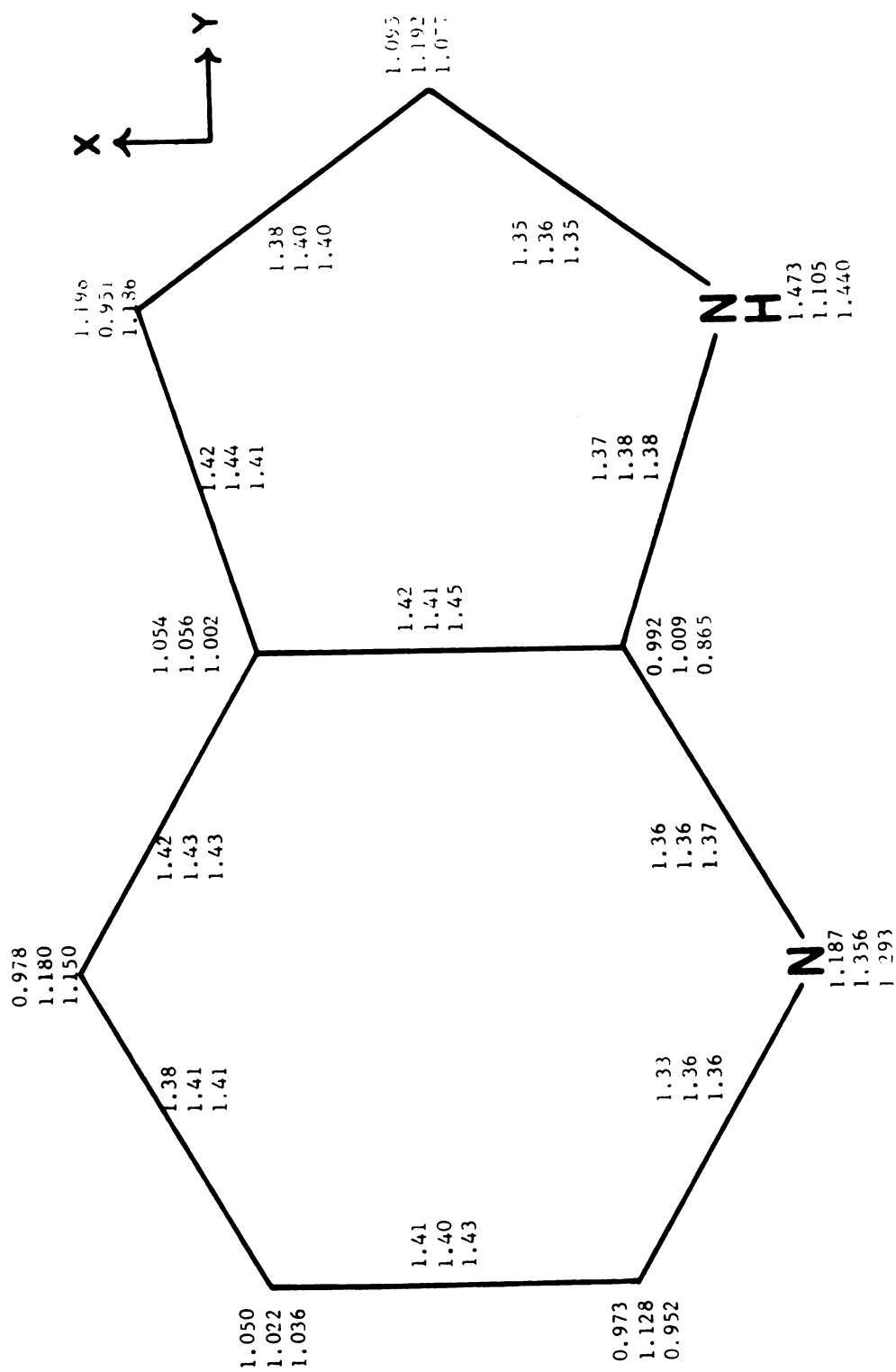


Figure 13.

acute angle relative to each other and neither moment is expected to parallel a molecular primary axis. The calculated permanent dipole moments of the ground and excited states correlate well with the observed Stokes' shifts. The permanent dipole moments appear from the observed solvent shifts to follow the sequence  ${}^1L_a > {}^1L_b > \text{ground state}$ . This sequence is also predicted by the calculations. Thus the solvent dipole moment interacts strongly with the  ${}^1L_a$  state moment to produce the experimentally noted Stokes' shifts. This interaction seems to be the dominant influence governing the shifts in various solvents.

The calculated charge densities for the ground and excited states also correlates quite well with the absorption spectra shifts observed between solvents. It appears that H-bonding alone at either the pyrrolic or pyridinic nitrogen will induce a red-shift. However a solvent proton- $\pi$ -electron interaction at the pyrrolic nitrogen should induce a blue-shift while a similar interaction at the pyridinic nitrogen should induce a red-shift. The observed blue-shift when changing solvents from ethanol to water appears to be due to an interaction between the more acidic water proton and the pyrrolic nitrogen  $\pi$ -electronic charge. The preferential interaction at this center indicates a wider change between the ground and excited state  $\pi$ -electron densities there than at the pyridinic nitrogen. This hypothesis correlates with the calculated charge density values.

Both the critical solvent dependency of the absorption spectra and the presence of emission from a proton tautomerized excited state indicate that 7-azaindole possesses an unusual electron structure. One of the unexplained mysteries of this structure is the absence of emission from the tautomer in water solution. The explanations of this

excited state proton tautomerization would not preclude this process from occurring in water; but it does not appear to occur or at least is not manifested as emission. Anyhow the uniqueness of the spectral properties of this molecule has prompted much work to be done at this laboratory in an attempt to further elucidate the electronic mechanisms involved in provoking the observed spectra. Due to the energetic closeness of the  $^1L_a$  and  $^1L_b$  states a set of polarization experiments should be performed to determine which state emits. Since the Stokes' shifts for 7-azaindole are quite large one would be tempted to look again for dual emission. A superposition of the  $^1L_a$  and  $^1L_b$  transitions and large Stokes' shifts also characterized the indole spectra and fluorescence apparently emanates from both states in that molecule. The polarization measurements should also yield useful information about the tautomer emission. At present there is no information available about the tautomer transition moment relative to the transition moments of the non-tautomerized species. The tautomer transition moment may not lie in the same direction as the moment of the "normal" molecule.

Finally the vapor absorption spectra again show an increase of the  $^1L_a$  transition relative to the  $^1L_b$  transition as the temperature is increased. This fact coincides with the vapor spectra observed for the previous molecules. Thus again the vibronic coupling mechanism may be invoked as a possible explanation of these results.

I. Y

The

rich

tran

lat

bro

ref

par

mo

lo

as

ti

tr

bo

m

u

a

t

t

t

c

## BENZOTRIAZOLE

I. Vapor Absorption Spectra.

Figure 19 shows the vapor absorption spectrum of benzotriazole. The most striking feature of this spectrum is the noticeable lack of rich, sharp, vibrational structure which characterized the  ${}^1L_b \leftarrow {}^1A$  transition of the previously examined molecules. There are some undulations present but they are relegated to minor perturbations of the broad lowest energy transition. This new spectral feature undoubtedly reflects the additional replacement of a carbon with a nitrogen. This particular replacement results in three contiguous nitrogens in this molecule. Two reasonably well separated transitions are apparent. The lowest energy transition is centered at 275 nm and is tentatively assigned as  ${}^1L_b \leftarrow {}^1A$ . The next transition centered at 242 nm is tentatively assigned as  ${}^1L_a \leftarrow {}^1A$ . The separation and assignment of these transitions coincides with the results obtained for indazole and benzimidazole. However the  ${}^1L_b$  transition observed for benzotriazole is much broader and more intense relative to the  ${}^1L_a$  transition. This is unique compared with transitions observed for the previously discussed azaindoles. A factor which must always be considered when interpreting this spectrum is the possibility of an  $n-\pi^*$  transition. There are now two nitrogens which could contribute to such a transition. Since this transition is usually weak, broad and contains very diffuse structure it could underlie the  ${}^1L_b$  transition. This would lead one to erroneously think the  ${}^1L_b$  transition was intense. It is thus possible that an  $n-\pi^*$  transition centered approximately at 275 nm occurs in benzotriazole.

Although the vibronic structure was slight, an attempt was made to assign the  ${}^1L_b$  0-0 transition and to locate vibrational sequences. The

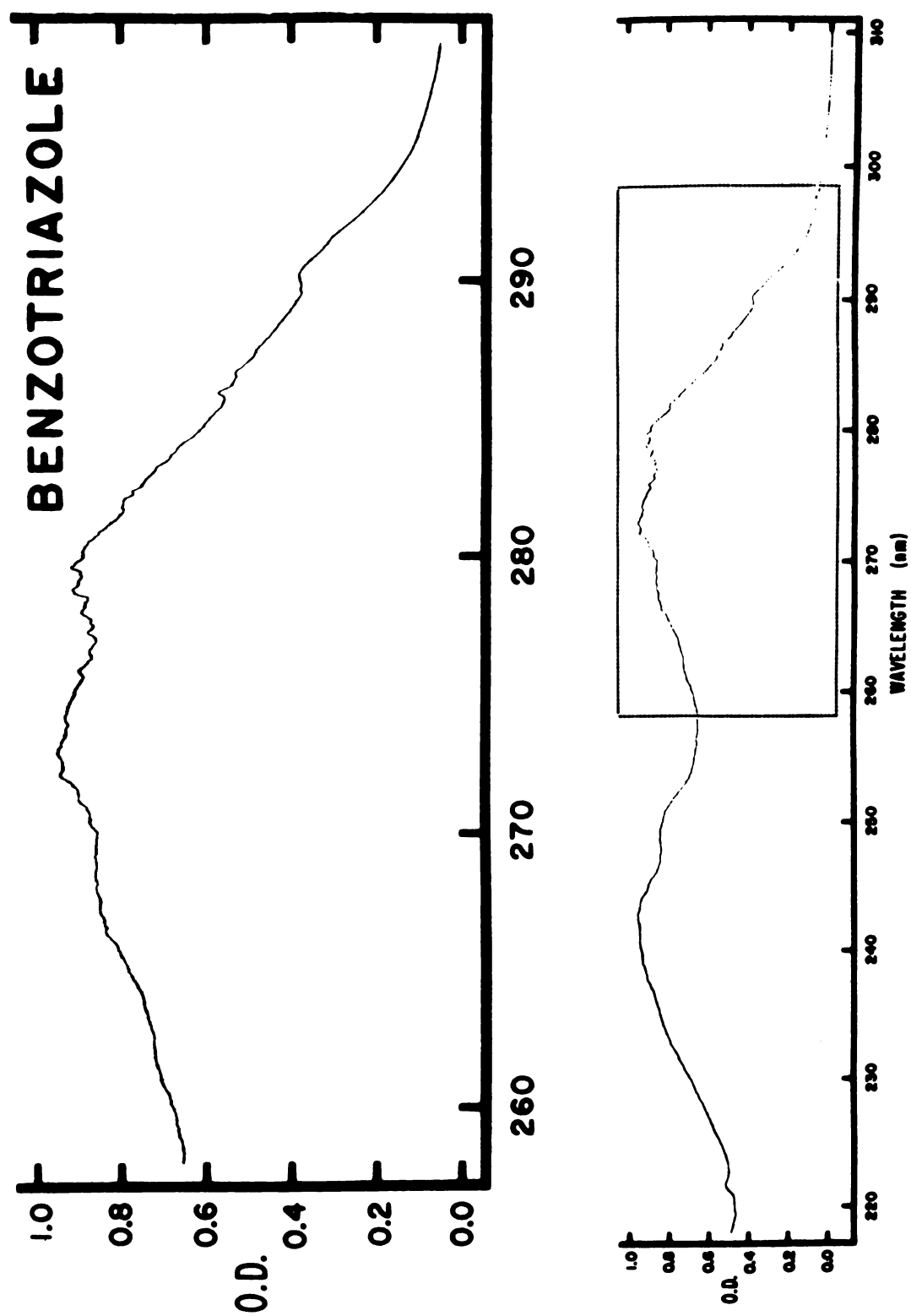


Figure 19. Benzotriazole Vapor Absorption Spectrum.

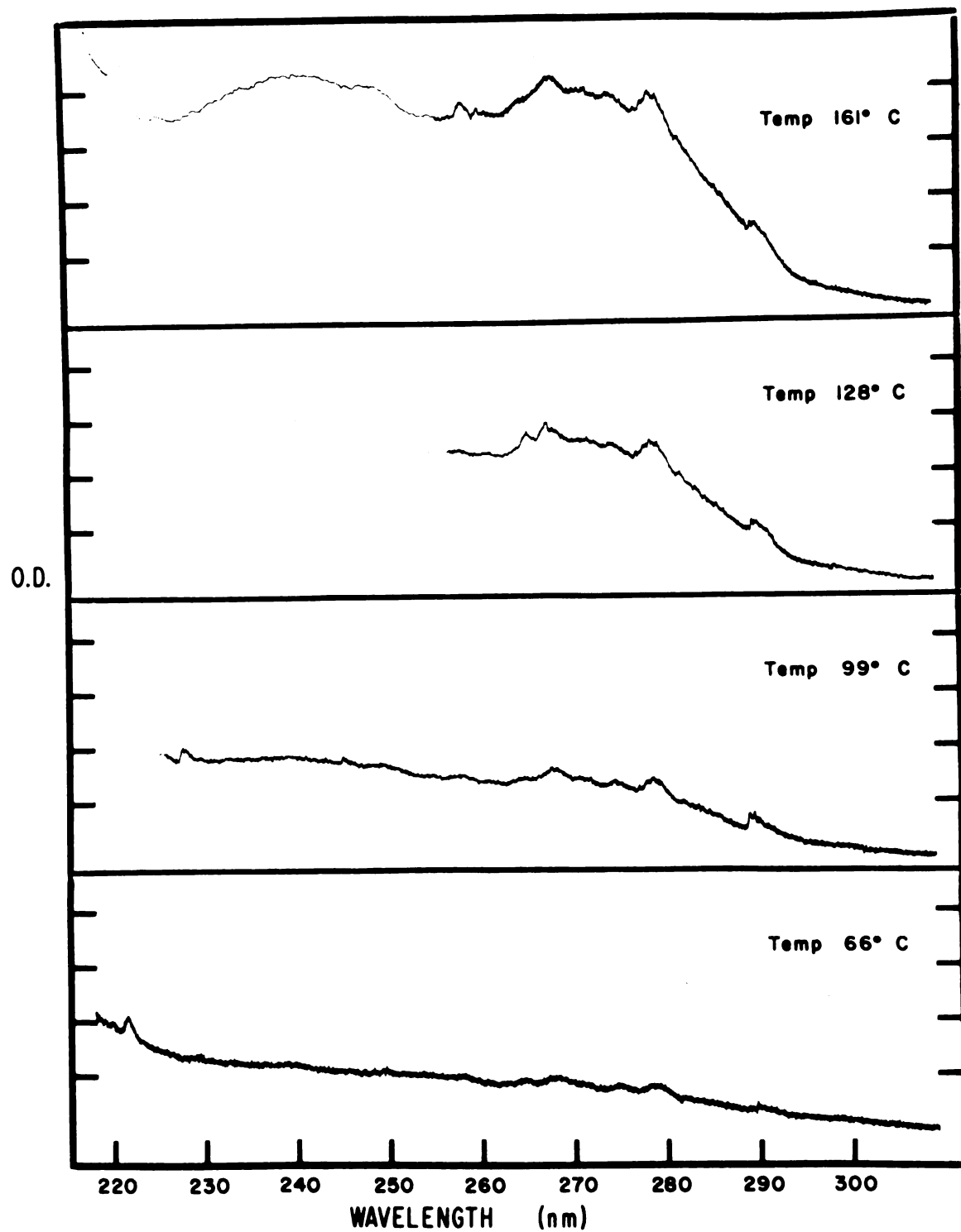


Figure 20. Benzotriazole Vapor Absorption Spectra as a Function of Temperature.



$^1L_b$  0-0 transition was assigned at  $35826\text{ cm}^{-1}$  ( $2791\text{ Å}$ ) and other sequences in this transition appeared to occur at 266 and 272 nm. The average separation between these  $^1L_b$  transition sequences is  $820\text{ cm}^{-1}$ . The  $^1L_a$  transition vibrational groups appear to occur at 238, 242, and 249 nm with an average separation of  $937\text{ cm}^{-1}$ . The  $^1L_a$  transition 0-0 remains unassigned. It was again observed that the higher energy members of the  $^1L_b$  transition sequences again consisted of doublets with an average individual peak separation of  $16\text{ cm}^{-1}$  within each doublet. It must be emphasized that the sequence and 0-0 assignments are quite tentative and based primarily on intuition fostered by similar assignments for the previous molecules.

As for the previous molecules a hot band analysis was carried out for benzotriazole. The results are depicted in Figure 20. Contrary to the results obtained for the previous molecules it is apparently impossible to discern a temperature dependent growth of the  $^1L_a$  transition relative to the  $^1L_b$  transition. Both transitions seem to grow simultaneously by the same amount. It seems strange that this heretofore expected result is an exception rather than the rule for these molecules. The broadness of the  $^1L_b$  transition probably contributes to the temperature dependent simultaneous growth phenomenon observed for this molecule. Thus either this result is an optical illusion or the  $^1L_b$  transition contains some character which allows its intensity to vary in the same manner as the  $^1L_a$  transition.

Confirmation of the  $^1L_b$  0-0 transition was impossible to achieve with this hot band analysis. The vibronic structure was so prohibitively broad that such a task was incapable of being performed. However an effect was noted which was similar to one observed for benzimidazole. The

first benzotriazole vibronic peak to appear as the temperature was slowly increased occurred at 290 nm. Its origin remains unexplained.

## II. Polarization Measurements of Fluorescence Excitation.

The only reported measurements of this type were those of Schutt and Zimmermann<sup>14</sup> in ethanol at  $-180^{\circ}\text{C}$ . Monitoring the fluorescence at 330 nm they found an increase in polarization from 0.15 to 0.35 as the excitation wavelength was increased from 255 to 300 nm. These data indicate that the  $^1\text{L}_b$  state emits and that there is some  $^1\text{L}_a$  transition character in the excitation spectrum down to 300 nm. Since the polarization values never reach 0.5 one may posit some character other than  $^1\text{L}_b$  in the lowest excitation band. This character may be either  $^1\text{L}_a$  or possibly  $n\text{-}\pi^*$  in nature. The absorption spectrum in ethanol does exhibit a general diffuseness and merging of the  $^1\text{L}_a$  and  $^1\text{L}_b$  bands so there is probably character of both transitions in varying proportions from 250 to 300 nm. The two  $\pi\text{-}\pi^*$  transition moments would not be expected to be parallel to each other and the nonnegative polarization values in the predominantly  $^1\text{L}_a$  transition region of the spectrum indicates these moments are also not perpendicular.

When Schutt and Zimmermann made excitation polarization measurements for the cation the observations differed from those seen with the neutral molecule. The  $^1\text{L}_a$  and  $^1\text{L}_b$  transitions had merged into one broad band whose peak occurred midway between the respective transition maxima of the neutral molecule. The polarization was 0.3 at 240 nm, decreased to about zero at the transition maximum and then rapidly increased to approximately 0.5 at 300 nm. These results show that the cation and neutral species have quite different spectral features. In fact these are the most drastic differences yet observed for this group

of molecules when comparing a charged with a neutral species. It appears that fluorescence again emanates from the  $^1L_b$  state in the cation. However the transition shifts and polarization data strongly suggest an  $n-\pi^*$  transition underlies the  $^1L_b$  transition of the neutral molecule. This  $n-\pi^*$  transition is blue shifted in the cation as would be expected. Together with the  $^1L_a$  transition this blue-shifted  $n-\pi^*$  transition could give the appearance of a  $^1L_b$  and  $^1L_a$  transition merger as well as the observed polarization minimum. The increase in polarization at higher energies is probably due to the more parallel orientation of the  $^1L_a$  and  $^1L_b$  transition moments compared with the more perpendicular orientation of the  $^1L_b$  and  $n-\pi^*$  transition moments. In addition the  $^1B_b$  transition moment which probably is closely parallel to the  $^1L_b$  moment could contribute to the more positive polarization at the short wavelengths. It must be iterated that this interpretation is very tentative and more experimental data must be obtained for support of this hypothesis. The strict merger of the  $^1L_a$  and  $^1L_b$  transitions does not explain the polarization data unless one postulates a very broad  $^1L_b$  transition upon which a narrow  $^1L_a$  transition is superposed. This picture is exactly opposite the one constructed for all the previously discussed molecules which had much supportive data.

### III. Solution Absorption Spectra.

The data in Table 7 show the characteristic broadening of the vibronic structure which occurs in hydrocarbon solvents compared with the vapor spectra. However as the solvents are changed in the sequence hydrocarbon, ethanol and water the  $^1L_b$  transition blue-shifts and the  $^1L_a$  transition red-shifts until they become one broad band in the latter solvent. Antagonistic dipole-dipole and H-bonding interactions are

probably responsible for this merger. The lower acidity and smaller dipole moment of ethanol compared with those of water explains the smaller shifts of the bands in ethanol. An  $n \rightarrow \pi^*$  band underlying the  ${}^1L_b$  transition band would undergo a blue shift in changing solvents from hydrocarbon to ethanol to water. This may contribute to the appearance of a single absorption band in water.

The blue shift of the  ${}^1L_b$  band and the red shift of the  ${}^1L_a$  band in going from hydrocarbon to ethanol is unique and can be explained in terms of an increase in the charge densities at one nitrogen upon excitation and a simultaneous decrease of the charge densities at another nitrogen. This situation is not unlikely. However the magnitude of these changes must be of such proportions that H-bonding at either site are equally probable in order to promote a concurrent red and blue shift of the two transitions. In addition one site must have the interaction primarily affecting the  ${}^1L_b$  state while at the other site the interaction primarily affects the  ${}^1L_a$  state.

#### IV. Fluorescence Spectra.

The fluorescence of benzotriazole is quite broad and exhibits vibronic structure. In addition a sizeable Stokes' shift is evident in polar solvents. This indicates that the emitting excited state permanent dipole moment is much larger than the ground state's moment. The fluorescence band is red-shifted with the solvent sequence ethanol, water and acidic medium. This reflects excited state stabilization via dipolar and H-bonding interactions. The relative importance of each of these interactions in promoting the stabilization cannot be assessed from these data.

Fluorescence polarization measurements in ethanol were slightly positive and flat throughout the emission spectrum.<sup>14</sup> Since excitation was monitored midway between the  ${}^1L_a$  and  ${}^1L_b$  transition bands the low polarization value indicates the mutual overlap of these bands. The flatness of this polarization spectrum shows that emission emanates from a single state, probably the  ${}^1L_b$  state. The same fluorescence polarization results were also obtained for the cation. Again the transition overlap could explain these observations.

#### V. Phosphorescence Spectra.

The data of Schutt and Zimmermann show phosphorescent emission for both the neutral molecule and the cation. Both emissions display some vibronic structure. The phosphorescence of the cation is somewhat red-shifted relative to the neutral molecule's emission. This red-shift probably reflects the excited state stabilization due to H-bonding.

Phosphorescence excitation and emission polarization measurements were performed by Schutt and Zimmermann for the benzotriazole cation. The excitation polarization was negative indicating that the phosphorescence is predominantly polarized out-of-plane. The fact that the polarization was not -0.33 probably means either that the triplet transition is not exactly perpendicular to the plane of the molecular nuclei or that there is some  $n-\pi^*$  transition contribution in the region of this excitation polarization spectrum.

#### VI. Correlations and Summary.

Benzotriazole exhibits two distinct transition bands in the vapor phase and in hydrocarbon solution. The lowest energy transition is assigned  ${}^1L_b \leftarrow {}^1A$  and the next higher transition is assigned  ${}^1L_a \leftarrow {}^1A$ . The vapor spectrum does not show the well resolved vibronic structure

observed with the previously discussed molecules. The  $^1L_b$  transition for this molecule appears to be more intense than previously observed. The breadth of this transition makes a distinction between it and the  $^1L_a$  transition more difficult to perceive when compared with a similar distinction for indazole or benzimidazole. In polar solvents these transitions merge such that they become almost indistinguishable. In fact the cation's absorption spectrum exhibits only a single peak whose position is midway between the peaks observed in hydrocarbon solvents.

One of the difficulties fostered by the lack of vibronic resolution in the vapor spectra is the difficulty in assigning the  $^1L_b$  0-0 transition. It was tentatively assigned at 2791 Å on the basis of the  $^1L_b$  transition band shape in comparison with the  $^1L_b$  bands of the previously discussed molecules.

Another "unique" feature of the benzotriazole vapor spectra was the lack of a disproportionate intensity growth for the  $^1L_a$  transition compared with the  $^1L_b$  transition as the temperature was increased. This result adds further support for the  $^1L_a$  transition intensity growth observed for the previously discussed molecules not being an experimental artifact. Using the same interpretation as previously discussed vibronic coupling apparently does not occur for benzotriazole. The reason for the lack (or even presence) of this vibronic coupling remains obscure.

Since a number of spectral features for benzotriazole differed from those of previously discussed molecules it is obvious that more spectral work should be concentrated on this molecule. It is evident that the introduction of a second aza nitrogen has a noticeable effect on the spectral properties and characteristics of the indoles.

## 4-AZABENZIMIDAZOLE

I. Vapor Absorption Spectra.

The vapor absorption spectrum of 4-azabenzimidazole is shown in Figure 21. This spectrum exhibits two well-separated bands centered at 235 and 280 nm. The lower energy transition displays some resolved vibronic structure although not as much as was observed for indole and the mono-azaindoles. The higher energy transition is quite broad and displays very diffuse vibronic structure. Comparing this spectrum with those of the previously discussed molecules the higher energy transition is assigned  ${}^1L_a \leftarrow {}^1A$  and the lower energy transition is assigned  ${}^1L_b \leftarrow {}^1A$ . For this molecule the  ${}^1L_b$  transition intensity is larger than that of the  ${}^1L_a$  transition. This observation is opposite the results obtained for indole and the mono-azaindoles. Even for benzotriazole the two transition were at most of equal intensity. A possible explanation of this large  ${}^1L_b$  transition intensity is that an  $n-\pi^*$  transition underlies this  $\pi-\pi^*$  transition. If so one would expect the presumed  $n-\pi^*$  transition to significantly blue-shift in H-bonding solvents.

The  ${}^1L_a$  0-0 transition remains unassigned but for the  ${}^1L_b$  transition the 0-0 is assigned at  $35201\text{ cm}^{-1}$  ( $2833\text{ \AA}$ ). Since the higher energy members of the  ${}^1L_b$  0-0 transition sequence were actually doublets the highest energy peak of the first doublet was chosen as the  ${}^1L_b$  0-0. Other vibrational sequences in the  ${}^1L_b$  transition occur at 272 and 277 nm with an average sequence separation of  $720\text{ cm}^{-1}$ . Vibrational groups in the  ${}^1L_a$  transition occur at 232, 236 and 239 nm with an average separation of  $800\text{ cm}^{-1}$ .

The results of the hot-band "analysis" for this molecule are shown in Figure 22. These results indicate that the above  ${}^1L_b$  0-0 transition

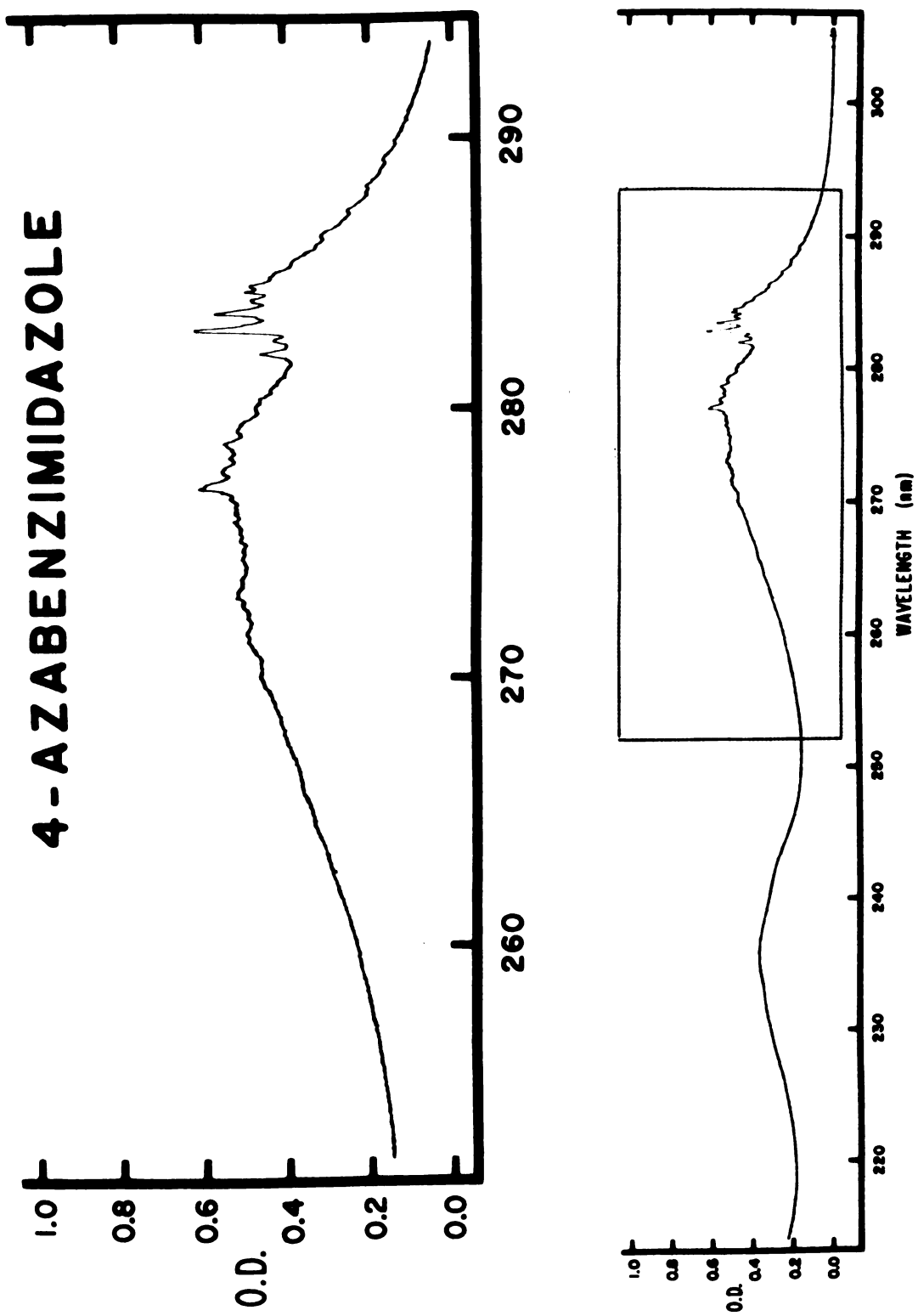


Figure 21. 4-Azabenzimidazole Vapor Absorption Spectrum.



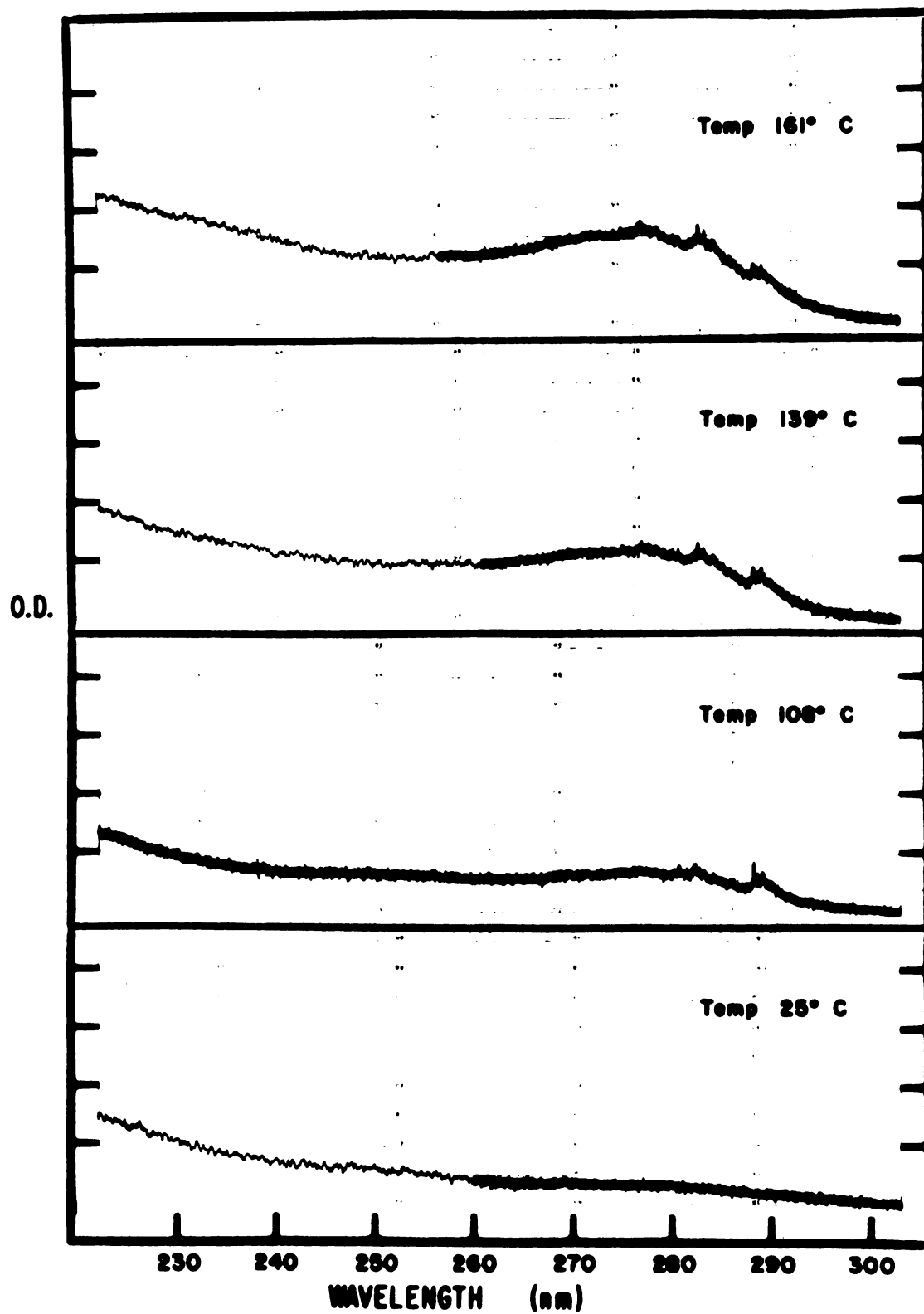


Figure 22. 4-Azabenzimidazole Vapor Absorption Spectra as a Function of Temperature.

assignment was correct. Another observation is that the  $^1L_a$  and  $^1L_b$  transitions do not exhibit any intensity growth disproportion between them. This result is similar to that observed for benzotriazole. Thus it does not appear that any intensity borrowing occurs for the  $^1L_a$  and  $^1L_b$  transitions in 4-azabenzimidazole.

However the temperature dependent spectra do exhibit the existence of a vibronic series of transitions at 288 nm before the  $^1L_b$  0-0 transition sequence appears. This phenomenon was also noticed with benzimidazole and benzotriazole and remains unexplained.

## II. Absorption and Fluorescence Spectra

The solution absorption data in Table 7 indicate very little or no shifts when comparing spectra obtained in cyclohexane with those obtained in water. There appears to be a red-shift for the cation relative to the spectrum in water. The lack of spectral shifts is probably due to different specific solvent-solute interactions which induce antagonistic shifts. It would be expected that the excited state permanent dipole moment magnitudes exceed the ground state moment magnitude. This would lead to a demonstrable red-shift in water relative to the spectrum in hydrocarbon solvents. The lack of any shift indicates that there is an H-bonding interaction at a site whose excited state charge density is less than the ground state charge density. The resulting blue-shift would tend to cancel the dipolar interaction induced red-shift. The net result would be little, if any, spectral shift.

The apparent red-shift which occurs in acidic media is probably caused by an interaction between the "excess" protons and a  $\pi$ -electron site in the molecule whose excited state charge density exceeds its ground state density. The most likely position for this interaction is one of

the pyridinic nitrogens. Obviously this site must differ from the one described above which was the center for a proposed blue-shift interaction. That center could be the other pyridinic nitrogen but more probably would be the pyrrolic nitrogen.

In a basic solvent there is a red-shift of both bands. This shift probably reflects the effect of the negative charge at the pyrrolic nitrogen on the  $\pi$ -electron system. The Coulombic repulsion presumably destabilizes the  $\pi$ -electronic structure. Thus less energy is required to excite this structure.

The fluorescence of this molecule probably emanates from the  $^1L_b$  state. It exhibits a moderate Stokes' shift in polar solvents. This indicates that the emitting state permanent dipole moment is larger than the ground state moment. This coincides with the above assumption concerning the dipolar interaction effects on the absorption spectra. The fluorescence maximum in water is blue-shifted compared with that in ethanol. This shift could be caused by the solvent proton- $\pi$ -electron interaction at a site whose ground state  $\pi$ -electron charge density exceeds the emitting state charge density. This mechanism corresponds with one of those proposed above to explain the lack of absorption spectrum shift between hydrocarbon and water solvents. Thus either a pyridinic nitrogen or the pyrrolic nitrogen is a candidate for the interaction site. The most likely choice is the pyrrolic nitrogen. Fluorescence from the cation is slightly red-shifted compared with the spectrum in water. This corresponds with the observed absorption spectrum shift of the cation vs. the neutral species.

### III. Theoretical Calculations.

Using the calculated oscillator strengths of Table 8 the first excited state was assigned  $^1L_b$  and the second excited state was assigned  $^1L_a$ . It should be recalled that normally the  $^1L_a$  transition oscillator strength exceeds that of the  $^1L_b$  transition. The calculated transition moment orientations were of little use in making this assignment since they were oriented at approximately the same angle from the principal axes of the molecule. However these calculated orientations do not parallel a principal axis. Their mutual orientation, though, is predicted to be almost perpendicular. The predicted energies of these two lowest transitions are not too disparate. The calculated ionization potential and electron affinity of 4-azabenzimidazole are respectively 7.3 eV and 1.8 eV. Calculations were not performed for either the excited state permanent dipole moments or their  $\pi$ -electron charge densities.

### IV. Correlations and Summary.

The first ( $^1L_b$ ) and second ( $^1L_a$ ) singlet transitions are energetically quite well separated. Although this fact is well established in the vapor absorption spectra it is not predicated by the calculations. This demonstrates the possible amount of error inherent in these calculations. However the error in predicting the second singlet transition is less than 0.5 eV so it is not too unsatisfactory. The vapor absorption spectra also show that the  $^1L_b$  transition oscillator strength apparently exceeds the  $^1L_a$  transition oscillator strength. This was not observed for any of the previously discussed molecules. A possible explanation of this occurrence is that one or more  $n-\pi^*$  transitions underlie the  $^1L_b$  transition. Thus the lowest energy transition band

would be composed of several transitions. Although no supportive evidence for the existence of an  $n-\pi^*$  transition was found, its occurrence still cannot be eliminated since very little spectral data has been obtained for this molecule.

Fluorescence probably emanates from the  $^1L_b$  state. Spectral shifts of both fluorescence and absorption indicate there are a number of possible solvent-solute interactions. The moderate Stokes' shifts imply that the emitting state permanent dipole moment exceeds the ground state moment. Thus polar solvent-solute interactions must occur and cause absorption spectra red-shifts when compared with the spectra in hydrocarbon solvents. However no such shift was evident for water solutions. Some antagonistic blue-shift must be occurring in this solvent. This shift could be caused by a solvent proton- $\pi$ -electron interaction at a site whose  $\pi$ -electronic charge density in the ground state is larger than in the excited states. This site is probably the pyrrolic nitrogen or possibly a pyridinic nitrogen. This scheme also could explain the blue-shift of the fluorescence in water compared with the emission in ethanol. In acidic media the fluorescence and absorption spectra are red-shifted relative to the spectra in neutral media. Apparently the additional protons interact at another  $\pi$ -electron site whose excited charge density exceeds its ground state charge density. This site is probably a pyridinic nitrogen. The anion absorption spectrum is red-shifted relative to the spectrum of the neutral species. This reflects the destabilization of the  $\pi$ -electron structure which is a result of the Coulombic repulsion between the  $\pi$ -electron system and the negative charge at the pyrrolic nitrogen.

The vapor absorption spectra obtained as function of temperature indicate that there is no intensity stealing which occurs for this molecule. That is, both  $^1L_a$  and  $^1L_b$  transition oscillator strengths maintain the same relative proportion throughout the range of utilized temperatures. This proportion constancy further supports the experimental evidence of relative oscillator strength proportionality changes which were obtained for many of the previously discussed molecules.

Due to the lack of symmetry the lowest two singlet transition moments are not expected to be oriented parallel to the principal axes of the molecule. This correlates well with the calculated moment orientations. However the calculated moments for the two lowest transitions are approximately perpendicular. This occurrence may be coincidental.

#### 5-AZABENZIMIDAZOLE

##### I. Absorption and Fluorescence Spectra.

Again Table 7 shows there are scanty data available for 5-azabenzimidazole. There appears to be a blue-shift in the absorption spectrum when the solvent is changed from water to an acidic medium. There is a progressive blue-shift in the fluorescence spectrum when the solvent sequence of ethanol, water and acid is followed. A moderate Stokes' shift is also observed in polar solvents. This indicates that the emitting state's permanent dipole moment is somewhat larger than the ground state's moment. Thus one would expect dipolar interaction induced red-shifts of the absorption and fluorescence spectra in more polar solvents. The fact that these red-shifts are not reported means that some other interaction is occurring which produces the observed blue-shifts. This interaction is probably between solvent protons and the  $\pi$ -electronic charge at certain sites on the molecule. All three

nitrogens interact with the solvent protons to produce these shifts. Their ground state  $\pi$ -electronic charge densities must exceed their excited state densities to cause these blue-shifts. The difference between the ground and excited state  $\pi$ -electron densities probably differs for these three nitrogens. Thus as the acidity of the solvent increases, more nitrogens become involved in this blue-shift producing interaction. For example in acidic media the additional proton could predominately interact at a nitrogen which had hardly been involved in the interactions with water and ethanol. The feebleness of interaction for this nitrogen in these latter solvents would probably be due to the relatively small  $\pi$ -electron density change between the ground and excited states compared with the change at the other two nitrogens.

## II. Theoretical Calculations.

Based on the calculated results in Table 8 the first singlet excited state is assigned as  ${}^1L_b$  and the second singlet excited state is assigned as  ${}^1L_a$ . This assignment is based on the calculated oscillator strengths only since the first two transition moment orientations were at approximately the same angle but at opposite directions to the principal axes of the molecule. These transition moment orientations are predicted to be neither parallel to a principal axis nor perpendicular to each other. The two lowest singlet transitions are predicted to lie energetically close to each other. The excited state permanent dipole moments and  $\pi$ -electron charge densities were not calculated for this molecule. The ionization potential and electron affinity were predicted to be 7.3 eV and 1.8 eV respectively.

### III. Correlations and Summary.

The sequence of blue-shifts in both the fluorescence and absorption spectra which was reported from 5-azabenzimidazole has not been observed for any of the previously discussed molecules. This result may indicate that all three nitrogens have the same  $\pi$ -electronic charge density pattern between the ground and excited state. That is, the ground state charge density exceeds that in the excited states. This pattern explains the observed blue-shifts as the medium becomes more acidic provided these shifts are caused by solvent proton- $\pi$ -electron interactions. If this interpretation becomes verified, 5-azabenzimidazole is a unique indole since it contains three nitrogens with the same  $\pi$ -electron density change pattern between the ground and excited states.

The first singlet excited state is assigned as  $^1L_b$  and the second singlet excited state is assigned as  $^1L_a$ . Their transition moments are not expected to parallel a molecular principal axis or to be perpendicular to each other. The fluorescence probably emanates from the  $^1L_b$  state. No  $n-\pi^*$  transition has been reported for this molecule. However on the basis of the data analyses for benzotriazole and 4-azabenzimidazole an  $n-\pi^*$  transition may occur in 5-azabenzimidazole and probably underlies the more intense  $\pi-\pi^*$  transitions.

## PURINE

### I. Vapor Absorption Spectra.

The vapor absorption spectrum of purine has been reported by El-Bayoumi, et. al.<sup>8</sup> It is identical with the spectrum obtained in this laboratory and shown in Figure 23. The most remarkable characteristic of this spectrum is the complete lack of sharp vibrational structure



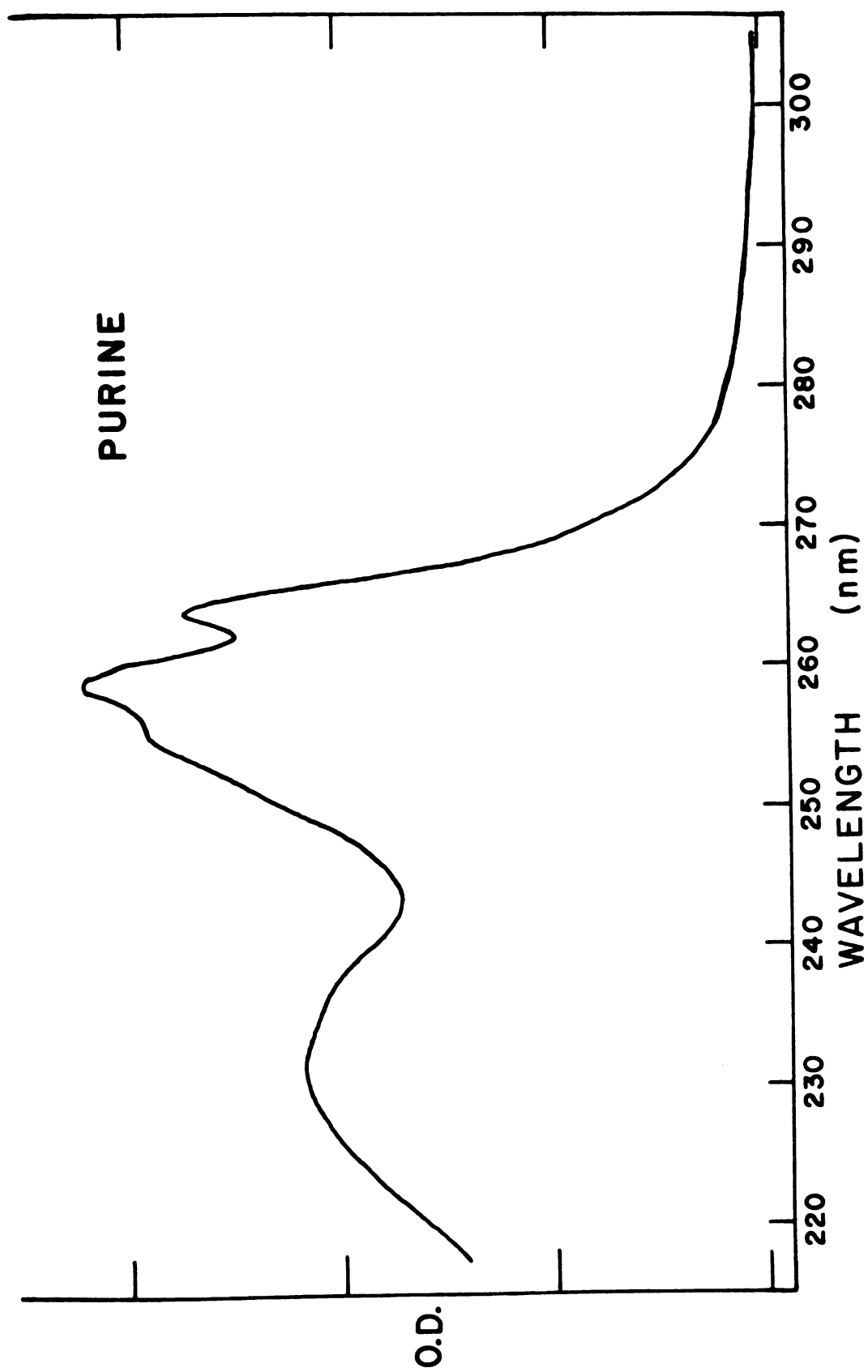


Figure 23. Purine Vapor Absorption Spectrum.

which was evident in indole and the mono and di-azaindoles. That is, in this triazaindole the existing vibrational structure has very broad, overlapping envelopes. Overall the features of this absorption spectrum resemble those of the azaindoles recorded in a polar solvent. However, there is even less evident vibronic structure in the purine vapor spectrum than was often observed in the solution spectra of the previously discussed molecules. For this reason transition assignments and spectral analyses based on solvent shifts are difficult to perform and were not attempted here. In addition a hot band analysis was not attempted. One of the factors which thwarted this type of analysis was the low vapor pressure of purine. Even when the solid was introduced directly into the 10 cm absorption cell a relatively high temperature was needed to obtain a vapor absorption spectrum.

## II. Transition Assignments.

Assignment of the transitions was first made by Clark and Tinoco<sup>60</sup> from a methylcyclohexane solution absorption spectrum. The first  $\pi-\pi^*$  transition had three broad peaks at 259, 262, and 267 nm. A less pronounced, weak peak at about 240 nm was ascribed to the second  $\pi-\pi^*$  transition by comparing purine's absorption spectrum with that of benzimidazole. Purine also exhibited a long absorption tail from 280 - 310 nm which was ascribed as an  $n-\pi^*$  transition. When these authors used trimethylphosphate as a solvent they noticed that the first  $\pi-\pi^*$  transition became more rounded with a loss of vibrational structure and was slightly red-shifted. The second  $\pi-\pi^*$  transition was more red-shifted and lost absorptivity. In addition a third  $\pi-\pi^*$  transition was found with peaks at 190 and 200 nm.

A different assignment was made on the basis of polarized reflectance measurements of a single purine crystal.<sup>61</sup> It should be noted that these assignments were based on a numerical analysis of the reflectance measurements and are thus subject to any assumptions made when performing this analysis. The transitions at 294 and 250 nm were assigned as out-of-plane  $n-\pi^*$  transitions originating from nitrogens at positions 5 and 7 (using the same numbering system as that for indole). The  $\pi-\pi^*$  transition at 263 nm was found to lie in-plane and had its moment lying  $48^\circ$  counterclockwise from the short molecular axis--that axis formed by the line from  $C_8$  to  $C_9$ . The  $\pi-\pi^*$  transition at 200 nm was also in-plane and had its moment  $51^\circ$  counterclockwise from the short axis. The strong transition at 190 nm had its transition moment out-of-plane and was unassigned regarding its character.

These two analyses show a major discrepancy in the assignment of the transition at 245 nm. This discrepancy is more remarkable since Clark was involved in both assignment attempts. However both analyses do show an  $n-\pi^*$  transition at lower energies than the lowest energy  $\pi-\pi^*$  transition. Thus an  $n-\pi^*$  transition becomes readily apparent when there are three aza nitrogens in the indole skeleton. A feature of the crystal polarization measurements worth noting is that the long wavelength  $\pi-\pi^*$  transition moment (at 263 nm) was not found to be polarized parallel to one of the principal axes of the molecule. This is a result which has been expected for all the indoles.

### III. Absorption and Fluorescence Spectra.

The available absorption and emission data for purine in various solvents are shown in Table 9. Another series of experiments were performed on purine which monitored absorption or fluorescence as a

Table 2. Purine Absorption and Luminescence.

Solvent	Temp.	$\lambda_{\text{abs}}$	$\lambda_{\text{fluor}}$	$\lambda_{\text{phos}}$	Ref.
Me-Cyclohex.	RT	240, 262, 280			60
Me-Cyclohex.	RT		none		62, 63
Me-Cyclohex.	77°K			351, 370, 395	62
Dichloroethane	RT		377		62
Isopropanol	RT	263 only			62
Methanol	RT		362		62
Ethanol	RT	310	350		54
E P A	77°K	263		364, 380, 400	64
Glycerol	77°K			351, 370, 395	62
Water	RT	263	387		62
Water	77°K			351, 370, 395	62
Water	RT	281	370		54
Water	RT		380		65

function of pH. These results are listed in Table 10. The existence of conflicting data as well as the breadth and lack of vibronic structure in the absorption spectra do not allow an analysis based on solvent shifts. Although no fluorescence spectrum has been published the data from tables indicate that this emission is also broad band. Some error in reporting the fluorescence maxima would be expected. The data do show that a moderate Stokes' shift occurs in polar solvents. This indicates that the emitting state permanent dipole moment exceeds the ground state moment. Thus, in general, dipolar interactions should produce red-shifts.

Although some of these data are conflicting certain general trends seem to be evident and are used to hypothesize what is occurring in the molecule which lead to these spectroscopic results. In hydrocarbon non-hydrogen bonding solvents the lone pair electrons are unperturbed and an  $n-\pi^*$  transition has lowest energy. Since its oscillator strength is very low its fluorescence lifetime is quite long. Thus radiationless processes may easily occur before fluorescence can take place. In this case very little if any fluorescence would be expected and little occurs according to the data. However if purine is put in a hydrogen bonding solvent these lone pair electrons are stabilized which in turn shifts the  $n-\pi^*$  transition to higher energies. Now a  $\pi-\pi^*$  transition is of lowest energy and fluorescence is predicted and observed. Dipolar and solvent proton  $-\pi-$  electron interactions also probably occur in the polar solvents which alter the energy of fluorescence. These perturbations would be manifested as solvent shifts. The data show that such shifts occur.

Table 10. Effects of pH on Purine Absorption or Fluorescence.

A or F	$\lambda_{\max}$	$pK_a$	$\phi_f$	Ref.
A	<220, 260 @ pH 0.28	2.39		57
	<220, 263 @ pH 5.70	8.93		
	219, 271 @ pH 11.0			
F	400 @ pH 2	3.2	0.008 @ pH 2.46	65
	380 @ pH 5.2	9.2	0.002 @ pH 8	
	370 @ pH 11		0.045 @ pH 10.6	

Table 11. Calculation Results for Purine.

Trans. Energy ( $\text{cm}^{-1}$ )	Trans. Energy (nm)	Trans. Moment (Debyes)	Trans. Polar (deg. from x-axis*)	f
36425	274.5	0.384	81	0.058
36542	273.7	0.598	-33	0.142
48889	204.5	0.982	72	0.512
49958	200.2	0.564	-43	0.172

\*See Figure 24

On the basis of this scheme Borreson analyzed the pH effect on the purine fluorescence.<sup>65</sup> From pH 3.2 to pH 9.2 the  $n-\pi^*$  transition has lowest energy and little fluorescence is expected or observed. Between pH 2.5 and pH 3.2 protons are stabilizing the lone pair electrons causing the  $n-\pi^*$  transition to be stabilized relative to the lowest energy  $\pi-\pi^*$  transition and fluorescence is predicted and observed. Below pH 2.5 an  $n-\pi^*$  transition is again the lowest energy transition due to a stabilizing of the electrons by the additional protons and fluorescence is not expected nor observed. Above pH 9.2 the pyrrolic nitrogen has a negative charge since the base has pulled a proton away from it. Borreson believes this negative charge is pulled up into the system. He states that further evidence for this attraction is provided by the experimental result that this  $pK_a$  (9.2) is lower than that of other azaindoles such as benzimidazole. This additional charge in the  $\pi$  system repels the lone pair electrons thus stabilizing them. The  $\pi-\pi^*$  transition now has lowest energy and fluorescence is predicted and observed. Borreson's interpretation of the anion fluorescence is vague and does not explain the anion red shift in absorption. An alternative explanation for the existence of anion fluorescence is that the Coulombic repulsion due to the negative charge on the pyrrolic nitrogen causes a rearrangement of the  $\pi$ -electron system. This rearrangement could have such a destabilizing effect that the  $\pi-\pi^*$  transition energy would be below the  $n-\pi^*$  transition energy. Fluorescence would be expected and is observed. This explanation would explain the observed absorption spectra shifts between the neutral and anion species in Table 10.

It should be noted at this point that some investigators report fluorescence occurrence for purine under certain experimental conditions while other do not. This is due to the relative sensitivity and signal-to-noise figures for various experimental setups. Purine has a low fluorescent quantum yield, especially at neutral pH's. In a 50:50 propane-1,2-diol: 0.01M phosphate buffer solution at pH 7 the quantum yield is  $0.02^{63}$  (see also Table 10).

#### IV. Phosphorescence Spectra.

In contrast to those phenomena regarding fluorescence, phosphorescence is readily observed in most solvents (see Table 9). For example in propane-diol phosphate buffer the phosphorescence to fluorescence ratio is  $1.9^{63}$  so phosphorescence becomes more readily observed. From excitation polarization studies the phosphorescence is concluded to be emitted from the  $\pi-\pi^*$  triplet state. That is, when excitation was via the lowest energy  $\pi-\pi^*$  transition the excitation polarization was negative while  $n-\pi^*$  excitation gave positive polarization.<sup>64</sup> This is consistent with the notion that  $\pi-\pi^*$  phosphorescence is out-of-plane polarized making it perpendicular to  $\pi-\pi^*$  singlet transitions and parallel to  $n-\pi^*$  transitions. In addition the relatively long lifetimes of observed phosphorescence (1.6 sec) and large singlet-triplet separation energies are consistent with the  $\pi-\pi^*$  phosphorescence emission conclusion.

Another set of phosphorescence excitation polarization experiments confirmed the negative polarization when the lowest  $\pi-\pi^*$  transition was excited.<sup>66</sup> In addition these investigators found that excitation via the second  $\pi-\pi^*$  transition (the one at 240 nm in Clark and Tinoco's assignment scheme) also gave negative polarizations. This further



indicated that phosphorescence emission is out-of-plane. Their results also indicated the two in-plane  $\pi-\pi^*$  transitions were not parallel but they could not say these transitions were perpendicular with any certitude. They also noted some structure in their phosphorescence emission polarization measurements which maintained position and magnitude when excitation was either the first or second  $\pi-\pi^*$  transition. The structural features consisted of relative maxima and minima of the negative polarization which were quite well aligned with structural features on the phosphorescence emission itself. The explanation given for this structure was that the more negative minima were due to direct spin-orbit interaction or coupling of the  $n-\pi^*$  singlet and the emitting  $\pi-\pi^*$  triplet while the less negative maxima were due to vibronic interactions between the  $n-\pi^*$  triplet and the  $\pi-\pi^*$  triplet.

#### V. Theoretical Calculations.

The results of these calculations are shown in Table 11 and Figure 24. Provided one may still use the same excited state nomenclature as was used for the other molecules the first singlet excited state is assigned as  $^1L_b$  and the second singlet excited state is assigned as  $^1L_a$ . The transition moment orientations, transition oscillator strengths and the ground and excited state permanent dipole moments all agree with this assignment. Neither transition is predicted to parallel a principal axis of the molecule. Also the two transitions are not predicted to be mutually perpendicular.

The two lowest singlet transitions are calculated to lie energetically very close to each other. The close proximity of these transitions does not allow an assignment of the fluorescence emitting state to be made. However the permanent dipole moment of the  $^1L_a$  state is much lower than the ground state dipole moment. This correlates with the

Figure 24. Calculated Charge Densities and Bond Lengths for Purine.

Legend:

Numbers at each atomic position denote  $\pi$ -electron charge densities in electron units.

Numbers at each bond denote bond lengths in Angstrom.

The top number corresponds to the ground state.

The middle number corresponds to the first excited singlet state ( $^1L_b$ ).

The bottom number corresponds to the second excited singlet state ( $^1L_a$ ).

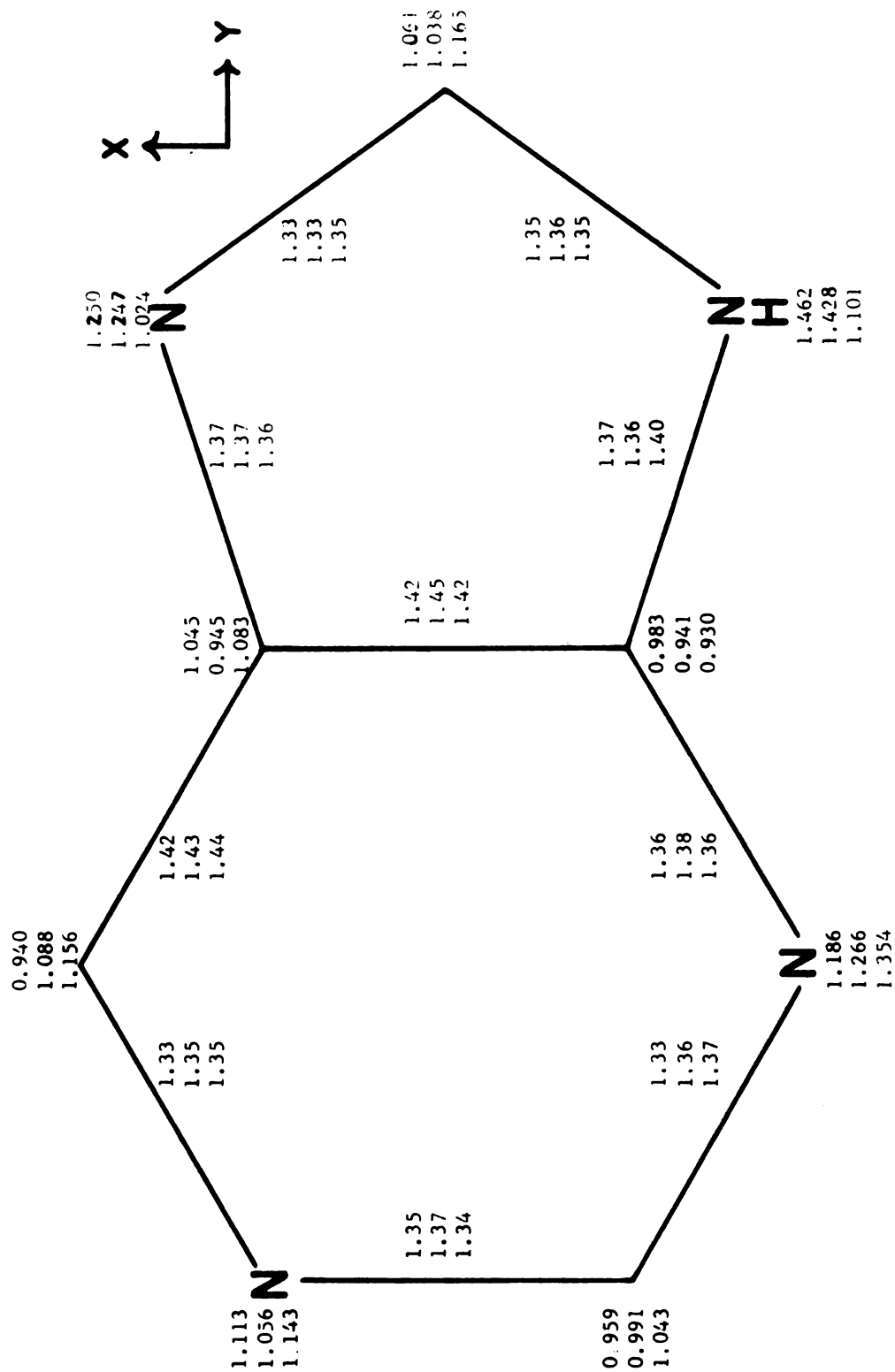


Figure 24.

experimentally observed Stokes' shifts in polar solvents. The correlation suggests that fluorescence emanates from the  $^1L_a$  state in polar media.

The calculated bond lengths do not vary drastically between the ground and excited states. At the pyrrolic nitrogen position the calculated  $\pi$ -electronic charge density does not noticeably change between the ground and  $^1L_b$  state. However this nitrogen is predicted to be much more acidic in the  $^1L_a$  state than in either the ground or  $^1L_b$  states. The calculated basicities at the pyridinic nitrogen positions are: 3 position - ground  $> ^1L_b > ^1L_a$ ; 5 position -  $^1L_a > \text{ground} > ^1L_b$ ; 7 position -  $^1L_a > ^1L_b > \text{ground}$ . It is interesting to note that the magnitude and direction of solvent induced shift as a result of H-bonding with aza nitrogens depends on the position of that nitrogen and the excited state ( $^1L_a$  or  $^1L_b$ ). The ionization potential is calculated to be 7.4 eV and the electron affinity is calculated to be 1.8 eV.

#### VI. Correlations and Summary.

Purine exhibits two features which were not readily apparent for the rest of the azaindoles. First there is a defineable  $n \rightarrow \pi^*$  transition which occurs at longer wavelengths than the longest energy  $\pi \rightarrow \pi^*$  transition. The existence of this transition has been verified by the vapor absorption spectra, polarization data and the solution absorption experiments. Second, very little vibronic structure is evident in the  $\pi \rightarrow \pi^*$  transitions. This structure is even absent in the vapor absorption spectrum. It is quite possible that these two features are a manifestation of the incorporation of a third aza nitrogen into the indole molecule.

Some controversy has been raised concerning the type of transition which occurs at 245 nm. I believe this is the second ( $^1L_a$ )  $\pi-\pi^*$  transition. This belief is based on a number of facts. First there have been two  $\pi-\pi^*$  transitions in the range 220 to 300 nm for every molecule in this study. The second transition for indazole, benzimidazole, benzotriazole, and the azabenzimidazoles have occurred in the region of 240 nm. Purine may be considered as a diazabenzimidazole so it also should have its second  $\pi-\pi^*$  transition in this region. In addition the phosphorescence excitation and emission spectra<sup>64,66</sup> indicate this is a  $\pi-\pi^*$  transition. Also if this transition were  $n-\pi^*$  it should be blue-shifted in protic solvents. The opposite result was experimentally observed for the only published spectra.<sup>62</sup> In fact the observed red-shift was so large that it partially merged the two  $\pi-\pi^*$  transitions. This red-shift would be expected and large if the appropriate excited state ( $^1L_a$ ) permanent dipole moment significantly exceeded the ground state moment. This trend is predicted by the calculations. The only data which refutes this assignment of the 245 nm transition is that of Chen and Clark,<sup>61</sup> Their data analysis is contingent on certain assumptions and is somewhat subjective. Perhaps some of these assumptions aren't fulfilled.

The calculations position the  $^1L_b$  transition moment at  $82^\circ$  and the  $^1L_a$  transition moment at  $-34^\circ$  relative to the axis formed by  $C_8$  and  $C_9$  in the molecule. Chen and Clark's data place the lowest energy  $\pi-\pi^*$  transition moment at  $-48^\circ$ . Although the accuracy of calculated angles is not good this discrepancy is somewhat unsettling and warrants further investigation. Possibly Chen and Clark were observing the  $^1L_a$  transition but this seems unlikely. Anyhow the two singlet transition

moments are not predicted to parallel a molecular principal axis nor be perpendicular to each other. This is an unexpected result.

The phosphorescence emission polarization reported by Drobnik, et. al.<sup>66</sup> exhibited some spectral structure. These authors attributed this structure to the relative importance, across the phosphorescence spectrum, of the vibronic mixing of the triplet ( $n, \pi^*$ ) and ( $\pi, \pi^*$ ) states and the direct spin-orbit coupling of the singlet ( $n, \pi^*$ ) state and the triplet ( $\pi, \pi^*$ ) state. An alternative explanation for this structure is dual emission polarization structure is dual emission from the  $^3L_a$  and  $^3L_b$  states. This phosphorescent emission polarization structure is reminiscent of that observed for indole and an interpretation of that polarization structure was dual emission. In polar solvents, at least, the two lowest singlet transitions apparently are energetically close. The lowest singlet transition was assigned as  $^1L_b$  and the second transition was assigned as  $^1L_a$ . However the fluorescence emitting state was assigned as  $^1L_a$  on the basis of the large Stokes' shifts exhibited in polar solvents. There is no guarantee that such shifts would be present in nonpolar solvents. Thus one would be tempted to investigate the existence of dual emission.

The calculated charge densities are also in accord with the experimental observation of electrophilic attack of ethanol at the 4 position when purine is in the excited state.<sup>70</sup> This carbon's calculated  $\pi$ -electron density changes more than any other carbon atom in the molecule upon excitation. In addition its excited state density is only rivaled by the  $\pi$ -electron excited state density of a carbon at the 2 position. Experimentally it was found that excitation of purine in ethanol at 2537 Å caused a decrease in absorption at 260 nm and an increase in absorption at 290 nm with an isosbestic point at 270 nm.

This photolysis reaction was claimed to be an alcohol adduct at the 4 position as analyzed by NMR spectroscopy.<sup>70</sup> On the basis of the calculated charge densities it would appear that there should also be electrophilic attack at the 2 position. However electrophilic attack may occur only at the site which exhibits the maximum charge density change between the ground and excited states.

It must be noted that no vibronic coupling mechanism was contemplated for this molecule. This may be another facet of the addition of a third aza nitrogen.

## CHAPTER V

### INTERMOLECULAR CORRELATION OF THE SPECTRAL DATA

There are certain trends, similarities and dissimilarities which characterize this group of molecules. This chapter will discuss the evident aspects which wed these molecules into a family. The discussion will be general with specific examples used only for illustrative purposes.

Consistent structural patterns were exhibited in the vapor absorption spectra of these molecules. The features which formed these patterns by their predictable presence became the diagnostic crutches for assigning the singlet transitions. The  ${}^1L_b \leftarrow {}^1A$  transition exhibited much more vibronic structure than the  ${}^1L_a \leftarrow {}^1A$  transition. This structure however became more diffuse as more aza nitrogens were incorporated into the molecule. The number of vibronic sequences also diminished with the number of aza nitrogens. This diffusivity and diminution was climaxed in the purine spectrum which exhibited no vibronic structure in the  ${}^1L_b$  transition. For most molecules the  ${}^1L_b$  transition oscillator strength was less than that of the  ${}^1L_a$  transition. Again as the number of incorporated aza nitrogens increased the relative transition intensities also changed. For benzotriazole the two transitions appeared to have equal intensities and for 4-azabenzimidazole the  ${}^1L_b$  transition oscillator strength surpassed that of the  ${}^1L_a$  transition. Purine's vapor spectrum was more difficult to decipher but the lower energy (supposedly the  ${}^1L_b$ ) transition intensity appeared to be decidedly larger than the higher energy ( ${}^1L_a$ ) transition intensity. Thus the  ${}^1L_b$  transition vibronic structure vanishes and the transition intensity ratio



${}^1L_b/{}^1L_a$  progresses from less than unity to greater than unity as the aza nitrogen population increases. These are major trends which occur. Minor variations of these trends are exhibited which depend on the positions of these nitrogens as illustrated above with benzotriazole and 4-azabenzimidazole.

Another consistent feature for all the molecules but purine was the relative separation between vibronic sequences or groups in the  ${}^1L_b$  and  ${}^1L_a$  transitions. The average sequence separation in the  ${}^1L_b$  transition was always less than the vibronic group separation in the  ${}^1L_a$  transition for each molecule. Presumably the  ${}^1L_a$  transition groups are reasonable representatives of vibronic sequences so group separations should reflect sequence separations. There did not seem to be any pattern which correlated the sequence or group separations with the number of aza nitrogens or their positions. In addition the  ${}^1L_b$  transition sequence separation for some molecules exceeded the  ${}^1L_a$  transition group separation for other molecules. The only predictable pattern was that the average  ${}^1L_a$  transition group separation would exceed the average  ${}^1L_b$  transition sequence separation for a given molecule. The variation between sequence or group separations was nonzero but nominal for each molecule. However this variation increased as the number of aza nitrogens increased. There were also fewer sequences or groups for molecules with more aza nitrogens. For example the diazaindoles had only two sequences and two groups. Thus this increased variation with increased aza nitrogen population undoubtedly reflects the diffuseness of vibronic structure and the concomitant imprecision in vibronic band position.

The average sequence separation in the  ${}^1L_b$  transition ranged from  $629\text{ cm}^{-1}$  to  $820\text{ cm}^{-1}$ . The average group separation in the  ${}^1L_a$

transition ranged from  $723\text{ cm}^{-1}$  to  $1064\text{ cm}^{-1}$ . These energies probably represent whole molecule breathing modes. This assertion is based on the little reported correlation that has been made between IR spectra and these energies.

When aza nitrogens were introduced into the pyrrole ring the  $^1L_a$  and  $^1L_b$  transitions were quite well separated. But for aza nitrogen substitution into the benzene ring only or for no aza nitrogen substitution the two transitions were merged. Distinction between the two transitions was difficult and was based on the recognizable vibronic sequence or group contours. For molecules with aza nitrogen substitution in both rings the transition separation was again distinct. This transition separation vs. aza nitrogen position phenomenon was first recognized by Mason<sup>57</sup> and was verified in this study. One may conceptualize these two lowest singlet transitions as normally overlapping such that they are merged. Aza nitrogen substitution into the benzene ring does not destroy the normalcy of this merger. However aza nitrogen substitution into the pyrrole ring does alter the transition positions by blue-shifting the  $^1L_a$  transition approximately  $5000\text{ cm}^{-1}$ . Further aza nitrogen substitution has no effect on the transition positions. Parenthetically there was no apparent pattern of either  $^1L_a$  or  $^1L_b$  transition position as a function of actual aza nitrogen position other than the gross effect just described.

A measure of the drastic amount of  $^1L_a$  transition shift is found in the relative positions of the lowest energy sequences of the  $^1L_a$  and  $^1L_b$  transitions. For indole and 7-azaindole the lowest energy sequence of the  $^1L_a$  transition is apparently at longer wavelengths than the lowest energy sequence of the  $^1L_b$  transition. The vapor spectra for

the other molecules all exhibited well separated transitions; thus the lowest energy sequence of the  $^1L_a$  transition must be at shorter wavelengths than the lowest energy sequence of the  $^1L_b$  transition. One of the difficulties in assigning the  $^1L_a$  transition 0-0 sequence was the inability to locate this sequence. This inability was attributed to two factors. First the broad, diffuse, overlapping nature of the vibronic groups made distinguishability between these groups very difficult. Second the pattern of these groups indicated that the 0-0 sequence must have low intensity. This is in contrast with the observations of the  $^1L_b$  transition 0-0 sequence. This transition intensity was strong enough to make the individual members in the  $^1L_b$  0-0 sequence easily discernable. Thus it appears that the  $^1L_b$  transition 0-0 sequence is Franck-Condon allowed and the  $^1L_a$  transition 0-0 sequence is Franck-Condon forbidden. In other words the ground state and first excited singlet state potential surfaces have similar contours and their minima occur at approximately the same general coordinate positions. However the  $^1L_a$  state potential surface probably has a different contour and its minimum occurs at a different position than the ground or  $^1L_b$  state.

The most puzzling aspect of the vapor absorption spectra was the temperature dependence of the  $^1L_a/^1L_b$  transition oscillator strength ratio for some of the studied molecules. This phenomenon became apparent when hot-band analyses were being performed to verify the  $^1L_b$  0-0 transition position (verification was accomplished in most cases). The nonexistence of this phenomenon for benzotriazole and 4-azsbenzimidazole further strengthens the contention that this phenomenon is not experimental artifact. The actual mechanism for explaining its

occurrence is not known. Certainly the mechanism must incorporate the fact that populating higher vibrational and rotational levels in the ground state increases the  ${}^1L_a \leftarrow {}^1A$  transition probability. This was exemplified by the experimental observation that there was a  ${}^1L_a$  transition intensity increase relative to the  ${}^1L_b$  transition intensity as the temperature was increased. In other words the value of the  ${}^1L_a$  transition moment,  $R = \langle \psi_f | \hat{M} | \psi_i \rangle$ , was changed as the temperature changed. In this expression  $\psi_i$  is the initial state wave function,  $\hat{M}$  is the transition dipole operator and  $\psi_f$  is the final state wave function. For any molecule  $\psi$  can be expressed as a product of functions,  $\psi_e \psi_v \psi_r$ , which respectively represent the purely electronic, vibrational and rotational components of the given wavefunction. As the temperature is increased the number of molecules in a given  $\psi_v$  in  $\psi_i$  can change. If this change is serendipitous it could increase the value of  $R$ . Usually the intensity of one transition cannot change without affecting the intensity of some other transition within a given transition manifold. Hence this  ${}^1L_a/{}^1L_b$  transition intensity ratio variation may involve intensity borrowing through vibronic coupling. That is the  $\psi_{i,v}$  at higher temperatures may readily couple with a vibrational mode of a higher excited state and consequently the  ${}^1L_a$  transition becomes more allowed. The excited states generally exhibit less symmetry than the ground state.

Another puzzling result was the appearance at lower temperatures vibronic bands to the red of the  ${}^1L_b$  0-0 transition sequence in the  ${}^1L_b$  transition band. The appearance of these vibronic bands preceded the  ${}^1L_b$  0-0 transition sequence as the temperature was increased. This occurred for benzimidazole, benzotriazole and 4-azabenzimidazole.

Another fact which must be considered is that the solution spectra of all the molecules, which exhibited these anomalous transition intensity changes, displayed a static  ${}^1L_a/{}^1L_b$  transition intensity ratio - even at different temperatures. The static ratio displayed in the solution spectra was the same as observed in the "concentrated" vapors. This ratio also appeared to be asymptotically reached at higher temperatures in the "equilibrium concentration" vapor spectra. Again the vibronic coupling mechanism could explain the stability of the  ${}^1L_a/{}^1L_b$  transition intensity ratio. Stability would be accomplished if one postulated that the solvent or other colliding solute molecules interacted with a solute molecule such that the  ${}^1L_a$  transition was maximally allowed. The interaction could be either through solute-solvent (or solute-solute) vibronic coupling or via a solute-solvent perturbation which enhances transition borrowing in the solute molecule.

If the proposed vibronic coupling mechanism is true there are still some unanswered questions: What is the specific vibrational coupling? Why does this coupling occur for some molecules but not for others? Why does the  ${}^1L_a/{}^1L_b$  transition intensity ratio always increase with increasing temperature and not decrease? It seems that some of the answers to these questions are inherently related to the role which the aza nitrogens have in formulating the  $\pi$ -electron structure. This is evident from the fact that the  ${}^1L_a/{}^1L_b$  transition intensity ratio doesn't appear to vary when at least two aza nitrogens are present. In addition the premature appearance of vibronic bands at energies below the  ${}^1L_b$  0-0 transition sequence only occurred when an aza nitrogen was present at the 3 position. Obviously the answers to these and other questions must await further experiments including

observations with different molecules.

One might wonder why these vapor absorption spectra anomalies only occurred in this study, i.e. why this is the first report of such anomalies. The answer is twofold and involve the fact that our spectra were obtained photometrically while most vapor spectra are obtained photographically. The latter method is used to more accurately make vibronic band assignments. Usually, though, only a specific portion of the spectrum is scrutinized since resolution is lost as more of the spectrum is encompassed. With the photometric method resolution is maintained no matter what wavelength limits are used. This is due to the fact that the photometric scan is displayed on a chart with optional length while the photographic scan is displayed on a plate with specified length. Thus the relative transition intensities were easily discernable photometrically since both the  $^1L_a$  and  $^1L_b$  transitions were easily scanned at any temperature. The second reason for our observation of this phenomenon is that its presence requires accurate determinations of relative transition intensities. The photometric method is designed to accomplish these determinations and the photographic method isn't so designed. The emulsion change versus light intensity is usually not linear or logarithmic. Thus our experimental procedures were luckily optimized for the chance observance of this anomalous phenomenon.

Turning attention now to the solution absorption and fluorescence spectra, it would seem to be quite difficult to ascribe solvent induced spectral shifts from the data in Table 7. The trick was to focus attention on the spectral data presented by only one author at a time. When an assessment was made of one author's data the spectra of another author was analyzed. Usually these data verified each other. Often

the data of several authors were so well interrelated that the solvent shifts became established beyond reasonable doubt.

It was possible to correlate the solvent-induced shifts for those molecules which displayed sufficient absorption and fluorescence data. The fact that this correlation was accomplished is probably the single most positive contribution of this dissertation. The correlation consisted of explanations of the solvent shifts using specific known solvent-solute interactions. These explanations were based somewhat on physical intuition about the types of expected interactions. However the explanations were also fashioned in a logical pattern. That is specific interactions were used to explain only a specific experimental observation. Each interaction could have only one effect. There was no ambivalence about specific cause and effect. The observed shifts were thus explained as a result of a combination of specific interactions. Further aid in forming these explanations was provided by the  $\pi$ -electronic charge density calculations. These calculations were used to gain some insight into the charge pattern differences between the ground and excited states. These calculations also were helpful in verifying which solvent-solute interactions were pertinent for explaining the observed shifts. Thus the experimental observations and the calculated results were meshed to provide a consistent explanation of the solvent-induced spectral shifts.

An example of the verificative correlation between the calculations and the observed spectra was the amount of Stokes' shift exhibited by various molecules in polar solvents. Those molecules which exhibited large Stokes' shifts were also calculated to have much larger excited state permanent dipole moments than ground state moments. Those

molecules with small Stokes' shifts also had smaller calculated differences between their ground and excited state permanent dipole moments. In fact the relative amount of Stokes' shift was easily predicted from the calculated magnitude of the change between the ground and excited state moments for all molecules where this comparison was made. This is a strong correlation because the Stokes' shifts are caused by dipolar interactions between the solvent and solute molecules. Large increases in the solute molecule permanent dipole moment magnitudes upon excitation cause a stabilizing rearrangement of polar solvent molecules. This stabilization is manifested as a large Stokes' shift. The confidence fostered by the Stokes' shift correlation with calculated permanent dipole moments allowed predictions to be made for those molecules whose permanent dipole moments hadn't been calculated. That is, a prediction was made concerning the relative difference between the ground and fluorescence-emitting state permanent dipole moment magnitudes for those molecules whose moments weren't calculated. Predictions could also be made via calculations for molecules whose spectra had not been examined. However this was not attempted here. Indazole, benzimidazole and 4-azabenzimidazole exhibit small Stokes' shifts. Indole, benzotriazole and 5-azabenzimidazole exhibit moderate Stokes' shifts. Those molecules with a single aza nitrogen substitution in the benzene ring and purine exhibit large Stokes' shifts. Thus the position of the aza nitrogens has a profound effect on the permanent dipole moment magnitude differences between the ground and excited states. These differences occur in the  $\pi$ -electron structure so the aza nitrogen positions must have strong influences on the  $\pi$ -electron rearrangement which occurs upon excitation.



The dipolar interactions which were responsible for the Stokes' shifts are also involved in the shifts observed between a solute's electronic transitions in different solvents. However, the observed solvent induced shift effects were not as pronounced as the Stokes' shift effects. Other effects which contribute to these shifts are H-bonding and solvent proton- $\pi$ -electron interactions. These three interactions were thus combinatorially used to explain the observed absorption and fluorescence shifts. At an aza nitrogen the solvent proton- $\pi$ -electron interactions and H-bonding were postulated to manifest the same effect. However, at the pyrrolic nitrogen these two interactions would lead to shifts in opposite directions. Thus at a pyrrolic nitrogen the proton- $\pi$ -electron interactions would cause a blue-shift and H-bonding would cause a red-shift if the  $\pi$ -electron charge densities at this nitrogen decreased upon excitation. The two effects would be reversed if the charge densities increased upon excitation. At pyridinic nitrogens both interactions would cause a red-shift if the  $\pi$ -electron densities at these nitrogens increased upon excitation. The interactions would cause a blue-shift if the densities decreased upon excitation. It was expected that solvent protons would preferentially interact at the pyridinic nitrogens since these species possessed lone pair electrons. Dipolar interactions would cause a red-shift if the excited state permanent dipole moment magnitude exceeded the ground state moment magnitude. A blue-shift would occur if the excited state moment magnitude was less than the ground state moment magnitude.

These three interactions were correlated with the excited and ground state  $\pi$ -electron charge density calculations to explain the observed solvent induced shifts in the absorption and fluorescence

spectra. Subtle shifts and reversals in shift trends were explained as due to combinations of these interactions or as interactions at different sites in the molecule. The nitrogens were chosen as the interaction sites because intuitively they should have more  $\pi$ -electron density and/or undergo larger  $\pi$ -electron charge density alterations upon excitation than should occur at the carbons. This supposition was verified with the charge density calculations. There are obviously other possible explanations for the solvent-induced spectral shifts. However, the correlations found here adequately explain these shifts and are reasonable. Based on physical intuition the explanations are sound.

The experimental data seemed to indicate that there were solute dependent differences in the amount of vibronic structure present in a given solvent. Apparently the differences depended on which solute molecule was being investigated. These differences seemed to occur for the absorption as well as the fluorescence spectra. Benzimidazole displayed sharp vibronic structure in its fluorescence spectra even in polar solvents. Indole in nonpolar solvents and indazole and 7-azaindole in both polar and nonpolar solvents displayed diffuse vibronic structure in their fluorescence spectra. These four molecules as well as purine also exhibited some vibronic structure in their solution absorption spectra. No absorption or fluorescence structure was reported for the other molecules. The presence or absence of this vibronic structure is probably not phenomenologically significant. Instead the structure probably reflects the resolving ability of the spectrometers used in making the spectral measurements. Thus there is presently little information pertaining to the electronic structures of these molecules which is derivable from the presence or absence

of vibronic structure in solution. Experiments must be performed with instruments possessing good resolution capabilities before any analysis of this structure is undertaken.

The pH of a solution had demonstrable effects on the spectral properties of these molecules. These effects were correlated with the data obtained in other solvents to give a consistent causal picture for the observed spectral shifts. A somewhat disturbing aspect of these observations is the fact that anions or cation supposedly were not formed unless a spectral change had occurred compared with that in neutral solutions. This presumes that the anion or cations species have different spectral characteristics than the neutral species. For most molecules this presumption is probably quite valid. However this statement may not be true for all molecules. One might be observing spectral changes for dications or dianions rather than cations or anions. This could occur if the doubly charged species was formed as a result of an interaction which strongly perturbed the molecule's  $\pi$ -electron structure and the singly charged species was formed without perturbing the  $\pi$ -electron structure.

The species in acidic media whose spectra differed from those in neutral solutions did not exhibit a consistent shift relative to the spectra obtained in neutral solutions. It was impossible to predict whether a red-shift or a blue-shift would be observed. This was probably due to the type of proton- $\pi$ -electron interaction which occurred in a specific molecule. On the other hand the "anion" regularly displayed a red-shift relative to the spectra in neutral solutions. The only reported exception of this statement for these molecules was the anion fluorescence of benzotriazole. The red-shift was attributed

to a  $\pi$ -electron structure destabilization caused by the Coulombic repulsion between this structure and the negative charge at the pyrrolic nitrogen. This residual charge was the hypothesized result of a proton extraction at this nitrogen's hydrogen by the basic solvent. This hypothesis could be easily tested by replacing the pyrrolic nitrogen's hydrogen with a methyl group and again observing the spectra in basic solution. The spectral changes should not occur at the same pH as the  $pK_a$  of the normal nonmethylated molecule if this hypothesis is correct. Another consistency noted for the anion was that the  $pK_a$  of the molecule in the excited state was lower than that molecular  $pK_a$  in the ground state. This supposedly reflects the relative acidity of the pyrrolic nitrogen in the ground and excited states. However very scanty data were available to verify this hypothesis. Again the hypothesis could be checked with molecules methylated at the pyrrolic nitrogen. In summary it would be fruitful if concentrated experimental effort were devoted to studying the effects of pH on the spectral properties of molecules.

The amount of available phosphorescence data was remarkably scarce. Thus very little comparison of such data between molecules was possible. A disappointing feature of the phosphorescence data analyses was the poor correlation between the calculated and the experimentally determined transition energies. This reflects the inadequacy of the calculations. The inadequacy could probably be corrected with better parametrization. Phosphorescent emission from the "cation" was red-shifted relative to emission from the neutral species for the few molecules whose emission was monitored in the two media. This red-shift paralleled the fluorescence shifts for these molecules between the cation and neutral species. Thus the same proton- $\pi$ -electron

interaction probably stabilizes the emitting state for both emissions. In contrast with this parallel between the cation and neutral species' emissions there was no apparent correlation between the observed Stokes' shifts and the phosphorescence position for these molecules. This indicates that dipolar interactions do not play an important role in determining the phosphorescence position. It should be noted that all phosphorescence spectra exhibited a moderate amount of vibronic structure. An analysis of this structure was not attempted. However this analysis could be performed and might yield information about the vibrational modes in the lowest triplet state for these molecules.

Two other experimental aspects were noted for these molecules. These were dual emission and  $n-\pi^*$  transitions. The dual emission explanation was hypothesized to occur for indole, purine, benzotriazole and indazole. The bases for this type of emission was discussed in appropriate sections in the discussion for these molecules. Purine displayed an  $n-\pi^*$  transition. In addition benzotriazole and 4-azabenzimidazole were hypothesized to exhibit this transition. These di- and triazaindoles were the only instances where this type of transition seemed to occur.

The results of the theoretical calculations were reasonably correlative with the spectral properties of the studied molecules. This heartening correlation fostered trust in most of the calculated quantities whose corresponding experimental parameters had not been measured (excluding the calculated quantities associated with phosphorescence as noted above). This included properties of singlet transitions for those molecules which had not been extensively experimentally examined. Unfortunately the calculated singlet transition energies were not

discriminatory for the first two transitions. That is the separation between states was about the same for all molecules whose transitions were calculated. Separation of the first two transitions was not predicted for benzimidazole and 4-azabenzimidazole although this fact was experimentally observed. Likewise merging of these transitions was not predicted for indole and 7-azaindole. The lack of these predictions was not considered an inconsistency for the calculations. The calculations and observed energy of the first transition agreed within 0.2 eV for all molecules where this comparison could be made. Such a comparison for the second transition yielded agreement within 0.3 eV. Such agreement is all that can be reasonably expected. The separation or merger of these two transitions are subtle differences which can be experimentally observed but not easily discernable with calculations.

Assignment of the two lowest calculated singlet transitions was based on three criteria: transition moment orientation, oscillator strength and excited state permanent dipole moment magnitude. The  ${}^1L_a$  state was postulated to possess the higher dipole moment magnitude and the  ${}^1L_a$  transition was presumed to be preferentially oriented along the short axis of the molecule and have the larger oscillator strength. The  ${}^1L_b$  state was postulated to have the lower moment magnitude and the corresponding transition was presumed to be primarily oriented along the long axis and possess the smaller oscillator strength. These assignments were based on experimental observations of indole and related molecules. The permanent dipole moment criterion was derived from polar solvent induced shifts. Indole's and 7-azaindole's  ${}^1L_a$  transition shifted more than the  ${}^1L_b$  transition when a solvent-solute dipolar interaction was involved. The transition orientation criterion

was based on the observed orientations in naphthalene which is iso-electronic with indole. The oscillator strength criterion was based on experimental observations for naphthalene and indole. This criterion does not appear to be correct for 4-azabenzimidazole and possibly benzotriazole or purine. However, further experimental data must be obtained before a final judgement of this criterion's applicability is made.

Other than for these three possible exceptions the experimental observations and the assigned transitions based on these criteria agreed perfectly. That is the criteria for the assignments of the calculated transitions and the experimentally observed spectral parameters coincided for all molecules where a comparison could be made. Such a remarkable amount of correlation was surprising and lent credence to the validity of the calculations.

For these molecules the calculated singlet transition moment orientations did not parallel a molecular primary axis and were not predicted to be perpendicular to each other. Although the criterion was used that they preferentially possess a major component along a particular axis it was not experimentally expected that the moments parallel an axis. Thus the calculated results reinforced our naive physical conception of these transitions. There was also general agreement between the calculated angle between the two lowest transitions and the available polarization data. However, this statement must be tempered with the fact that small adjustments in the parameters used for the calculations significantly altered the resultant transition moment orientation. Thus these calculated orientations must not be interpreted literally. There is still negligible chance that the moments would be predicted to parallel a

primary axis of the molecule.

The good correlation between experimental observations and calculated observables for the singlet transitions and states engendered trust in the plausibility of the  $\pi$ -electron charge density calculations for these states. This trust was further enhanced by the correlation between these density calculations and the relative reactivities of the atomic centers in the molecules. The correlation was quite good although little reactivity data was cited. More data is probably available and could be used to further substantiate these density calculations. It was also noted above that the calculated densities provided realistic values for the interactions involved in the solvent shift interpretations.

All this evidence for the believability of the calculated  $\pi$ -electronic charge densities provides confidence in the picture of the molecular electronic structure which these densities portray. Thus the relative shifts in  $\pi$ -electronic charge between the ground and excited states appears to be an accurate picture of the actual physical processes. In addition these calculated densities appear to accurately reflect the relative position of the charge in the ground and excited states. This pictorial representation of the electronic charge is the most powerful and perhaps the most useful result of the calculations. Experimental observations alone could not develop such a picture. This conceptualization of the electronic structure is the culmination of the previous paths of correlations. It is the essence and was the goal of this thesis.

One of the conclusions from this study is that minor variations in the relative  $\pi$ -electron charge densities at various positions can be



effected by or can affect the spectral properties of these molecules. For example the absorption and fluorescence spectra of benzimidazole in neutral and basic solutions are quite different. The difference occurs between the two processes as well as between the two solvents. This large variation occurs as a result of the solvent change which presents only a small perturbation to the  $\pi$ -electron structure. A second example is the differences in values of the permanent dipole moments for the ground and excited states. An electronic transition can drastically alter the value of the molecular dipole moment. Another example is presented by the charge density calculations for any two molecules. Although the charge density variations between molecules are small at any position the spectral characteristics are quite different. These spectral characteristics are so discernably unique that they provide identifying features of these molecules. These spectral differences were not unexpected. However, the minor rearrangement of  $\pi$ -electron charge accompanying these differences was surprising and enlightening.

There were two spectroscopic phenomena discussed in this study which appear to be relatively unique properties of these molecules. These phenomena are the hypothesized vibronic coupling which occurs during excitation and the dual emission from two excited states which occurs for some molecules. The question arises concerning the biological significance of these phenomena. These processes signify close communication between electronic states. Is this biologically relevant? Since the normal biological function of these molecules does not depend on interactions of the molecules with light there does not seem to be any relevance of these processes. However, the natural environment of

these molecules includes electromagnetic radiation. UV light can induce mutations in DNA. UV irradiation can severely disrupt the function of enzymes. Also the chemical reactions of these molecules must involve the  $\pi$ -electron system since these electrons are an integral part of the molecules. But there still does not seem to be any biological function in which these molecules participate that depends upon these unique electronic properties. Similar chromophores which did not exhibit these phenomena could probably participate in the biological activity. Yet the nagging unanswered question still remains that these specific chromophores are the actual ones involved in biological viability. Perhaps these electronic properties are important but their relevance remains unknown. A related unanswered question regards the properties of these molecules which dictate their use in different biological functions. It is still unknown why these molecules which form a chromophoric family display diverse biological roles. The position and/or type of substituent as well as the aza nitrogen position may be implicated. These position differences were manifested in the spectral data so they are important.

Finally it is hoped that this study has shown that a coordination of spectroscopic data is feasible and can yield information about the electronic structure of molecules. In addition the data can be used to compare properties within a family of molecules. The exhibited spectroscopic information isn't composed of isolated features. There are aspects of this information which are interrelated. Coordinating the information can reveal these interrelationships.

## BIBLIOGRAPHY

## BIBLIOGRAPHY

1. I. N. Levine, Quantum Chemistry, Allyn and Bacon (1970).
2. F. L. Pilar, Elementary Quantum Chemistry, McGraw-Hill (1968).
3. R. G. Parr, Quantum Theory of Molecular Electronic Structure, W. A. Benjamin (1963).
4. P. Hochman and R. Wagner, Description of the TE DEUM Program, internal publication (1970).
5. P. Hochmann, V. Kleinwachter, and M. A. El-Bayoumi, to be published.
6. W. J. Potts, Jr., J. Chem. Phys. 20, 809 (1952).
7. J. M. Hollas, Spectrochim. Acta 19, 753 (1963).
8. M. A. El-Bayoumi, C. A. Taylor, M. Kasha, to be published.
9. J. R. Platt, J. Chem. Phys. 19, 101 (1951).
10. S. V. Konev, Fluorescence and Phosphorescence of Proteins and Nucleic Acids, Plenum Press 1967, a) p. 16-17 b) p. 29-35 c) p. 19 d) p. 39-53.
11. D. P. Craig, J. M. Hollas, M. F. Redies and S. C. Wait, Jr., Phil. Tran. Roy. Soc. 253A, 543 (1961).
12. G. Weber, Biochem J. 75, 335 (1960).
13. H. Zimmermann and N. Joop, Z. Elektrochem., Ber. Bunsenges Physik. Chem. 65, 61 (1961).
14. H.-U. Schutt and H. Zimmermann, Z. Elektrochem., Ber Bunsenges. Physik. Chem. 67, 54 (1963).
15. E. A. Chernitskii, S. V. Konev, and V. P. Bobrovich, Dokl. Akad. Nauk BSSR 7, 628 (1963).
16. A. N. Sevchenko, S. V. Konev, and M. A. Katibnikov, Dokl. Akad. Nauk SSSR 153, 875 (1963).
17. E-S. Song and W. E. Kurtin, J. Am. Chem. Soc. 91, 4892 (1969).
18. J. Zuclich, J. Chem. Phys. 52, 3586 (1970).

19. B. L. Van Duuren, J. Org. Chem. 26, 2954 (1961).
20. D. A. Chignell and W. B. Gratzner, J. Phys. Chem. 72, 2934 (1968).
21. S. Nagakura, J. A. Chem. Soc. 76, 3070 (1954).
22. E. G. McRae, J. Phys. Chem. 61, 562 (1957).
23. R. D. Gordon and R. F. Yang, Can. J. Chem. 48, 1722 (1970).
24. E. A. Chernitskii and S. V. Konev, Dokl. Akad. Nauk BSSR 8, 258 (1964).
25. S. V. Konev, V. P. Bobrovich and E. A. Chernitskii, Biofizika 10, 42 (1965).
26. V. P. Bobrovich, G. S. Kembrovskii, and N. I. Marenka, Dokl. Akad. Nauk BSSR 10, 936 (1966).
27. N. Mataga, Y. Torihashi, and K. Ezumi, Theor. Chim. Acta. 2, 158 (1964).
28. B. L. VanDuuren, Anal. Chem. 32, 1436 (1960).
29. C. M. Chopin and J. H. Wharton, Chem. Phys. Lett. 3, 552 (1969).
30. M. S. Walker, T. W. Bednar, and R. Lumry, J. Chem. Phys. 47, 1020 (1967).
31. G. S. Kembrovskii, V. P. Bobrovich and S. V. Konev, Zh. Prikl. Spektrosk. 5, 695 (1966).
32. I. Weinryb, Biochem. Biophys. Res. Comm. 34, 865 (1969).
33. L. F. Gladchenko, M. Y. Kostko, and L. G. Pikulik, A. N. Sevchenko, Dokl. Akad. Nauk. BSSR 9, 647 (1965).
34. J. Eisinger and G. Navon, J. Chem. Phys. 50, 2069 (1969).
35. R. F. Chen, G. G. Vurek and N. Alexander, Science 156, 949 (1967).
36. H. Sprince, G. R. Rowley, and D. Jameson, Science 125, 442 (1957).
37. R. W. Cowgill, Arch. Biochem. Biophys. 100, 36 (1963).
38. H. V. Drushel, A. L. Sommers and R. L. Cox, Anal. Chem. 35, 2166 (1963).
39. G. Weber and F. W. J. Teale, Trans. Faraday Soc. 53, 646 (1957).
40. J. W. Bridges and R. T. Williams, Biochem. J. 107, 225 (1968).
41. M. G. M. Balemans and F. C. G. Van De Veerdonk, Experientia 23, 906 (1967).

42. S. V. Konev and E. A. Chernitskii, Dokl. Akad. Nauk. BSSR 9, 328 (1965).
43. S. V. Konev and E. A. Chernitskii, Biofizika 9, 520 (1964).
44. M. S. Walker, T. W. Bednar and R. Lumry, J. Chem. Phys. 45, 3455 (1966).
45. L. Stryer, J. A. Chem. Soc. 88, 5708 (1966).
46. L. G. Pikulik, L. F. Cladchenko and M. Y. Kostko, Zh. Prikl. Spektrosk. 6, 210 (1967).
47. R. C. Heckman, J. Mol. Spect. 2, 27 (1958).
48. V. L. Ermolaev, Optika i Spektroskopiya 11, 492 (1961).
49. S. Freed and W. Salmre, Science 128, 1341 (1958).
50. C. Cailly and A. Bourkhors, C. R. Acad. Sci., Paris, Ser. C264, 480 (1967).
51. G. M. Barenboim, Biofizika 7, 227 (1962).
52. R. Pariser, J. Chem. Phys. 24, 250 (1956).
53. R. L. Hinman and J. Lang, Tetrahedron Lett. 21, 12 (1960).
54. T. K. Adler, Anal. Chem. 34, 685 (1962).
55. J. Derkosch, O. E. Polansky, E. Rieger and G. Derflinger, Monatsh Chem. 92, 1131 (1961).
56. G. H. Beaven, E. R. Holiday, E. A. Johnson, Spectrochim. Acta 4, 338 (1951).
57. S. F. Mason, J. Chem. Soc. 1954, 2071.
58. Present work.
59. K. C. Ingham, this laboratory.
60. L. B. Clark and I. Tinoco, J. Am. Chem. Soc. 87, 11 (1965).
61. H. H. Chen and L. B. Clark, J. Chem. Phys. 51, 1862 (1969).
62. J. Drobnik and L. Augenstein, Photochem. Photobiol. 5, 13 (1966).
63. J. W. Longworth, Biochem. J. 84, 104p (1962).
64. B. J. Cohen and L. Goodman, J. Am. Chem. Soc. 87, 5487 (1965).
65. H. C. Borreson, Acta Chem. Scand. 17, 921 (1963).

66. J. Drobnik, V. Kleinwachter and L. Augenstein, Photochem. Photobiol. 6, 147 (1967).
67. R. Guermonprez, C. Helene and M. Ptak, J. Chim. Phys. 64, 1376 (1967).
68. C. Helene, Biochem. Biophys. Res. Comm. 22, 237 (1966).
69. M. A. Slifkin, Biochim. Biophys. Acta 103, 365 (1965).
70. H. Linschitz and J. S. Connelly, J. Am. Chem. Soc. 90, 2979 (1968).
71. J. W. Longworth, R. O. Rahn and R. G. Shulman, J. Chem. Phys. 45, 2930 (1966).

MICHIGAN STATE UNIVERSITY LIBRARIES



3 1293 10798 5396